AD-A036 211 STANFORD RESEARCH INST MENLO PARK CALIF F/G 17/5
EVALUATION OF TECHNOLOGIES FOR INFRARED IMAGING.(U)
NOV 76 K S KRISHNAN, J S OSTREM F33615-75-C-1142
UNCLASSIFIED AFAL-TR-76-82 NL

1 OF 2
AD
A036211

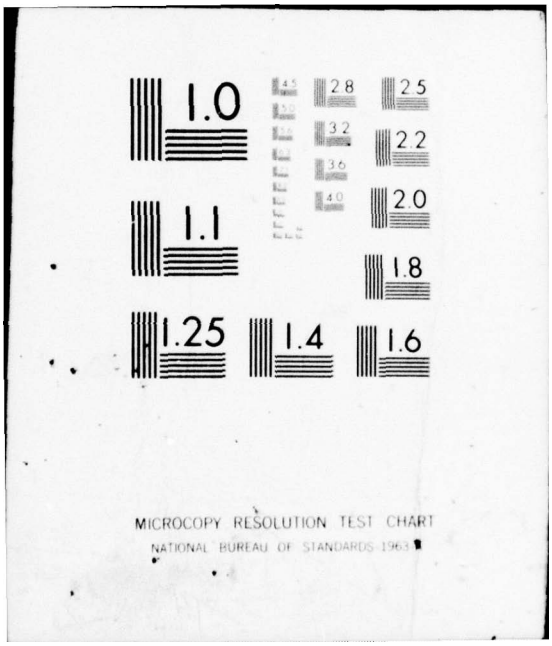
1.0
1.1
1.25
1.4
1.6
2.8
2.5
3.2
2.2
3.6
2.0
4.0
1.8
MICROCOPY RESOLUTION TEST CHART
NATIONAL BUREAU OF STANDARDS-1963

AFAL-TR-76-82

EVALUATION OF TECHNOLOGIES FOR INFRARED IMAGING

STANFORD RESEARCH INSTITUTE
MENLO PARK, CA 94025

NOVEMBER 1976

FINAL REPORT FEBRUARY 1975 - NOVEMBER 1975

AIR FORCE AVIONICS LABORATORY
AIR FORCE WRIGHT AERONAUTICAL LABORATORIES
AIR FORCE SYSTEMS COMMAND
WRIGHT-PATTERSON AIR FORCE BASE, OHIO 45433

NOTICE

When Government drawings, specifications, or other data are used for any purpose other than in connection with a definitely related Government procurement operation, the United States Government thereby incurs no responsibility nor any obligation whatsoever; and the fact that the government may have formulated, furnished, or in any way supplied the said drawings, specifications, or other data, is not to be regarded by implication or otherwise as in any manner licensing the holder or any other person or corporation, or conveying any rights or permission to manufacture, use, or sell any patented invention that may in any way be related thereto.

This report has been reviewed by the Information Office (OI) and is releasable to the National Technical Information Service (NTIS). At NTIS, it will be available to the general public, including foreign nations.

This technical report has been reviewed and is approved for publication.

Donald J. Peacock

DONALD J. PEACOCK, Actg. Chief
Electro-Optic Detectors Group
Electro-Optics Technology Branch

FOR THE COMMANDER

William C. Schoonover

WILLIAM C. SCHOONOVER, Chief
Electro-Optics Technology Branch
Electronic Technology Division

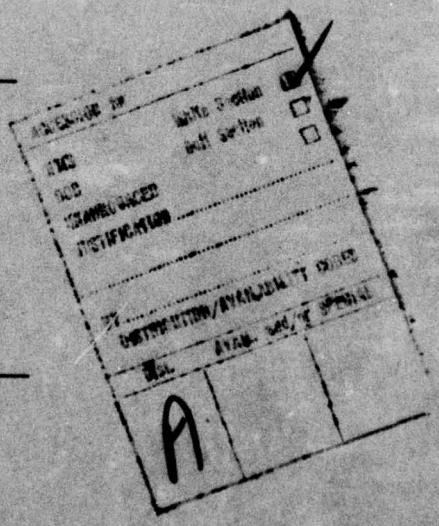

Copies of this report should not be returned unless return is required by security considerations, contractual obligations, or notice on a specific document.

AIR FORCE - 29 DECEMBER 76 - 100

UNCLASSIFIED

SECURITY CLASSIFICATION OF THIS PAGE (When Data Entered)

REPORT DOCUMENTATION PAGE

READ INSTRUCTIONS BEFORE COMPLETING FORM

1. REPORT NUMBER: AFAL-TR-76-82
2. GOVT ACCESSION NO.
3. RECIPIENT'S CATALOG NUMBER
4. TITLE (and Subtitle): EVALUATION OF TECHNOLOGIES FOR INFRARED IMAGING.
5. TYPE OF REPORT & PERIOD COVERED: Final Technical Report. 5 Feb [redacted]-15 Nov [redacted]75
6. PERFORMING ORG. REPORT NUMBER: SRI Project ISE 4047
7. AUTHOR(s): Kamala S. Krishnan [redacted] John S. Ostrem
8. CONTRACT OR GRANT NUMBER(s): F33615-75-C-1142
9. PERFORMING ORGANIZATION NAME AND ADDRESS: Stanford Research Institute, 333 Ravenswood Avenue, Menlo Park, CA 94025
10. PROGRAM ELEMENT, PROJECT, TASK AREA & WORK UNIT NUMBERS: 2001 0346
11. CONTROLLING OFFICE NAME AND ADDRESS: Air Force Avionics Laboratory (AFAL/DHO-3), Air Force Systems Command, United States Air Force, Wright-Patterson AFB, Ohio 45433
12. REPORT DATE: Nov [redacted]76
13. NO. OF PAGES: 129
14. MONITORING AGENCY NAME & ADDRESS (if diff. from Controlling Office)
15. SECURITY CLASS. (of this report): UNCLASSIFIED
15a. DECLASSIFICATION/DOWNGRADING SCHEDULE

16. DISTRIBUTION STATEMENT (of this report)

Approved for public release; distribution unlimited

17. DISTRIBUTION STATEMENT (of the abstract entered in Block 20, if different from report)

62204F

18. SUPPLEMENTARY NOTES

To be submitted for publication in Applied Optics. To be presented in IRIS 1976.

19. KEY WORDS (Continue on reverse side if necessary and identify by block number)

Infrared detection	Four-frequency imaging
Infrared imaging	Metal-vapor upconversion
Passive imaging	Two-photon pumped upconversion
Active imaging	Parametric upconversion
Infrared upconversion	Nonlinear crystal upconversion
	Infrared quantum counter

20. ABSTRACT (Continue on reverse side if necessary and identify by block number)

This report assesses the practical value of a new technique of upconverting infrared radiation using two-photon pumped alkali metal vapors and compares the relative merits of several approaches to IR imaging. Performance criteria of passive and active IR imaging systems are chosen and practical configurations are defined.

DD FORM 1 JAN 73 1473
EDITION OF 1 NOV 65 IS OBSOLETE

Over

UNCLASSIFIED

SECURITY CLASSIFICATION OF THIS PAGE (When Data Entered)

332507

19. KEY WORDS (Continued)

20 ABSTRACT (Continued)

The principles of IR upconversion using alkali metal vapors and the infrared quantum counter are detailed. The upconversion efficiency, acceptance angle and IR bandwidth are evaluated. Upconversion with nonlinear crystals and direct detection of IR are also briefly treated.

Detailed and practical systems are designed for passive and active imaging based on the several approaches and the performance indicators are evaluated. The upconversion methods in their present stage of development are not found to perform as well as the state-of-the-art direct-detection methods. The infrared quantum counter (IRQC) is at present the best upconversion candidate for thermal imaging because of its ability to integrate the thermal radiation. Upconversion in sodium vapor is promising in both the passive and active cases approaching, in the latter, the performance of direct detection. The IRQC does not appear to have any merit for active imaging. The performance of nonlinear crystal upconverters is significantly poorer than the metal-vapor upconverters.

PREFACE

This final technical report describes the research performed under Air Force Contract F33615-75-C-1142 during the period 5 February 1975 through 15 November 1975.

This work was supported by the U.S. Air Force Systems Command and monitored by the Air Force Avionics Laboratory, Wright-Patterson Air Force Base, Ohio. The project engineer was Mr. Charles H. Stevens (AFAL/TEO).

The following SRI personnel contributed to the work under SRI Project ISE 4047 and to this report: Dr. Kamala S. Krishnan (Principal Investigator), Dr. John S. Ostrem, and Dr. Richard C. Honey.

During the course of the work, Mr. Eddie A. Stappaerts of W. W. Hansen Microwave Laboratory, Stanford University, was retained as a consultant and contributed substantially to the work on metal-vapor upconversion.

During the work, Drs. J. Chivian, D. Eden, and A. Sobey of LTV Advanced Technology Center, Dallas, Texas, and Drs. K. Sewell, J. Herrington, and W. Volz of Varo, Inc., Garland, Texas, were consulted on their respective versions of the infrared quantum counter. Their cooperation is appreciated. Gratitude is expressed to Drs. B. Soffer and D. Tseng of Hughes Research Laboratories, Malibu, California, for discussions on coherent upconversion processes.

SUMMARY

Recent discovery of a new technique of upconverting infrared radiation into the visible or ultraviolet using two-photon pumped alkali metal vapors has stimulated questions regarding the practical value of the technique in thermal and active image upconversion. This report addresses these questions in detail for metal-vapor upconversion and examines several other approaches to IR imaging so as to elicit their relative merits.

The principles of passive and active infrared imaging are examined and a set of parameters is chosen as indicative of the performance of the devices. For the passive case, the noise-equivalent temperature difference (NETD), the field of view, and the number of resolution elements are chosen as the performance indicators. In active imaging, the signal-to-noise ratio (SNR) for a chosen range and illuminator power is chosen to replace NETD. The optical systems for the upconverters are examined to determine the limitations they impose on the field of view and resolution. Practical system configurations are defined.

The background and physical principles of IR upconversion using alkali metal vapors and the infrared quantum counter are described in detail. Expressions are developed for the upconversion efficiency and other characteristics of these upconversion processes. Realistic parameter values are used to evaluate these characteristics. To provide a comparative basis, nonlinear crystal upconverters and direct-detection-based imaging systems are also considered briefly.

Using this background, detailed and practical system designs are developed for passive and active imaging based on the several approaches.

The performance indicators are presented in detail and discussed. It is found that the upconversion methods in their present stage of development do not perform as well as the state-of-the-art direct-detection methods. The quantum counter is the best upconversion candidate for thermal imaging because of its ability to integrate the thermal radiation. Upconversion in sodium vapor is promising in both the passive and active cases approaching, in the latter, the performance of direct detection. The IRQC does not appear to have any merit for active imaging. The performance of nonlinear crystal upconverters is significantly poorer than the metal-vapor upconverters.

TABLE OF CONTENTS

TABLE OF CONTENTS (Concluded)

LIST OF ILLUSTRATIONS

LIST OF TABLES

SECTION I

INTRODUCTION

A. BACKGROUND AND OBJECTIVES

Detection and imaging of infrared (IR) radiation has been of sustained interest in many different applications. Direct detection of infrared radiation using infrared-sensitive detectors was an early method and is highly developed at the present time. With the advent of the laser, several novel ways have been invented for frequency-shifting ("upconversion") of infrared radiation into the ultraviolet, visible or near-infrared region. Since detectors for visible radiation have significantly better signal-to-noise performance than infrared detectors, detection of the upconverted radiation appears attractive. However, the overall desirability of an infrared detection and imaging system depends on several other factors. It is the objective of the work reported here to investigate in some detail the relation of these factors to different schemes for detection of infrared radiation.

The IR upconversion methods considered in this report are based on (1) nonlinear crystals, (2) alkali metal vapors, and (3) quantum counters. The first two depend on the parametric interaction between the infrared radiation and a pump radiation occurring in a material with the requisite nonlinear properties to yield radiation at the sum frequency. This demands a laser pump-source not only to provide the electric field intensities at which the nonlinearities become significant but also to provide the coherence necessary to achieve a traveling wave interaction. In the third method, the energy of the infrared photon is added to that of a visible or near-infrared photon in a material with a suitable set of energy levels. While a coherent laser pump is not necessary for this method, the high spectral brightness of a laser is convenient and useful in practice.

Parametric upconversion using crystals with second-order electric susceptibilities has been explored and fundamental as well as practical limitations have been shown to exist.* The nonlinear coefficients are not sufficiently large to provide good conversion efficiency at pump power levels low enough to avoid damaging the crystals. Furthermore, the requirement of phase-matching in these birefringent crystals restricts the field of view and the bandwidth over which the infrared radiation may be upconverted. This is particularly important in upconverting thermal images. It was the conclusion of the previous study* that crystal upconversion will be limited to special purpose active imaging.

Recently, a new upconversion technique using two-photon-pumped metal vapors has been developed.† When a natural frequency of the metal vapor is approached by the frequency of one or more of the photons involved, the third-order susceptibilities acquire very large values. As a result, sizable photon conversion efficiencies have been reported.‡ The method seems to offer several advantages. The expected conversion efficiencies are high. Since no permanent damage mechanism exists in metal vapors, higher pump power densities may be used if necessary. Problems associated with the preparation of the nonlinear material are minimal with the metal vapors, and since a nonallowed two-photon transistor is pumped, the upconverted or sum frequency is well separated from the pump frequency. Finally, for cesium and sodium metal vapors to be considered in this report, the sum frequencies are generated in a region where photocathodes have significantly better quantum efficiencies. Because of these advantages, a detailed examination of the metal-vapor upconversion applied to active and passive imaging was deemed to be a useful undertaking.

---

*A. Fenner Milton, "Upconversion--A Systems View," Appl. Optics, Vol. 11, p. 2311 (1972).

†S. E. Harris and D. M. Bloom, "Resonantly Two-Photon Pumped Frequency Converter," Appl. Phys. Letters, Vol. 24, p. 229 (1974).

‡D. M. Bloom, J. T. Yardley, J. F. Young, and S. E. Harris, "Infrared Up-Conversion with Resonantly Two-Photon Pumped Metal Vapors," Appl. Phys. Letters, Vol. 24, p. 427 (1974).

The infrared quantum counter (IRQC) method of detecting infrared radiation has been known for some time and had been thought to be of limited potential because of the need to obtain a good spectral match between the laser pump and the IRQC material. The availability of tunable lasers has eased this requirement. In addition, some progress has been reported recently in improving signal to noise by temporal discrimination* as well as in using polycrystalline material.† Because of the renewed interest in this area, the quantum-counter method was included so as to complete the examination of upconversion techniques.

The development of conventional detectors for infrared radiation has occurred over several decades and the pace of development has been enhanced by the advances in semiconductor materials, device, and processing technology. Forward-looking infrared (FLIR) systems based on semiconductor detectors, being in very advanced stages of development, represent the state of the art in performance and must be looked upon as the standard against which the promise of the upconversion techniques must be evaluated. It should be noted that in the imaging mode, the present-day FLIR systems must scan the image in the focal plane, whereas all the upconversion methods can upconvert the entire image at the same time. Aside from the mechanical complexity of scanning, scanning methods require faster detectors and cannot respond to fast events, including pulsed illumination. (Self-scanning focal-plane arrays of detectors are currently under intensive development.)

In the remainder of this report, an evaluation and a comparison of the various infrared imaging methods are presented with special attention

---

*J. R. Herrington, K. G. Sewell, and W. B. Volz, "A Thermal Imaging System Based on the $PrCl_3$ Quantum Counter," Appl. Phys. Letters, Vol. 26, p. 226, (1975).

†K. G. Sewell and W. B. Volz, "Direct Infrared Image Upconversion with a Praseodymium Chloride Quantum Counter," Appl. Phys. Letters, Vol. 23, p. 104 (1973).

to metal-vapor upconversion and the IRQC, since these have not been evaluated previously. The approach will be to identify the significant performance parameters of active and passive imaging systems, to examine the special and unique characteristics of the different upconversion schemes, and to obtain a realistic performance estimate for each system. Performance comparisons are given directly after these estimates. The necessary physical background is developed wherever it is not available directly from the literature.

B. ORGANIZATION

Passive and active infrared imaging systems are discussed in Section II. The basic approach to the performance estimation is developed and the important performance factors are defined. The different types of optical systems for upconverters are then discussed and the configurations of the upconversion systems are then described.

The basic phenomenology of upconversion in metal vapors, quantum counters and nonlinear crystals are presented in Section III. The metal vapors and quantum counters are discussed at length. Upconversion efficiencies, acceptance angles and bandwidths, and so on, are derived. To complete the descriptions, nonlinear crystal upconversion and infrared photodetectors are briefly discussed.

The expected performance of passive and active IR imaging systems, based on the above four methods, is developed in Section IV. Detailed system designs are presented and the performance of the systems are compared and the various constraints and trade-offs in the systems are detailed.

A brief summary of the findings and recommendations for future work are presented in Section V.

SECTION II

INFRARED IMAGING SYSTEMS

The operation of infrared detection and imaging devices depends on the IR radiance of the objects in the field of view of their optics. A simplified block diagram of an infrared imaging system is shown in Figure 1. The radiance from the object is from self-emission by virtue of its temperature as well as from reflection of radiation incident on the object. This radiation is modified during the transmission through the intervening atmosphere by absorption, atmospheric emission, and scatter. The optics collect the infrared radiation and make it available for the detection system, which converts it into video signals for display purposes.

Because the difference between the various schemes of infrared imaging lies in the detection system, this comparative study concentrates on the detection system and ignores in the main the effects due to common aspects of the system. For example, this study does not treat the emissivities and transmittances, the aberrations due to the atmosphere or the optical system, or the signal-to-noise ratio in the display electronics. In this sense, the performance parameters obtained are optimistic, but they are not expected to be far different from practical values.

The details of a scene are contained in the variations in the scene radiance arising from local variations in the temperature, emissivity, irradiance, and reflectance of the objects in the scene. The contrast present in the image is a function of both the variations in the scene as well as the average level of radiance in the scene. A fundamental limitation of thermal imaging arises from the fact that the changes in temperature and emissivity are small and the background radiance is large, resulting in poor contrast.

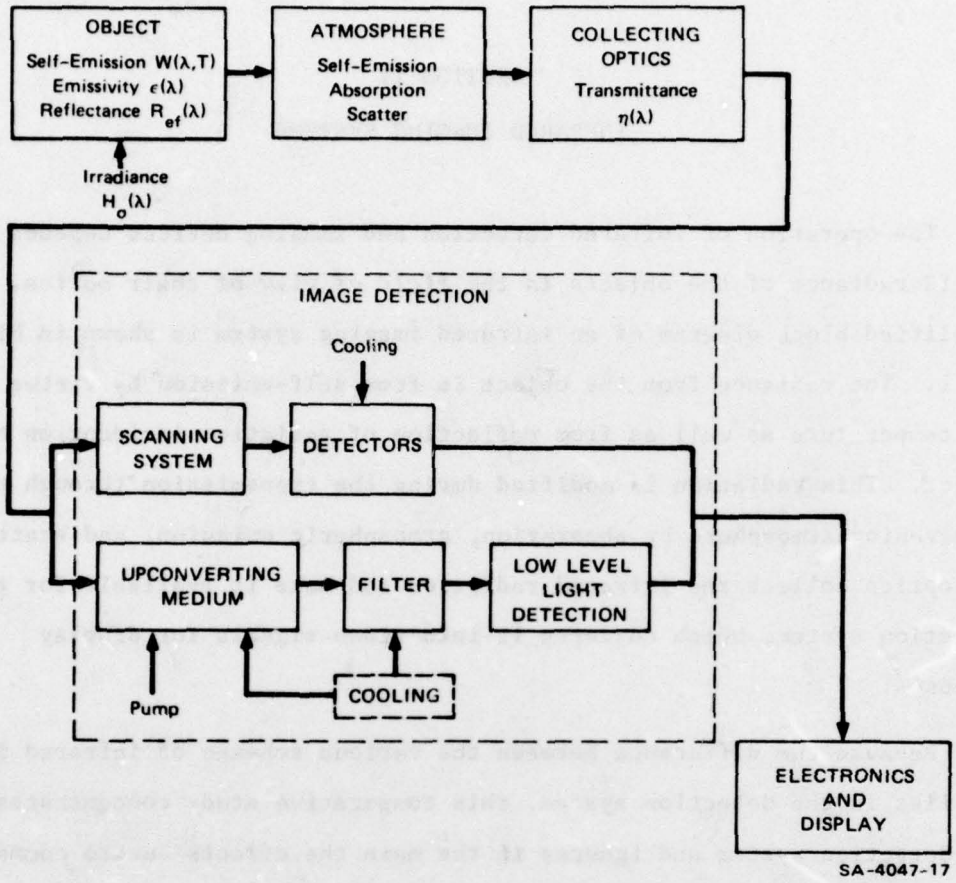

FIGURE 1 BLOCK DIAGRAM OF INFRARED IMAGING

Even though photodetectors for infrared radiation have somewhat higher quantum efficiencies than photocathodes for visible radiation, there are relatively noise-free amplification methods for the latter. Also, the room temperature "dark" current is much larger for IR detectors, necessitating cooling and shielding of the detectors from the surroundings.

A. PERFORMANCE CRITERIA FOR IMAGING SYSTEMS

The spectral radiance of the object to be imaged is given by

$$N(\lambda,T) = \frac{W(\lambda,T)}{\pi}\,\epsilon(\lambda) + \frac{H_o(\lambda)}{\pi}\,R_{ef}(\lambda)\ \left[W\ sr^{-1}\ cm^{-2}\ \mu m^{-1}\right] \quad , \quad (1)$$

where

$W(\lambda,T)$ = spectral emittance of a blackbody at temperature $T[°K]$

$\epsilon(\lambda)$ = spectral emissivity of the object

$H_o(\lambda)$ = spectral irradiance on the object

$R_{ef}(\lambda)$ = diffuse spectral reflectance of the object.

If the transmittance of the atmosphere over the bandwidth of interest is assumed to be unity and the self-emission and scattering from the atmosphere are ignored; and if an optical system with an aperture of diameter D[cm], focal length f[cm], and transmittance $\eta_t(\lambda)$, is used to collect the IR radiation at a range r[cm], then the spectral irradiance due to the object at the image plane ($f \ll r$) will be

$$H_{\lambda i}(\lambda,T) = N(\lambda,T)\,\frac{\pi D^2}{4r^2}\cdot\frac{r^2}{f^2}\,\eta_t(\lambda)$$

$$= \frac{\pi}{4\mathcal{F}^2}\,N(\lambda,T)\ \eta_t(\lambda)\ \left[W\ cm^{-2}\ \mu m^{-1}\right] \quad , \quad (2)$$

where $\mathcal{F}$ is the f-number of the optical system. If $H_o(\lambda)$ is unpolarized, each orthogonal polarization component will have one-half the above value.

The diffraction-limited angular resolution of the optical system is $1.22\,\lambda/D$. Therefore, the spectral power collected per optical resolution element will be

$$P_R(\lambda,T) = \frac{\pi}{4\mathcal{F}^2}\,N(\lambda,T)\ \eta_t(\lambda)\ \frac{\pi}{4}\ (1.22\,\lambda\mathcal{F})^2$$

$$= \left(\frac{1.22\pi}{4}\right)^2 \lambda^2\,N(\lambda,T)\ \eta_t(\lambda)\left[W\ \mu m^{-1}\right] \quad . \quad (3)$$

If, however, the resolution provided by the sensor is poorer than the optical resolution, the power collected per sensor element will be

$$P_d(\lambda,T) = \frac{\pi}{4\mathcal{F}^2} N(\lambda,T)\ \eta_t(\lambda)\ A_d$$

$$= \frac{\pi D^2}{4} N(\lambda,T)\ \eta_t(\lambda)\ \omega \left[W\ \mu m^{-1}\right] \quad , \tag{4}$$

where A_d is the area and $\omega = A_d/f^2$ is the (solid) angular field of view corresponding to the sensor element. If the sensor is responsive only to the spectral band (λ_1,λ_2), the irradiance in this band may be converted to a photon flux as follows:

$$J_d(T) = \frac{\pi}{4\mathcal{F}^2 hc} \int_{\lambda_1}^{\lambda_2} \lambda\ N(\lambda,T)\ \eta_t(\lambda)\ d\lambda \left[\text{photons sec}^{-1}\ \text{cm}^{-2}\right] . \tag{5}$$

1. Passive Imaging

For passive (or thermal) imaging under nighttime conditions, the spectral irradiance on the object is negligible compared to the self-emission, and Eq. (5) simplifies to

$$J_d(T) = \frac{1}{4\mathcal{F}^2 hc} \int_{\lambda_1}^{\lambda_2} \lambda\ W(\lambda,T)\ \varepsilon(\lambda)\ \eta_t(\lambda)\ d\lambda \left[\text{photons sec}^{-1}\ \text{cm}^{-2}\right] \tag{6}$$

Since the detector cannot distinguish between the several causes of the change in scene radiance, a given change in the image irradiance or photon flux may be treated as arising from an effective temperature difference, ΔT. It is reasonable to assume that this effective temperature will result whether the change in scene radiance occurs in the same

resolution cell over a period of time or at two different resolution cells. It is also evident that the changes will be averaged over a resolution cell. The change in the photon rate in a resolution area, A_d, constitutes the signal to be detected.

$$S_d(T, \Delta T) = A_d \frac{\partial J_d}{\partial T} \Delta T$$

$$= \frac{A_d \Delta T}{4\mathcal{F}^2 hc} \int_{\lambda_1}^{\lambda_2} \lambda \frac{\partial W(\lambda, T)}{\partial T} \epsilon(\lambda)\ \eta_t(\lambda)\ d\lambda \left[\text{photons sec}^{-1}\right] \quad . \tag{7}$$

If the responsivity of the detection scheme is $\rho(\lambda)$ volts W^{-1}, then the differential signal voltage, ΔV_s, from the resolution element will be

$$\Delta V_s = \rho(\lambda)\ S_d\ hc/\lambda \ [\text{volts}] \tag{8}$$

One may define the detectivity, $D^*(\lambda)$, in the manner of Hudson*

$$D^*(\lambda) = \frac{\rho(\lambda)\sqrt{A_d \Delta f}}{V_n} \left[W^{-1}\ \text{cm Hz}^{1/2}\right] \quad , \tag{9}$$

where V_n is rms noise voltage in the bandwidth, Δf, leading to the expression for the differential signal-to-noise ratio

$$\frac{\Delta V_s}{V_n} = \frac{\Delta T}{4\mathcal{F}^2} \sqrt{\frac{A_d}{\Delta f}} \int_{\lambda_1}^{\lambda_2} \frac{\partial W(\lambda, T)}{\partial T} D^*(\lambda)\ \epsilon(\lambda)\ \eta_t(\lambda)\ d\lambda \quad . \tag{10}$$

---

*R. D. Hudson, Jr., Infrared System Engineering, p. 322 (John Wiley and Sons, New York, New York, 1969).

The sensitivity of a detector or an imaging device is evidently related to the relative magnitudes of its response to a change ΔT, and the random fluctuations in its response due to various noise processes; therefore, one performance indicator of a thermal detector would be the noise-equivalent temperature difference (NETD), which may be defined as that effective temperature difference that causes a response equal to the rms noise fluctuations in the response of the detector, that is, when $\Delta V_s / V_n$ is unity. It follows that

$$\text{NETD} = 4\mathcal{F}^2 \sqrt{\frac{\Delta f}{A_d}} \left[\int_{\lambda_1}^{\lambda_2} \frac{\partial W(\lambda,T)}{\partial T} D^*(\lambda)\ \epsilon(\lambda)\ \eta_t(\lambda)\ d\lambda \right]^{-1} \quad [^\circ K] \quad . \tag{11}$$

In all the detection methods to be considered, it turns out that the noise contributed by the detectors is negligible compared to the photon noise in the detected radiation. When the detectivity is limited by the fluctuations in the arrival rate of photons from the background at a temperature T°K, the detector is said to be background-limited. Under these circumstances, the maximum theoretical value of D^* is

$$D^*(\lambda) = \frac{\lambda}{hc} \left(\frac{\eta(\lambda)}{2J_B} \right)^{1/2} \tag{12} \quad .$$

where $\eta(\lambda)$ is the quantum efficiency and J_B is the total photon flux incident on the detector from the background, and

$$J_B = \frac{1}{4\mathcal{F}^2} \int_{\lambda_1}^{\lambda_2} \frac{\lambda}{hc} W(\lambda,T)\ d\lambda \quad \left[\text{photons sec}^{-1}\ \text{cm}^{-2} \right] \tag{13}$$

It is assumed that the detector receives photons only over the solid angle defined by the f-number of the optical system in which it is placed.

Equation (12) for $D^*(\lambda)$ is the usual expression for photovoltaic detectors. In all the upconversion methods to be considered, there is no process equivalent to recombination noise, which is important in photoconductive sensors. (In the latter case D^* has a value smaller by the factor $\sqrt{2}$.) The expression for NETD now becomes

$$\text{NETD} = 2\mathcal{F}\lambda_2\sqrt{\frac{\Delta f}{A_d}}\left[D^{**}_{\text{BLIP}}\ (\lambda_2)\int_{\lambda_1}^{\lambda_2}\lambda\ \frac{\partial W(\lambda,T)}{\partial T}\ \epsilon(\lambda)\ \eta(\lambda)^{1/2}\ \eta_t(\lambda)\ d\lambda\right]^{-1}, \tag{14}$$

where

$$D^{**}_{\text{BLIP}} = \frac{\lambda_2}{hc}\left[2\int_{\lambda_1}^{\lambda_2}\frac{\lambda}{hc}\ W(\lambda,T)\ d\lambda\right]^{-1/2}. \tag{15}$$

The emissivity, transmittance, and the quantum efficiency may be considered to be approximately constant over the band (λ_1,λ_2). For comparison purposes, the emissivity of the object and the transmission losses in the atmosphere and the optics are not important and so ϵ and η_t may be taken to be unity. With these assumptions

$$\text{NETD} \cong \frac{2\mathcal{F}\lambda_2}{\eta^{1/2}}\sqrt{\frac{\Delta f}{A_d}}\left[D^{**}_{\text{BLIP}}\ (\lambda_2)\int_{\lambda_1}^{\lambda_2}\lambda\ \frac{\partial W(\lambda,T)}{\partial T}\ \partial\lambda\right]^{-1}. \tag{16}$$

It should be evident that this performance indicator must be combined with the spatial resolution and area coverage that the imaging system can provide so as to fully reflect the capabilities of the system. The angular field of view and the number of resolution elements are descriptors equivalent to area coverage and spatial resolution respectively. Therefore, the following three parameters are chosen as performance descriptors for comparative evaluation of passive infrared imaging devices:

(1) Noise equivalent temperature difference, NETD.

(2) Planar field of view, α_{ir}.

(3) Number of resolution elements in the (solid angular) field of view, R.

Equation (16) may be rewritten in terms of the field of view and the number of resolution elements as

$$NETD = \frac{4}{D\,\alpha_{ir}} \sqrt{\frac{\Delta f R}{\pi \eta}} \frac{\lambda_2}{D^{**}_{BLIP}\,(\lambda_2) \int_{\lambda_1}^{\lambda_2} \lambda \frac{\partial W(\lambda,T)}{\partial T}\, d\lambda}$$

$$\cong \frac{4}{D\,\alpha_{ir}} \sqrt{\frac{\Delta f R}{\pi \eta}} \frac{1}{D^{**}_{BLIP}\,(\lambda_2) \frac{\partial W(\lambda_2,T)}{\partial T} (\lambda_2 - \lambda_1)} \quad , \qquad (17a)$$

where it is assumed that the area of the elementary detector, A_d, limits the resolution of the system. For a diffraction-limited system, the expression becomes

$$NETD \cong \frac{4}{1.22\,\lambda_2} \sqrt{\frac{\Delta f}{\pi \eta}} \frac{1}{D^{**}_{BLIP}\,(\lambda_2) \frac{\partial W(\lambda_2,T)}{\partial T} (\lambda_2 - \lambda_1)} \quad . \qquad (17b)$$

It is useful to examine the implication of Eq. (17b) for the different approaches to imaging. The operating IR wavelength determines NETD to a large degree through the factors λ_1, λ_2, D^{**}_{BLIP}, and $(\partial W/\partial T)$, since these factors are strong functions of λ. NETD, strictly speaking, cannot be used to compare imaging devices that operate at widely different IR wavelengths, because the transmission characteristics of the atmosphere (that have been neglected in this analysis) are quite different. We note in passing that for ideal detectors, and when the atmospheric attenuation is neglected, the NETD for operation in the 8 to

14-μm region is 3.65 times better than that for operation in the 3.5 to 5-μm region when all other design parameters are equal.

For devices that operate in the same IR wavelength regime, the NETD is determined by the factors Δf, η and $(\lambda_2 - \lambda_1)$ and is independent of other system parameters. These factors are, respectively, the noise equivalent electronic bandwidth, the quantum efficiency, and the IR bandwidth to which the system is sensitive. The electronic bandwidth is equivalent to the reciprocal of a dwell or integration time, τ_d. It is then evident that the NETD will be superior (smaller) for the device with the largest values for τ_d, η, and $(\lambda_2 - \lambda_1)$. The importance of a large IR sensitivity bandwidth for a thermal imaging system thus becomes apparent.

The above derivation of NETD has followed the conventional approach used with semiconductor detectors. Nevertheless, it should be emphasized that the concepts used, such as D^* and D^{**}_{BLIP}, have wider application as long as proper interpretations are supplied for the different schemes. In this context, η should be consistently interpreted as the efficiency of conversion of the incident IR photons into electrons in the output of the detection system, regardless of the internal details.

Evidently the dwell time or integration time, τ_d, is related to the time required by the device to follow temporal changes. To faithfully record a fast event, the frequency response bandwidth of a device must be large. This study, considers active and passive imaging using nonscanning devices coupled to TV displays, thus the temporal response of the devices will be adequate if they exceed the TV frame rate.

It is emphasized that NETD is used in this study as one performance comparator, but it has various deficiencies as the summary measure of the quality of the image from a device.

2. Active Imaging

In an active imaging system a laser (called the laser illuminator) illuminates the IR scene, and the reflected radiation is collected to produce an image of the IR scene. The primary difference between active and passive imaging systems is that for passive imaging, broadband thermal radiation must be imaged but for active imaging the radiation to be detected is reflected or scattered laser light with a narrow bandwidth. For passive imaging, it is important to collect as much of the emitted IR scene radiation as possible. In fact, as we shall see in later sections, among the major disadvantages of the coherent upconverters as compared to the FLIRs for thermal imaging are their small bandwidths and small acceptance angles. For active imaging the situation is reversed. The smaller bandwidths of the coherent upconverters is an advantage when detecting radiation of a particular frequency, since this affords effective discrimination against the broadband thermal background without the need to employ a cooled filter in the system optics.

The noise-equivalent temperature difference is not applicable as a criterion of merit for an active upconverter system, since reflected laser radiation and not the thermal background constitutes the signal. Furthermore, the performance of an active system may be enhanced by increasing the power of the irradiating laser. Thus it will be more appropriate to compare the performance of the various upconverters for active imaging on the basis of a noise-equivalent power output of the irradiating laser. Equivalently, the comparison may be based on the signal-to-noise ratio achieved at each resolution element for a given irradiating power. Formulas for the signal-to-noise ratio of an active imaging system are derived in the following.

A schematic of the active imaging system is given in Figure 2. A laser is used to irradiate the object and the back-reflected radiation is collected by the receiver optics in a monostatic arrangement. If the irradiating laser emits n_L [photons sec^{-1}] into a solid angle Ω_L [sr], then the irradiance on the object at a distance r [cm] is

$$H_o(\lambda) = \frac{hc}{\lambda} \frac{n_L}{\Omega_L r^2} \text{ [Watts cm}^{-2}\text{]} \tag{18}$$

For a Lambertian reflector, the fractional energy reflected back toward the receiver per steradian is R_{ef}/π, where

$$R_{ef} = \frac{\text{laser power reflected into the back hemisphere}}{\text{laser power incident on the object}}$$

From Eq. (4), the number of (laser) photons incident on the upconverter per resolution element per second is

$$n_s = \frac{\pi D^2}{4} \frac{n_L}{\Omega_L} \frac{R_{ef}}{\pi} \frac{\omega}{r^2} \text{ [photons sec}^{-1}\text{]} \tag{19}$$

where ω is the (solid) angular field of view corresponding to the resolution element. If α_{ir} is the planar field of view of the receiver, and R is the number of resolution elements in the field of view, then

$$\omega R = \frac{\pi}{4} \alpha_{ir}^2 \triangleq \Omega_{FOV} \tag{20}$$

In deriving Eq. (19), it is implicitly assumed that $\Omega_{FOV} \leq \Omega_L$; for efficient use of laser power, one would choose $\Omega_{FOV} = \Omega_L$. From Eq. (5), the number of background photons incident on the upconverter per resolution element per second is

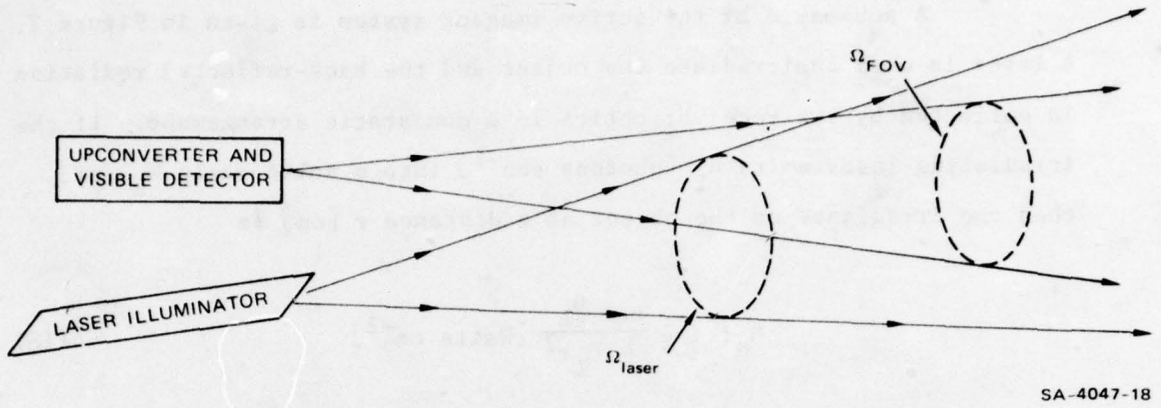

FIGURE 2 SCHEMATIC OF ACTIVE IMAGING SYSTEM

$$n_b \cong \frac{\pi D^2}{4} \frac{\lambda_2}{hc} \frac{W(\lambda_2, T)}{\pi} (\lambda_2 - \lambda_1)\, \omega$$

$$\triangleq \frac{\pi D^2}{4} \frac{J_\lambda}{\pi} \Delta\lambda_{ir}\, \omega \quad [\text{photons sec}^{-1}] \quad , \qquad (21)$$

where J_λ is the spectral photon emittance of a blackbody at T°K (=300°K for a room temperature background), and $\Delta\lambda_{ir} = (\lambda_2 - \lambda_1)$ is the IR bandwidth to which the upconversion system is sensitive. The upconversion system is assumed to have an overall efficiency

$$\eta = \frac{\text{number of electrons generated}}{\text{number of incident IR photons in } \Delta\lambda_{ir}} \quad .$$

The dominant source of noise in the output of the upconverter is the photon noise in the radiation incident on the upconverter. Though n_s represents the signal in the active imaging case, the noise is generated by the laser and background thermal radiation. Assuming Poisson statistics, the signal-to-noise ratio may be written as

$$SNR = \frac{\eta \bar{n}_s \sqrt{\tau_d}}{\sqrt{\eta \bar{n}_s + \eta \bar{n}_b + \bar{n}_D}} \quad , \tag{22}$$

where $\bar{n}_D$ is the dark current (electrons sec^{-1}) of the photocathode and τ_d is the time over which the laser and background radiation is collected.

Combining Eq. (22) with the preceding formulas for $\bar{n}_b$ and $\bar{n}_s$, and neglecting the dark current, yields

$$SNR = \frac{1}{2\sqrt{hc}} \; D \sqrt{\frac{\Omega_{FOV}}{R}} \sqrt{\eta \tau_d \lambda_{ir}} \; \frac{\left(P_L R_{ef} / r^2 \Omega_L\right)}{\left[\left(P_L \, R_{ef} / r^2 \, \Omega_L\right) + W \, \Delta\lambda_{ir}\right]^{1/2}} \quad , \tag{23}$$

where $P_L = h \nu_{ir} \bar{n}_L$, is the transmitted laser power. This gives the signal-to-noise ratio at each resolution element when R_{ef} refers to an average over that resolution element. If a polarized illuminator is used and if it may be assumed that the laser return is not depolarized, then the background may be reduced by a factor of two by the use of a polarizer in front of the receiver. Depending on the power of the irradiating laser, this expression can be further simplified.

a. Signal-to-Noise Ratio Under Background-Limited Conditions

When the background photons overwhelm the signal photons, then the noise is determined by the background. Or when

$$W \Delta\lambda_{ir} \gg P_L \, R_{ef} / \Omega_L \, r^2$$

$$SNR_{BL} = \frac{1}{2\sqrt{hc}} \; D \sqrt{\frac{\Omega_{FOV}}{R}} \; \frac{R_{ef}}{\Omega_L r^2} \sqrt{\frac{\lambda_{ir}}{W}} \sqrt{\frac{\eta \tau_d}{\Delta\lambda_{ir}}} \sqrt{P_L} \quad . \tag{24}$$

b. Signal-to-Noise Ratio Under Signal-Shot-Noise-Limited Conditions

When the laser return is much larger than the background, then the noise is essentially that due to the shot-noise in the signal. In other words, when

$$P_L R_{ef}/\Omega_L r^2 \gg W\Delta\lambda_{ir} \quad ,$$

$$SNR_{SL} = \frac{1}{2\sqrt{hc}} D \sqrt{\frac{\Omega_{FOV}}{R}} \sqrt{\frac{R_{ef}}{\Omega_L r^2}} \sqrt{\lambda_{ir}} \sqrt{\eta\tau_d} \sqrt{P_L} \quad . \tag{25}$$

The background and signal-shot-noise are of equal magnitude when

$$P_L R_{ef}/\Omega_L r^2 = W\Delta\lambda_{ir} \quad , \tag{26}$$

or when the transmitter (illuminator) laser power, $P_L = h\nu_{ir} N_L$, is

$$P_L = \frac{\Omega_L r^2}{R_{ef}} W \Delta\lambda \quad , \tag{27}$$

in which case,

$$SNR_{SB} = \frac{1}{\sqrt{2}} SNR_{SL} \quad . \tag{28}$$

Equation (23) is plotted in Figure 3 for the two important atmospheric windows in the infrared for a chosen set of values of the various parameters and assuming $\Omega_{FOV} = \Omega_L$. The log-log plot may easily be used for other values. The difference in the atmospheric transmittances is neglected. It is seen that the 4-μm region is better for low laser powers or for background-limited operation; at higher laser powers or for

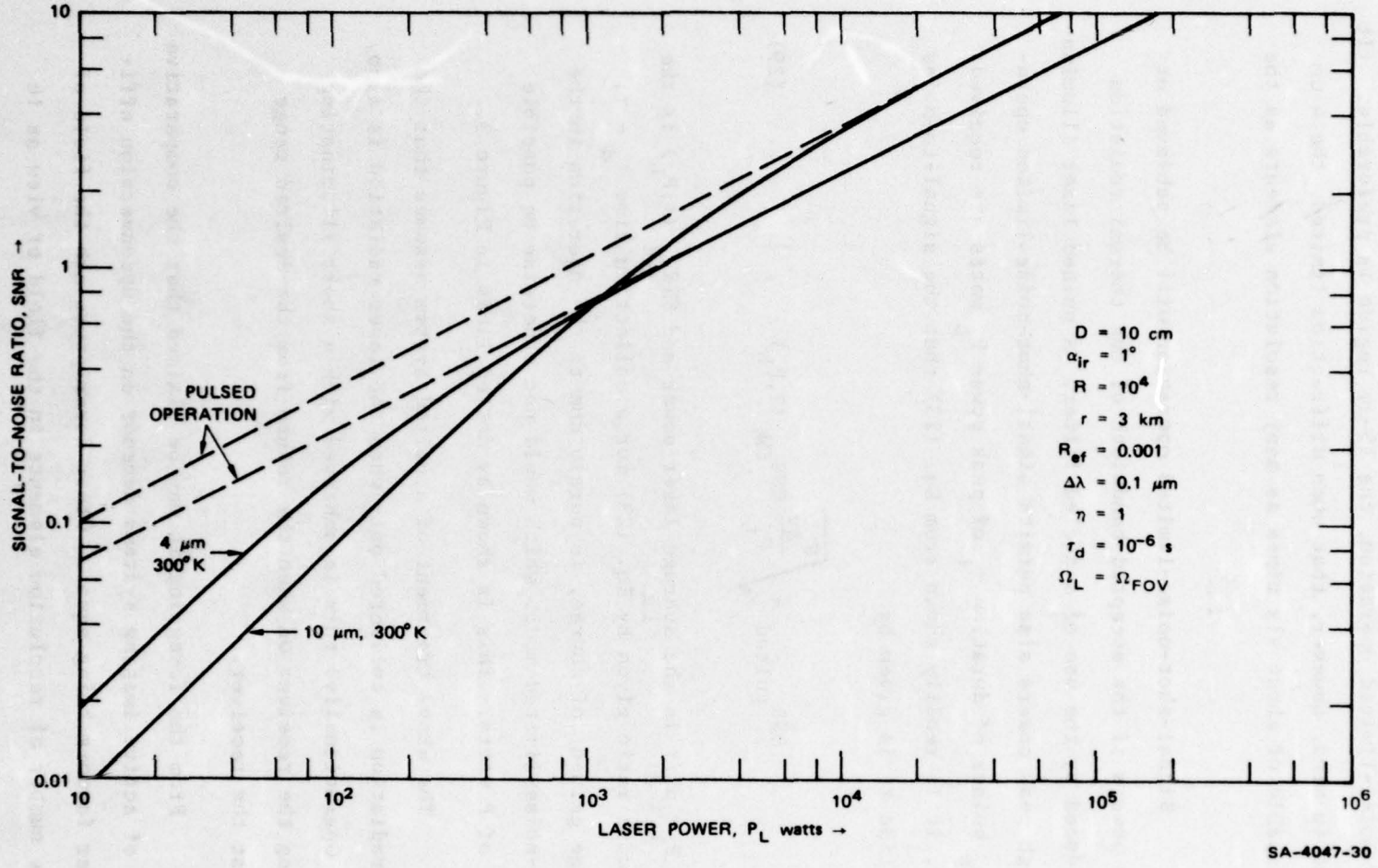

FIGURE 3 SIGNAL-TO-NOISE RATIO OF ACTIVE IMAGING SYSTEM AS A FUNCTION OF LASER ILLUMINATOR POWER

signal-shot-noise-limited operation, the 10-μm region is preferable. (It must be kept in mind, however, that when diffraction limited, the 4-μm system is capable of about six times as many resolution elements as the other.)

Signal-shot-noise-limited operation will be achieved at lower laser powers if the accepted bandwidth of the thermal radiation could be reduced by the use of a cooled filter. A pulsed laser illuminator with high peak powers also permits signal-shot-noise-limited operation. If n_p pulses of duration τ_i of peak power P_L watts are received in a time τ, it is readily shown from Eq. (23) that the signal-to-noise ratio (for time τ) is given by

$$SNR_{pulsed} = \sqrt{\frac{P_{av}}{P_L}}\, SNR_{CW}\ (\tau, P_L) \quad , \tag{29}$$

where $P_{av} = P_L \tau_i n_p / \tau$ is the average laser power and $SNR_{CW}\ (\tau, P_L)$ is the signal-to-noise ratio given by Eq. (23) for a collection time $\tau_d = \tau$. The advantage gained, of course, is purely due to the operation in the signal-shot-noise-limited mode, which would not otherwise be possible for a power of P watts. This is shown by dotted lines in Figure 3.

The above treatment of a pulsed system assumes that the background radiation is collected only when the laser radiation is also collected. Operationally, this is achieved with a short illuminating pulse, gating the receiver on when the return from the desired range segment is at the receiver.

From the foregoing it may be claimed that the comparative performance of active imaging systems depends on the upconversion efficiency, other factors being equal. Other descriptors are the field of view and the number of resolution elements in the field of view as in the case of passive imaging systems.

B. OPTICAL SYSTEMS FOR UPCONVERTERS

1. Optical Design Principles

Just as in the case of direct-detection-based FLIR systems, the design of the optical systems for upconverters is determined by the desired NETD (or SNR), α_{ir}, the field of view and N, the number of resolution elements, as well as a_d, the detector size. For parametric upconverters, the design will be constrained in addition by α, the acceptance angle (in air) of the upconverter. This acceptance angle is determined by the momentum-matching requirement for efficient upconversion (as detailed later). Further, from the same condition, an angular demagnification, $M = \lambda_s/\lambda_{ir}$, of the upconverted output results.

Three basically different types of optical systems for parametric upconversion have been discussed in detail by Andrews.* These are illustrated in Figure 4. Figure 4a illustrates the Type I optical system. The image of a point on the IR object is formed by a wavefront converging on a point in the upconverter. Different points on the IR object correspond to different points in the upconverter. The upconverted wave is then imaged onto the visible image detector. Upconversion employing a Type I optical system is also called upconversion in image space. In the Type II optical system shown in Figure 4b, nearly plane waves from the IR object are upconverted and the upconverted 'plane wave' is imaged onto the detector. Figure 4c shows the Type III optical system. In this case the objective lens forms the image of the IR object in the focal plane of a second lens, with the upconverter being placed just behind the second lens. The IR radiation from different object points become plane waves with different directions in the upconverter.

---

*R. A. Andrews, "IR Image Parametric Up-Conversion," IEEE J. Quantum Electron., Vol. QE-6, p. 68 (1970).

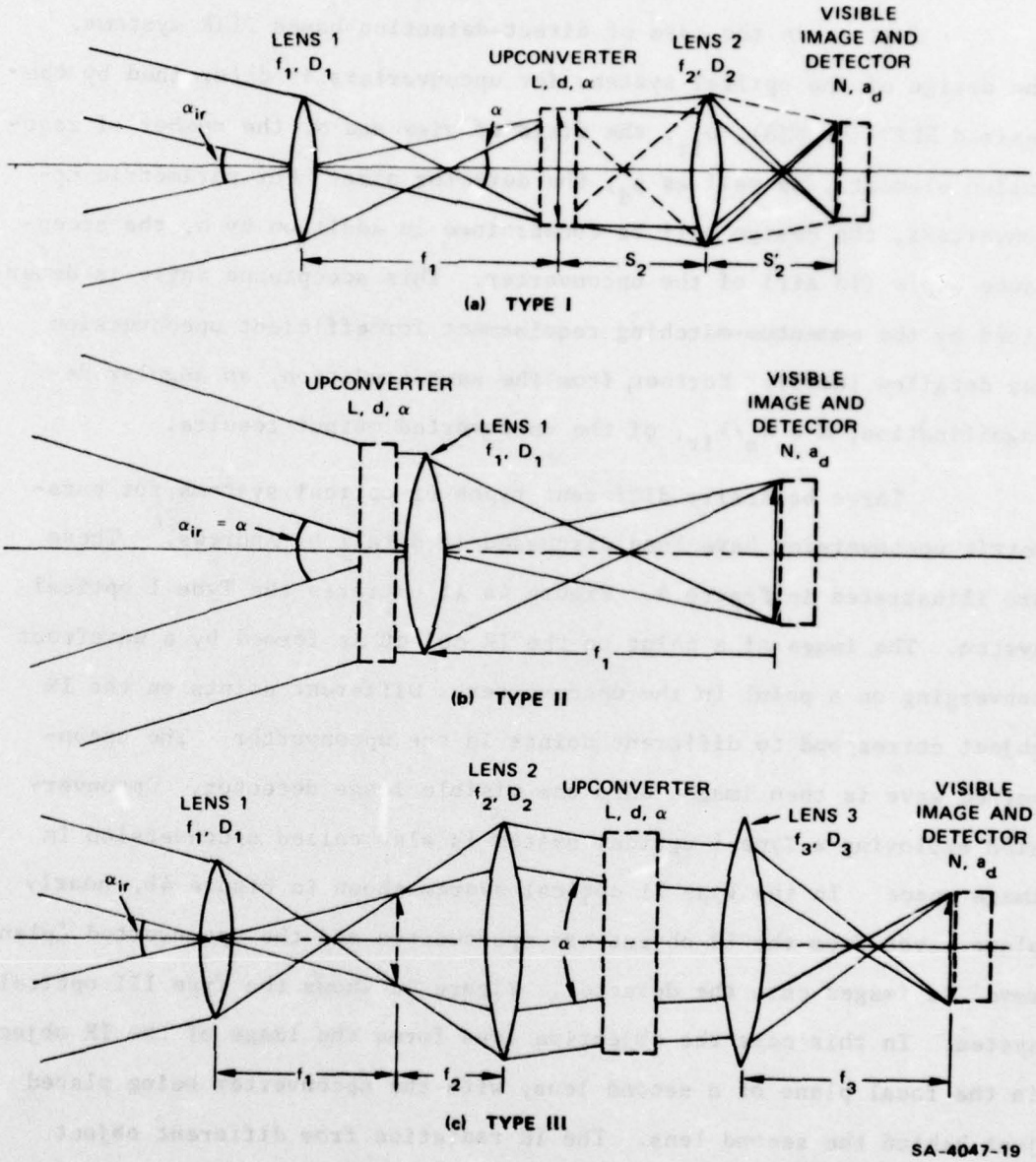

FIGURE 4 TYPES OF OPTICAL SYSTEMS FOR INFRARED UPCONVERSION

These plane waves interact with the plane-wave pump within the upconverter medium, and the upconverted wavefronts are then imaged at the visible image detector. Upconversion employing a Type III optical system is referred to as upconversion in Fourier space.

Optimum design of the optical systems (1) matches the acceptance angle of the upconverter to the angular spread of the incident IR radiation, (2) chooses the apertures of the various optical components so that all the IR radiation collected from the desired field of view, as well as all the upconverted radiation, is accepted, and (3) ensures that the resolution of the optical system is better than the resolution of the detector of the upconverted image. The practicality of the resulting f-numbers and the total length of the system are further considerations.

The design equations derived from the treatment of Andrews* are shown in Table 1. The critical aperture in the optical system is d, the diameter of the upconverter itself, which will be limited by practical reasons more than any other component. Further, since for a given IR collection aperture, the upconverted output will depend on the pump power-density at the upconverter, smaller upconverter diameters are desirable to reduce pump power. The upconverter diameter needed is shown in Figure 5 as a function of the field of view for the three types of optical systems for 100 (planar) resolution elements and 0.1 radian (5.7°) acceptance angle. These log-log plots may be used for other values of N and α with the help of the relations in Table 1. In particular, the parameters scale with N and $1/\alpha$ to a good approximation when $\alpha \ll 1$. It should be noted that the IR collection aperture D_1 shown is the smallest that will provide the required angular resolution, assuming that the resolution is limited by diffraction only.

---

*R. A. Andrews, "IR Image Parametric Up-Conversion," IEEE J. Quantum Electron., Vol. QE-6, p. 68 (1970).

TABLE 1

DESIGN FORMULAS FOR OPTICAL SYSTEMS OF PARAMETRIC UPCONVERTERS

Desired Characteristics: α_{ir}, N, a_d

Parameters Fixed by Technique: α, λ_{ir}, λ_s

Parameter	Type I	Type II	Type III
Choose	$\mathcal{F}_2$	--	$\mathcal{F}_1$
D_1	$> \frac{N\lambda_{ir}}{\alpha_{ir}}$	$> \frac{N\lambda_{ir}}{\alpha_{ir}}$	$> \frac{N\lambda_{ir}}{\alpha_{ir}}$
f_1	$D_1/(\alpha - \alpha_{ir})$	$\frac{Na_d}{M\alpha_{ir}}$	$D_1\mathcal{F}_1$
$\mathcal{F}_1$	$1/(\alpha - \alpha_{ir})$	a_d/λ_s	Chosen
d	$D_1\alpha_{ir}/(\alpha - \alpha_{ir})$	$\geq D_1$	$D_1 \frac{\alpha_{ir}}{\alpha}\left[1 + \frac{\mathcal{F}_1}{2}(\alpha + \alpha_{ir})\right]$
D_2	$d + S_2M\alpha$	--	$D_1 \frac{\alpha_{ir}}{\alpha}\left[1 + \mathcal{F}_1(\alpha + \alpha_{ir})\right]$
f_2	$D_2\mathcal{F}_2$	--	$D_1\mathcal{F}_1\alpha_{ir}/\alpha$
$\mathcal{F}_2$	Chosen	--	$\mathcal{F}_1/\left[1 + \mathcal{F}_1(\alpha + \alpha_{ir})\right]$
D_3	--	--	D_2
f_3	--	--	$a_dN/M\alpha$
$\mathcal{F}_3$	--	--	(limits D_1)
S_2	$\frac{\mathcal{F}_2(1 + m)d}{1 - \mathcal{F}_2(1 + m)M\alpha}$	--	--
S_2^1	S_2/m	--	--

Angular demagnification $M = \frac{\lambda_s}{\lambda_{ir}}$

Image demagnification $m = \frac{d}{Na_d}$

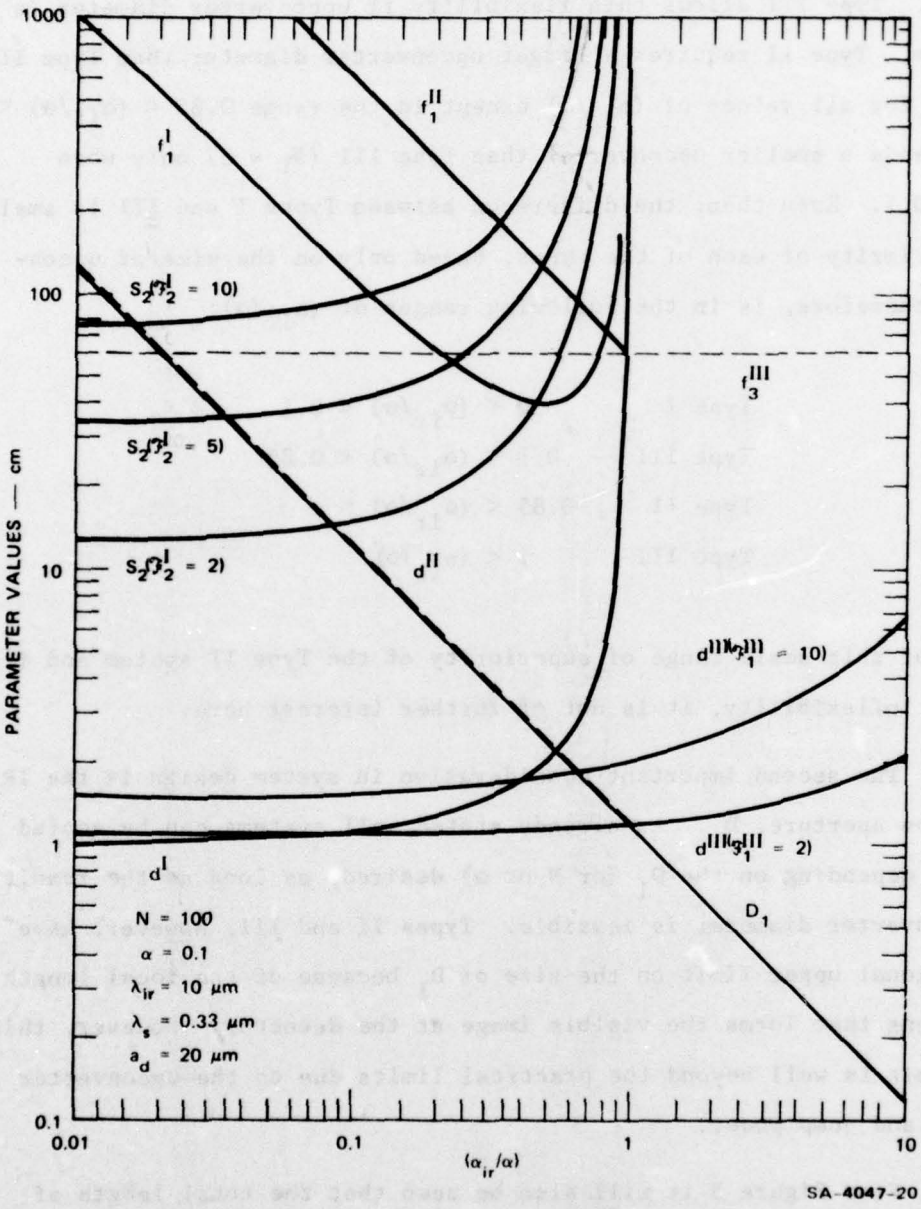

FIGURE 5 DEPENDENCE OF COHERENT UPCONVERTER SYSTEM PARAMETERS ON FIELD OF VIEW FOR THREE TYPES OF OPTICAL SYSTEMS

It is immediately seen from Figure 5 that Types I and II cannot be used when the desired field of view, α_{ir} is greater than the acceptance angle, α. Type III allows this flexibility if upconverter diameter is not a problem. Type II requires a larger upconverter diameter than Type III ($\mathcal{F}_1 = 2$) for all values of (α_{ir}/α) except in the range $0.85 < (\alpha_{ir}/\alpha) < 1$. Type I needs a smaller upconverter than Type III ($\mathcal{F}_1 = 2$) only when $\alpha_{ir}/\alpha < 0.1$. Even then, the difference between Types I and III is small. The superiority of each of the types, based only on the size of upconverter, therefore, is in the following ranges of (α_{ir}/α):

Type I	$0 < (\alpha_{ir}/\alpha) < 0.1$
Type III	$0.1 < (\alpha_{ir}/\alpha) < 0.85$
Type II	$0.85 < (\alpha_{ir}/\alpha) < 1$
Type III	$1 < (\alpha_{ir}/\alpha)$

Because of this small range of superiority of the Type II system and its relative inflexibility, it is not of further interest here.

The second important consideration in system design is the IR collection aperture, D_1. As already stated, all systems can be scaled directly depending on the D_1 (or N or α) desired, as long as the resulting upconverter diameter is feasible. Types II and III, however, have an additional upper limit on the size of D_1 because of the focal length of the lens that forms the visible image at the detector. However, this upper limit is well beyond the practical limits due to the upconverter diameter and pump power.

From Figure 5 it will also be seen that the total length of the system depends on the focal length of one of the lenses. The introduction of the pump and the polarizers and filters necessary to separate the pump radiation from the upconverted radiation is more easily and readily accomplished in the Type III system.

In imaging systems, the available resolution and the aberrations present are significant factors. In the absence of other considerations, the angular resolution of the systems is approximately $1.22\,\lambda_{ir}/D_1$. In the case of Type I, the length of the upconverter can degrade this resolution because upconversion of the IR radiation from a single object point occurs not at the image plane only but over the entire length of the upconverter, L, and the upconverted wavefront has a direction different from the IR wavefront. Since in the Type I system, the IR radiation forms convergent spherical wavefronts in the upconverter, the upconverted output appears to emanate from a disc instead of a point as shown in Figure 6. This loss in resolution evidently increases for smaller f-numbers, longer upconverters, and smaller demagnification factors. It can be shown that the minimum angular resolution for the Type I system because of thickness aberration is

$$<_{res} = \frac{L}{2f_1 \mathcal{F}_1 n_{ir}} \left[1 - \frac{n_{ir}\omega_{ir}}{n_s \omega_s} \right]$$

$$\approx \frac{L}{2f_1 \mathcal{F}_1 n_{ir}} = \frac{\lambda_{ir}}{D_1} \frac{L}{2\mathcal{F}_1^2 n_{ir} \lambda_{ir}} \quad . \tag{30}$$

For L = 1 cm, $\mathcal{F}_1 = 10$, $n_{ir} \approx 1$ and $\lambda_{ir} = 10\ \mu m$, this angular resolution is about four times the diffraction limit. (It may be noted that Type I systems using nonlinear crystals have better resolutions than when using metal vapors, since n_{ir} for crystals is typically about two, whereas that for metal vapors is about unity.) With the help of Table 1, it can also be shown that the thickness of the crystal limits the number of resolution elements along the image diameter is

$$N^t_{max} = \frac{2n_{ir}}{L} \frac{d(d + D_1)}{\alpha D_1} \quad , \tag{31}$$

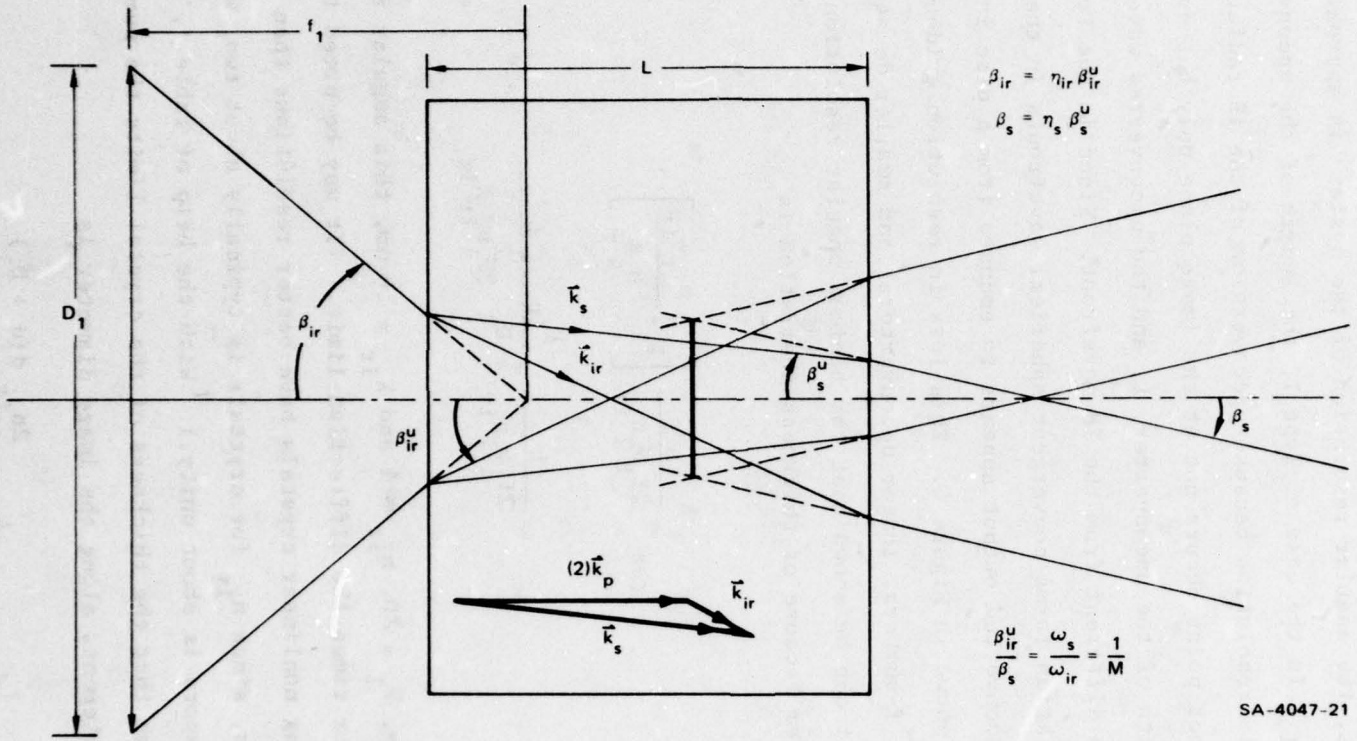

FIGURE 6 RESOLUTION LOSS DUE TO MEDIUM THICKNESS IN COHERENT UPCONVERTER

and that the diffraction limit and the thickness limit become equal when

$$d = D_1\left[\alpha\sqrt{L/2.44\ \lambda_{ir}n_{ir}} - 1\right] \quad . \tag{32}$$

Increasing the diameter of the upconverter to increase resolution also increases the required pump power.

Resolution loss due to the length of the upconverter is negligible in Types II and III because each object point gives rise to a plane wave instead of a spherical wave in the upconverter and the directional change of the upconverted wave is the same over the entire wavefront. Therefore, the number of resolution elements along the image diameter is given in the two cases by

$$N_{max}^{II} = \frac{\alpha D_1}{1.22\ \lambda_{ir}} \quad , \tag{33a}$$

and

$$N_{max}^{III} = \frac{D_1}{2.44\ \lambda_{ir}\mathcal{F}_1}\left[\sqrt{(2 + \mathcal{F}_1\alpha)^2 + (8\alpha\mathcal{F}_1 d/D_1)} - (2 + \mathcal{F}_1\alpha)\right] \quad . \tag{33b}$$

For essentially the same reasons as above, the resolution of the systems depends on the mode structure or angular divergence of the pump. Though the Type II and Type III systems suffer no loss of resolution due to divergence of the IR radiation, they are sensitive to pump divergence, and diffraction-limited resolution can be obtained only if a single-mode or uniform planewave pump is used. But the Type I system will be further degraded by a multi-mode pump only if the angular spread of the pump becomes comparable to that of the IR radiation. Type II and Type III systems using nonlinear crystals also have better resolution than those using metal vapors, when, in practice, a single-mode laser pump with a

Gaussian amplitude distribution is used. This is because the upconversion efficiency of metal vapors has a quadratic dependence on pump power, whereas that of crystals has a linear dependence. It can be shown that the angular resolution is degraded by a factor of $\sqrt{2}$. In other words, the maximum number of resolution elements in the solid angular field of view is decreased by a factor of two.

Chromatic aberration will be present in all systems when low f-numbers are used. It may be more noticeable in Type III systems where it may, in principle, be corrected. Because the upconversion of the radiation from each object point occurs over essentially the entire upconverter aperture, the Type III system demands less uniformity of the upconverting medium. Since the advantages of the Type III system over the others outweigh its disadvantages, it will be assumed henceforth that the coherent upconverters will employ Type III optics.

In the IRQC, an incoherent upconverter, the upconverted radiation is a spherical wave emanating from the various upconversion centers. All angular information present in the incoming IR radiation is lost upon upconversion; therefore, the choice of an optical system is limited to Type I. There is no limitation on the angular spread of the incident IR and the pump beam does not have any required orientation. The design restrictions of the coherent upconverters do not apply, but the basic consideration is to be able to collect as much of the upconverted emission that occurs over all 4π steradians. This requires clever design with low f-number optics that would still allow separation of the pump using spectral discrimination only. Polarization discrimination useful with crystals is not applicable. Some design considerations are presented in Table 2.

TABLE 2

DESIGN FORMULAS FOR OPTICAL SYSTEM OF IRQC UPCONVERTER

Desired Characteristics: α_{ir}, N, a_d

Parameters Fixed by Technique: λ_{ir} λ_s

Parameter	Formulas
D_1	$>N\lambda_{ir}/\alpha_{ir}$
f_1	d/α_{ir}
$\mathcal{F}_1$	Chosen
d	Chosen
D_2	$<f_2$, $<d$
f_2	$S_2/(1 + m)$
$\mathcal{F}_2$	~ 1
S_2	Chosen
S_2'	S_2/m

Image demagnification: $m = \dfrac{d}{Na_d}$

Collection efficiency $\eta_{coll} = \left[1/4n_s\mathcal{F}_2(1 + m)\right]^2$

The IR radiation from a single object point arrives at the upconverter over a finite angle ($\sim 1/\mathcal{F}_1$) and is absorbed by a finite thickness of the IRQC as shown in Figure 7. The upconverted emission corresponding to an object point, therefore, takes place from a volume of the IRQC. The resolution of the upconverter will thus be poorer than the diffraction limit set by the collection aperture D_1. When $L \ll S_2$ or D_2, the minimum angular resolution will be

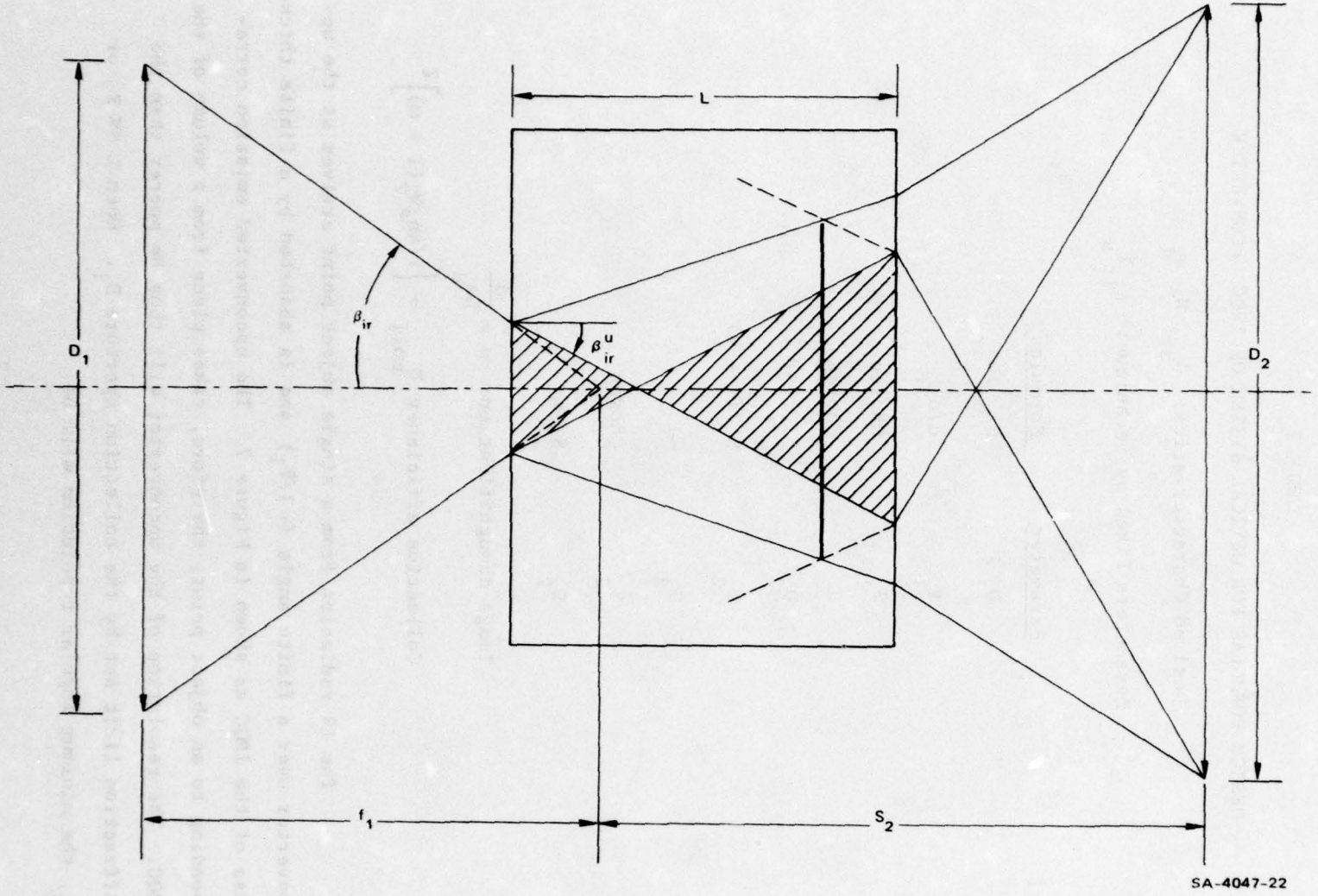

FIGURE 7 RESOLUTION LOSS DUE TO MEDIUM THICKNESS IN INCOHERENT UPCONVERTER

$$\theta_{res} = \frac{\lambda_{ir}}{D_1} \frac{L}{2\mathcal{F}_1 \lambda_{ir}} \left[\frac{1}{n_{ir}\mathcal{F}_1} + \frac{1}{n_s(1+m)\mathcal{F}_2} \right] \quad . \tag{34}$$

When $\lambda_{ir} = 5\ \mu m$, $\mathcal{F}_1 = 2$, $\mathcal{F}_2 = 1$, $m = 2$, $n_{ir} = n_s = 2$, and $L = 300\ \mu m$, the angular resolution given by Eq. (34) is about six times the diffraction limit.

The thickness of the crystal limits the number of resolution elements along the diameter to

$$N_{max} = \frac{2d}{L} \left[\frac{1}{n_{ir}\mathcal{F}_1} + \frac{1}{n_s(1+m)\mathcal{F}_2} \right]^{-1} \quad , \tag{35}$$

and the diffraction limit will equal the thickness limit only when

$$L = 2.44\ \lambda_{ir}\mathcal{F}_1 \frac{n_{ir} n_s (1+m)\mathcal{F}_1\mathcal{F}_2}{n_{ir}\mathcal{F}_1 + n_s(1+m)\mathcal{F}_2} \quad . \tag{36}$$

The collection efficiency of the second lens or the fraction of the sum frequency emission collected by the aperture D_2 is readily shown to be $[4n_s(1+m)\mathcal{F}_2]^{-2}$. Hence attempts to reduce resolution loss from thickness aberration, by the use of large $\mathcal{F}_2$ will reduce collection efficiency drastically. Increasing $\mathcal{F}_1$ implies reducing α_{ir} or D_1. The desirable procedure will therefore be to use as thin a crystal as possible. However, the thickness of the crystal should be adequate to absorb most of the incident IR. Therefore, a material with a high absorption coefficient for the IR is essential to obtain high resolution, with high conversion efficiency.

Since the process is incoherent, the mode structure of the pump has no bearing on the resolution or other characteristics of the IRQC. In addition, no angular relationships between the pump beam and the IR beam need to be met. This means the pump can be transverse to the IR,

thereby considerably reducing power requirements on the pump to provide a high power density across the small edge area of the thin IRQC.

Because the IRQC forms a self-luminous image, the diameter, D_2, of the optics for the collection will also affect the ultimate resolution of the system. The angular resolution limit can be easily shown to be $\lambda_s(1 + m)/D_2$. Since $\lambda_s \ll \lambda_{ir}$ and if $D_1 \approx D_2$, this loss of resolution can be neglected if m is not large.

In the case of direct-detection-based FLIRs, the optical system design is simple and the resolution is limited by the detector size. With focal-plane-array detectors now under development, the number of resolution elements is determined by the array and the field of view by the focal length of the collection optics. In currently available focal-plane scanning systems, the angular resolution is determined by the detector size and the focal length of the collection optics, and the number of resolution elements (and/or field of view) is determined by the scanning system. The field of view is directly proportional and the dwell time is inversely proportional to the number of resolution elements.

In Table 3, the resolution and field of view of the systems of interest are collected together. It is emphasized that the size and resolution of the detector of the upconverted image must also be considered in determining the performance of the system.

TABLE 3

CHARACTERISTICS OF INFRARED UPCONVERSION METHODS

Property	Type III Metal Vapor	Type III Nonlinear Crystal	Type I IRQC	Type I Direct Detection
Minimum angular resolution, radians	$\sqrt{2}\ 1.22\ \frac{\lambda_{ir}}{D_1}$	$1.22\ \frac{\lambda_{ir}}{D_1}$	$\frac{L}{2D_1\mathcal{F}_1}\left[\frac{1}{n_{ir}\mathcal{F}_1} + \frac{1}{n_s(1+m)\mathcal{F}_2}\right]$	$1.22\ \frac{\lambda_{ir}}{D_1}$
Maximum angular field of view	$\frac{1}{2\mathcal{F}_1}\left[\sqrt{\left(2+\mathcal{F}_1\alpha\right)^2 + \left(8\alpha\mathcal{F}_1 d/D_1\right)} - (2+\mathcal{F}_1\alpha)\right]$	$d/D_1\mathcal{F}_1$		$d_D/D_1\mathcal{F}_1$

2. Configurations of Upconversion Systems

In Figures 8 and 9, schematic diagrams of IR image-detection systems are presented, showing some of the details of and the differences among the various methods. The systems for the metal vapor and the nonlinear crystal are very similar. Both upconvert in Fourier space and require a single-mode laser pump. It is assumed that a linearly polarized laser is used in both cases. As discussed later, two pump beams at a small angle with respect to each other are used with metal vapors. The nonlinear crystal of the appropriate orientation is the upconverting medium in the one case and the metal vapor at the appropriate pressure in the other. At the present time, a heat-pipe oven appears to be the best method for generating and maintaining the metal vapor at the desired temperature and pressure. The upconverted radiation of low intensity must be separated from the high-intensity pump before imaging on the visible detector. The nonlinear crystal system can use both a polarizer and a spectral filter for pump removal, whereas the metal-vapor system must rely on a spectral filter. Because of the wide spectral separation between the pump and the sum frequency in the case of the metal-vapor system, even absorption filters can be considered. The crystal system must use multilayer dielectric filters, which must withstand the high power densities. No cryogenic cooling of any component is needed because the coherent upconverters are sensitive only to IR within their field of view and no cooled apertures are needed to restrict background radiation.

The IRQC upconverter uses a Type I system. Since the technique is incoherent, only an intense light source of the proper frequency is needed for the pump. A laser fills this requirement. If the transverse or edge-pumping configuration is used, the laser power requirements for a desired power density can be considerably reduced. This is possible because the IRQC is transparent to the pump frequency in the absence of IR radiation and the absorption of the pump is small even when the IRQC

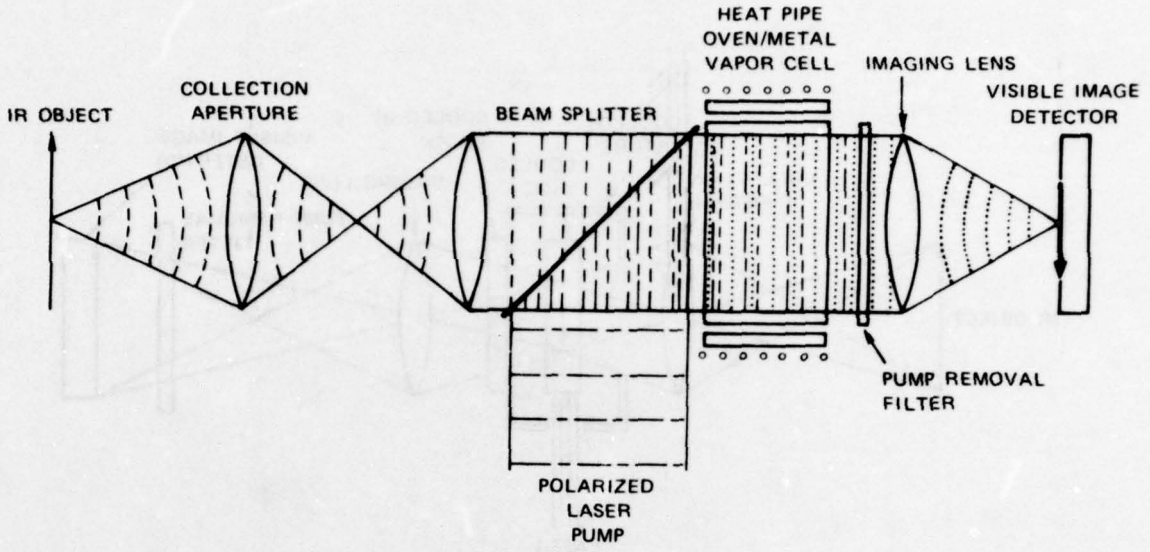

(a) METAL VAPOR UPCONVERTER

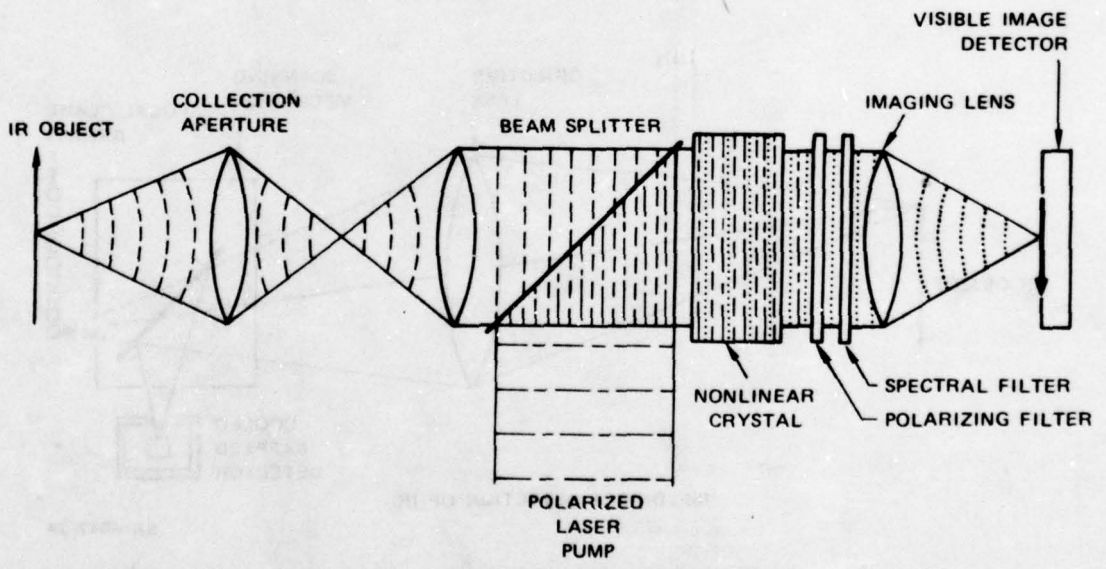

(b) NONLINEAR CRYSTAL UPCONVERTER

SA-4047-23

FIGURE 8 SCHEMATIC DIAGRAM OF PARAMETRIC UPCONVERTER SYSTEMS

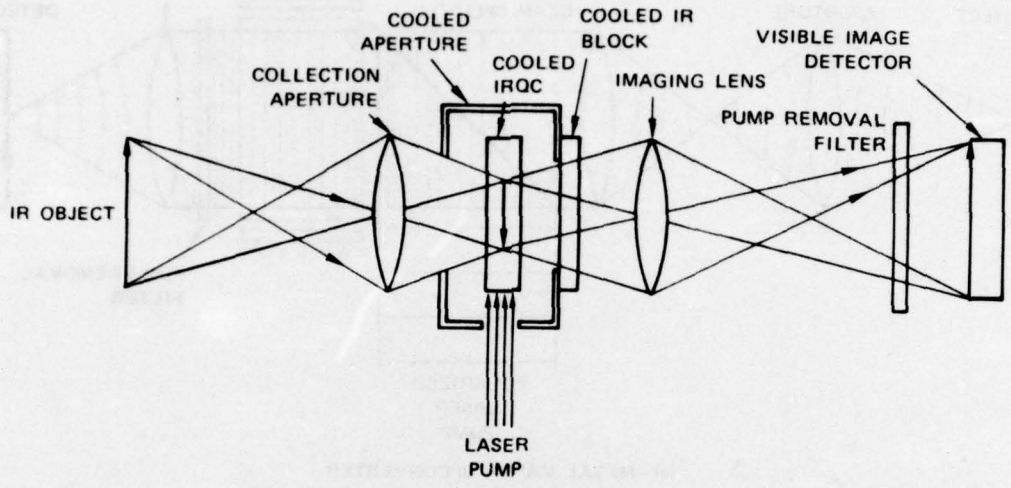

(a) IRQC UPCONVERTER

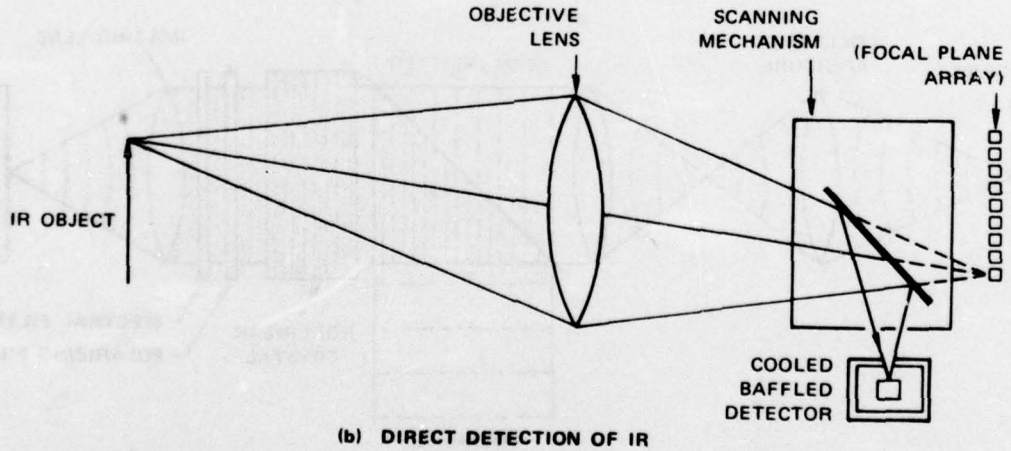

(b) DIRECT DETECTION OF IR

SA-4047-24

FIGURE 9 SCHEMATIC DIAGRAM OF INFRARED IMAGING METHODS

is exposed to IR radiation. The edge-pumping configuration has an additional advantage in that the amount of pump radiation collected along with the sum frequency by the imaging lens, being due mainly to scattering, should be small. Requirements on pump removal filters are less severe.

The IRQC must be cooled to cyrogenic temperature to minimize self-generated thermal noise. For the same reason, a cooled aperture tailored to the incoming IR beam must be used. Finally, the back of the IRQC must also be protected by a cooled infrared-blocking filter to prevent "fogging" of the IR image in the IRQC.

The direct-detection FLIR system employs a cooled detector, which scans the field of view with the help of a scanner. A cooled aperture is needed just as in the case of the IRQC.

SECTION III

PHENOMENOLOGY OF INFRARED UPCONVERSION METHODS

A. ALKALI METAL VAPORS

1. Introduction

Drawing on their experience with third-harmonic generation using metal vapors, Harris and coworkers have proposed and demonstrated point upconversion in metal vapors (see Harris* and Bloom†). The high photon-conversion efficiencies obtained in these initial experiments make metal-vapor upconversion an attractive prospect for infrared imaging applications. It is the primary purpose of the present report to investigate this potential of the method.

The basic principle of operation is that of a third-order nonlinear mixing process in which one IR photon and two pump photons are destroyed, and a visible photon is created. This is a coherent process, requiring that both the photon energy and momentum relations

$$\omega_s = 2\omega_p + \omega_{ir} \quad , \quad \text{conservation of energy} \quad , \tag{37}$$

$$\vec{k}_s = 2\vec{k}_p + \vec{k}_{ir} \quad , \quad \text{conservation of momentum} \quad , \tag{38}$$

be satisfied for efficient conversion of the IR input to visible output. Here ω_s, ω_p, ω_{ir} are the angular frequencies of the sum, pump, and IR photons; and $|\vec{k}_j| = n_j\omega_j/c$ are the wave vectors where n_j is the respective index of refraction.

---

*S. E. Harris and D. M. Bloom, "Resonantly Two-Photon Pumped Frequency Converter," Appl. Phys. Letters, Vol. 24, p. 229 (1974).

†D. M. Bloom et al., "Infrared Upconversion with Resonant Two-Photon Pumped Metal Vapors," Appl. Phys. Letters, Vol. 24, No. 9, p. 427 (May 1974).

The nonlinear medium is a metal vapor with the basic scheme of atomic energy levels shown in Figure 10.

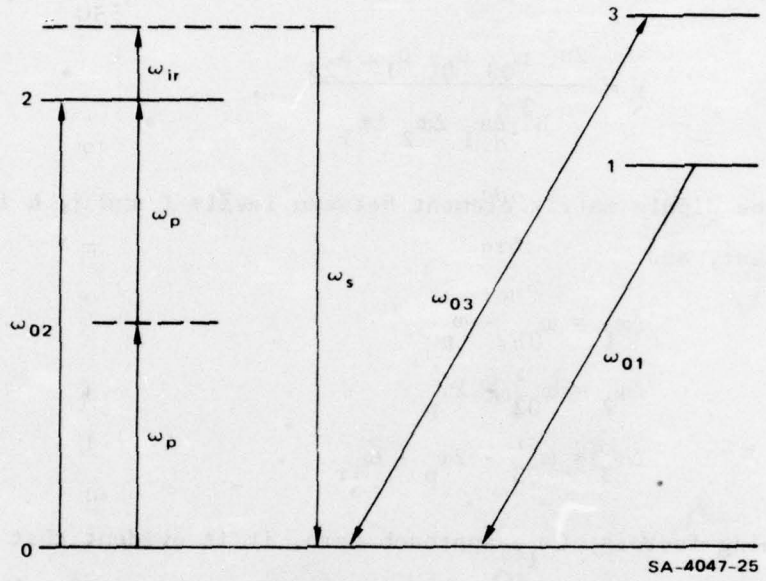

FIGURE 10 ENERGY LEVEL SCHEME IN METAL VAPORS

The metal vapor is irradiated with an intense pump source of radian frequency, ω_p, simultaneously with the infrared source of frequency, ω_{ir}. If the pump frequency is tuned to approximately half the frequency of the nonallowed (in first order) transition $|0\rangle \rightarrow |2\rangle$, that is, $2\omega_p \cong \omega_{02}$, and the IR frequency is such that $2\omega_p + \omega_{ir} \cong \omega_{03}$, then a strong polarization results at $\omega_s = 2\omega_p + \omega_{ir}$. If momentum conservation is simultaneously satisfied, then radiation at the sum frequency is observed. It should be noted that the frequencies ω_{ij} are the properties of the nonlinear medium, and ω_p and ω_{ir} are variable frequencies.

The efficiency of the upconversion process depends on the pump power density, the density of the metal atoms in the vapor, and on the third-order nonlinear susceptibility, which is given by*

$$\chi = \frac{2\pi^3 \mu_{03} \mu_{01} \mu_{12} \mu_{23}}{h^3 \Delta\omega_1 \Delta\omega_2 \Delta\omega_3} \quad , \tag{39}$$

where μ_{ij} is the dipole matrix element between levels i and j, h is Planck's constant, and

$$\begin{aligned} \Delta\omega_1 &= \omega_{01} - \omega_p \\ \Delta\omega_2 &= \omega_{02} - 2\omega_p \\ \Delta\omega_3 &= \omega_{03} - 2\omega_p - \omega_{ir} \quad . \end{aligned} \tag{40}$$

When the detuning factors, $\Delta\omega_i$, approach zero, it is evident that the susceptibility and hence the induced dipole moments become very large. This resonant enhancement of the nonlinear susceptibility can typically increase its value by several orders of magnitude higher than those for inert gases under otherwise similar conditions.

It must be pointed out that there should be no actual absorption of photons by the metal vapor at any of the three frequencies ω_p, ω_{ir}, and ω_s. The basic procedure is to choose these frequencies such that resonant enhancement is obtained but yet not so close to ω_{ij} that there is significant absorption. This is particularly important for the sum frequency, ω_s, which if too close to ω_{03} will be absorbed by other metal atoms. Two-photon absorption is not significant except at

---

*J. A. Armstrong et al., "Interactions Between Light Waves in a Nonlinear Dielectric," Phys. Rev., Vol. 127, p. 1918 (1962).

very high pump-power densities, and resonant enhancement at the two-photon-transition frequency is advantageous in that it contributes no loss and no dispersion at the input and sum frequencies. However, use of the two-photon transition does mean that the conversion efficiency will depend quadratically on the pump power rather than linearly as in the case of nonlinear crystal upconversion.

Metal vapor-upconversion is the result of a four-wave parametric interaction (third-order nonlinearity), whereas crystal upconversion is a three-wave parametric process. (The latter is due to a second-order nonlinearity that does not exist in metal vapors, since they are isotropic.) This leads to additional flexibility in achieving phase-matching to satisfy momentum conservation. The pump can consist of two beams at a suitable small angle $2\emptyset$, chosen such that the momentum mismatch is minimized. Because metal vapors are isotropic, they do not exhibit birefringence and there is no Poynting vector "walk-off," such as is observed in crystals where phase-matching is done using the birefringence of the crystal (except when 90° phase-matching can be accomplished). Since birefringent phase-matching is possible only for a given choice of the polarizations of pump, IR, and sum radiations, only half of an unpolarized IR input can be upconverted--metal vapors do not have this restriction. The bandwidth and the angular spread over which upconversion is possible, (that is, the length and orientation of the input IR wave vectors) is clearly related to the efficacy of phase-matching.

The subsequent treatment addresses two specific metal vapors, those of cesium and sodium, which have energy levels suitable for upconversion in the 2- to 5-μm and 8- to 12-μm atmospheric windows, respectively. The corresponding energy level diagrams are given in Figures 11 and 12. In both cases, the pumps are chosen to match the two-photon transition

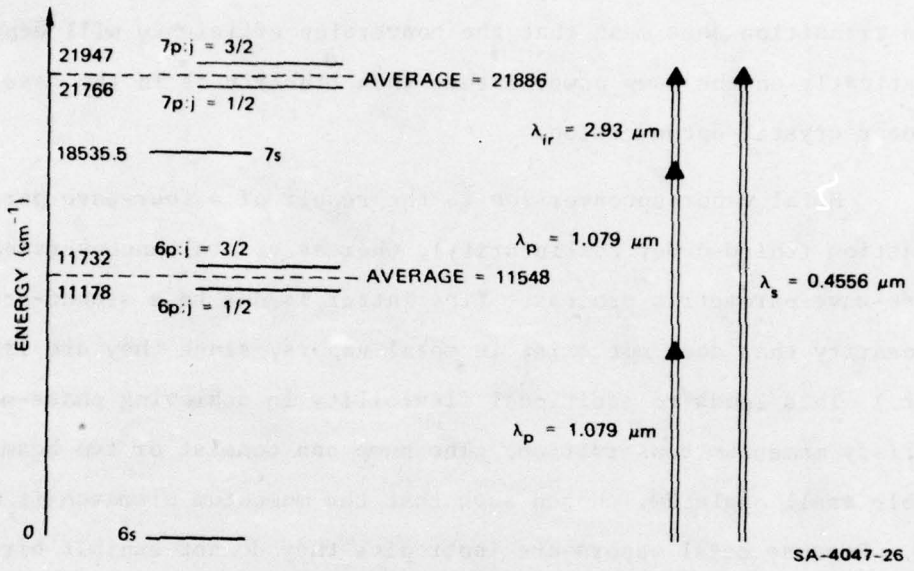

FIGURE 11 CESIUM ENERGY LEVELS

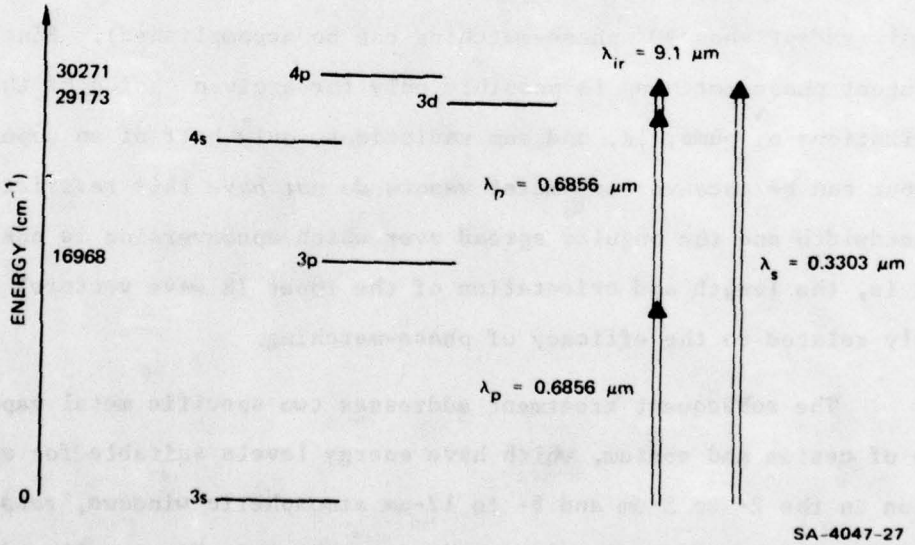

FIGURE 12 SODIUM ENERGY LEVELS

exactly. It can be shown that under these conditions Eq. (39) should be modified to*

$$\chi = \frac{4\pi^3 \mu_{01} \mu_{12} \mu_{23} \mu_{03}}{h^3 \Delta\omega_1 \Delta\omega_3 \sqrt{\Delta\omega_{laser} \Delta\omega_{atomic}}} , \qquad (41)$$

where $\Delta\omega_{laser}$ is the laser linewidth and $\Delta\omega_{atomic}$ is the linewidth of the two-photon transition. In Table 4, the atomic parameters of the two species are listed as well as the details about the pump, IR, and sum frequencies. Since the splitting of the doublet of the 7p level in cesium is large compared to the detuning or IR bandwidth to be considered, upconversion in cesium can be treated as occurring in two independent bands, one about each level of the doublet. The splitting of the 4p level in sodium, however, is small compared to the IR bandwidth, so that the doublet may be well approximated by the average of the two levels.

2. Photon Conversion Efficiency

The photon conversion efficiency for the upconverters is defined as the ratio of the number of IR photons upconverted to visible photons to the number of incident IR photons. An expression for η_{MV}, the photon conversion efficiency of the metal vapors, is derived in the following.

In general, four-wave interactions in a nonlinear medium can be described by a set of coupled-mode equations that relate the interdependence of the various wave amplitudes. These equations are derived as follows: The wave equation, including nonlinear polarization terms, is obtained from Maxwell's equations. Each of the four waves is represented as a plane wave of a particular frequency, and their sum substituted

*E. A. Stappaerts, Stanford University, Private Communication.

TABLE 4

PARAMETERS OF CESIUM AND SODIUM METAL VAPORS

Parameter[a]	Cesium	Sodium
$\bar{\nu}_{01}$, cm^{-1}	11,548	16,968
$\bar{\nu}_{02}$, cm^{-1}	18,535.5	29,173
$\bar{\nu}_{03}$, cm^{-1}	21,947	30,271
μ_{01}, C-cm	2.78×10^{-27}	2.13×10^{-27}
μ_{12}, C-cm	2.55×10^{-27}	2.54×10^{-27}
μ_{23}, C-cm	4.92×10^{-27}	4.09×10^{-27}
μ_{03}, C-cm	2.54×10^{-28}	1.93×10^{-28}
$\bar{\nu}_p = \frac{1}{2} \bar{\nu}_{02}$, cm^{-1}	9,267.75	14,586.5
$\Delta\bar{\nu}_1$, cm^{-1}	2,280	2,381.5
$\Delta\bar{\nu}_{atomic}$, cm^{-1}	0.1	0.1
$\Delta\bar{\nu}_{laser}$, cm^{-1}	0.1	0.1
$\bar{\nu}^o_{ir}$, cm^{-1}	3,411.5	1,098
$\bar{\nu}^o_s$, cm^{-1}	21,947	30,271
λ_p, μm	1.079	0.6856
λ^o_s, μm	0.4556	0.3303
λ^o_{ir}, μm	2.931	9.107

(a) To be consistent with the current literature on metal-vapor upconversion, frequencies are given in wave number. Note that $\bar{\nu} = \nu/c = \omega/2\pi c = \bar{\omega}/2\pi$.

into the wave equation. The resulting equation is then separated into four equations, each containing only terms oscillating at one of the four frequencies. These are the coupled-mode equations. For the purposes of the analysis of the metal-vapor upconversion, we assume one-dimensional propagation along the z-axis, negligible losses at the four frequencies in the nonlinear material, and no significant depletion of the pump during the upconversion process. In this case, the coupled-mode equations reduce to*

$$\frac{\partial E_s}{\partial z} = -j \kappa_s E_{ir} e^{j\vec{\Delta k}z}$$
$$\frac{\partial E_{ir}}{\partial z} = -j \kappa_{ir} E_s e^{-j\vec{\Delta k}z} \quad , \tag{42}$$

where

$$\kappa_s = \frac{1}{2} \mu_o v_s \omega_s E_p^2 N\chi \quad ; \tag{43}$$

$$\kappa_{ir} = \frac{1}{2} \mu_o v_{ir} \omega_{ir} E_p^2 N\chi \quad ; \tag{44}$$

$$\vec{\Delta k} = \vec{k}_s - \vec{2k}_p - \vec{k}_{ir} \quad ; \tag{45}$$

μ_o is the permeability of free space; E_p, E_{ir}, and E_s are the pump, IR, and sum wave amplitudes; v_s and v_{ir} are the phase velocities at the sum and IR frequencies; N is the atomic density; and χ is given by Eq. (41).

Equation (42) may be solved to yield the photon conversion efficiency:

---

*Similar equations are derived for crystal upconversion in J. Falk and W. B. Tiffany, "Theory of Parametric Upconversion of Thermal Images," J. Appl. Phys., Vol. 43, p. 3762 (1972); and F. Zernike and J. E. Midwinter, Applied Nonlinear Optics, p. 42 (John Wiley and Sons, New York, New York, 1973).

$$\eta_{MV} = \frac{\kappa_{ir}\kappa_{s}}{\kappa_{ir}\kappa_{s} + \left(\frac{|\vec{\Delta k}|}{2}\right)^2} \sin^2\left[\sqrt{\kappa_{ir}\kappa_{s} + \left(\frac{|\vec{\Delta k}|}{2}\right)^2}\, L\right]$$

$$= \kappa_{ir}\kappa_{s} L^2 \operatorname{sinc}^2\left[L\sqrt{\kappa_{ir}\kappa_{s} + \left(\frac{|\vec{\Delta k}|}{2}\right)^2}\right] \qquad (46)$$

where $\operatorname{sinc}(x) \triangleq \sin(x)/x$ and L is the interaction length.

Equation (46) is the general expression for the photon conversion efficiency, including saturation. It will be seen that η_{MV} is limited to values less than unity as required by physical considerations. In other words, the best that can be done is to upconvert every incident IR photon, in which case $\eta_{MV} = 1$. If saturation is neglected in Eq. (46), which is equivalent to assuming that $\kappa_{ir}\kappa_{s} \ll (|\vec{\Delta k}|/2)^2$, then

$$\eta_{MV} = \kappa_{ir}\kappa_{s} L^2 \operatorname{sinc}^2\left(\frac{1}{2}|\vec{\Delta k}|L\right) . \qquad (47)$$

The length corresponding to the first maximum of $\sin^2\left(\frac{1}{2}|\vec{\Delta k}|L\right)$ is called the coherence length L_c; that is,

$$L_c = \pi/|\vec{\Delta k}| . \qquad (48)$$

3. Pump Phase-Matching

Consider the most general geometry for the wave vectors involved in the four-wave parametric process, shown in Figure 13(a). Two beams at the pump frequency are inclined at angles ϕ with respect to the optical axis. In practice, this may be accomplished by splitting the pump into two beams and recombining them at the upconverter with an angle 2ϕ between them. They interact with the IR radiation arriving at an angle θ with respect to the optical axis, to generate the sum frequency. The direction

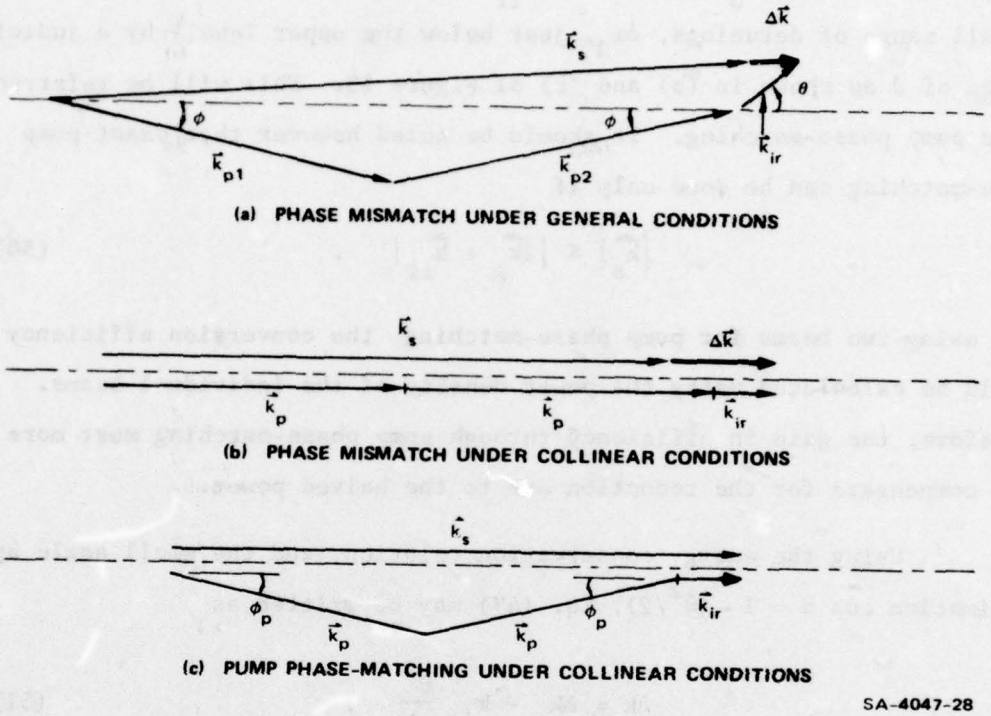

FIGURE 13 WAVE VECTOR GEOMETRY IN FOUR-WAVE PARAMETRIC UPCONVERSION WITH METAL VAPORS

of the sum wave-vector $\vec{k}_s$ may be determined by minimizing the momentum mismatch Δk. It can be shown that under these conditions

$$\Delta k = |\vec{\Delta k}| = k_s - 2k_p \cos \phi - k_{ir} \cos \theta \quad . \tag{49}$$

In the i...age-upconversion of broadband IR, one expects k_{ir} and θ to vary over a considerable range. It is clearly impossible to obtain phase match

for all ω_{ir} and θ; but it is feasible to arrange Δk to have the value zero or any other value Δk_o for a given ω_{ir} and θ (except, as we shall see, for a small range of detunings, $\Delta\omega_3$, just below the upper level) by a judicious choice of ϕ as shown in (b) and (c) of Figure 13. This will be referred to as pump phase-matching. It should be noted however that exact pump phase-matching can be done only if

$$|\vec{k}_s| \leq |2\vec{k}_p + \vec{k}_{ir}| \quad . \tag{50}$$

When using two beams for pump phase-matching the conversion efficiency should be calculated using the power density of the individual beams. Therefore, the gain in efficiency through pump phase-matching must more than compensate for the reduction due to the halved power.

Using the energy conservation relation, and the small angle approximation $\cos\theta = 1 - (\theta^2/2)$, Eq. (49) may be written as

$$\Delta k = \Delta k_o + k_{ir} \frac{\theta^2}{2} \quad , \tag{51}$$

where

$$\Delta k_o = (n_s - 1)\frac{\omega_s}{c} - (n_p \cos\phi - 1)\frac{2\omega_p}{c} - (n_{ir} - 1)\frac{\omega_{ir}}{c}$$

$$\cong (n_s - 1)\frac{\omega_s}{c} - (n_p \cos\phi - 1)\frac{2\omega_p}{c} \quad , \tag{52}$$

assuming $n_{ir} \approx 1$. The latter is a very good approximation for sodium and cesium since they do not have any natural frequencies in the infrared.

The Kramers-Heisenberg dispersion formulas give

$$(n_s - 1) = \frac{N}{2\epsilon_o \hbar}\frac{\mu_{03}^2}{\omega_{03} - \omega_s} \tag{53a}$$

$$(n_p - 1) = \frac{N}{2\epsilon_o \hbar}\frac{\mu_{01}^2}{\omega_{01} - \omega_p} \tag{53b}$$

and
$$(n_{ir} - 1) = \frac{N}{2\epsilon_o \hbar} \frac{\mu_{01}^2}{\omega_{01} - \omega_{ir}} \tag{53c}$$

When
$$(n_s - 1)\frac{\omega_s}{c} >> (n_p \cos \phi - 1)\frac{2\omega_p}{c} \quad , \tag{54}$$

it is readily shown that

$$L_c = \frac{\pi}{\Delta k} = \frac{2\pi\hbar \Delta\omega_3}{R_o N \omega_s \mu_{03}^2} \quad , \tag{55}$$

at $\theta = 0$. Here R_o is the impedance of free space. We call L_c given by Eq. (55) the coherence length as set by the upper level, since it was derived under the assumption that the dispersion of the upper level limits the length over which phase-matched interaction can occur.

4. Acceptance Angle and Pump Phase-Matching Angle for a Single IR Frequency

It is convenient at this time to derive the acceptance angle for the upconversion of single-frequency IR radiation arriving over a range of angles. These conditions obtain in an active imaging system where a very narrow band of frequencies (reflected laser radiation), collected by an optical system, is to be upconverted.

Equation (46) may be rewritten as

$$\eta_{MV}(\Delta k) = \left(\frac{\pi L}{2\Lambda}\right)^2 \operatorname{sinc}^2 \left[\sqrt{\left(\frac{\pi L}{2\Lambda}\right)^2 + \left(\frac{\Delta k L}{2}\right)^2}\right] , \tag{56}$$

where

$$\Lambda \triangleq \pi \Big/ \left(2\sqrt{K_{ir} K_s}\right)$$

$$= \text{const.} \; |\Delta\bar{\nu}_3| \; / \; [N(P/A)] \quad . \tag{57}$$

For $\Delta\nu_3 = -20\ \text{cm}^{-1}$, $N = 10^{18}\ \text{cm}^{-3}$, and $(P/A) = 10^6\ \text{W cm}^{-2}$, $\Lambda = 0.055$ cm for cesium and $\Lambda = 0.178$ cm for sodium. When $\Delta k = 0$,

$$\eta_{MV}(0) = \sin^2\left(\frac{\pi L}{2\Lambda}\right) \quad . \tag{58}$$

Note that Eqs. (56) and (57) predict that whenever $L = (2n + 1)\Lambda$ ($n = 0, 1, 2, \ldots$), and $\Delta k = 0$, the conversion efficiency is a maximum at unity.

Δk may have values in a range $-\Delta k_{max} < \Delta k < \Delta k_{max}$ and still provide conversion efficiencies within an acceptable fraction, q^2, of its peak value in the range. In other words,

$$\eta_{MV}(\Delta k_{max}) = q^2\, \eta_{MV}^{max} \quad . \tag{59}$$

A general solution for Δk_{max} is difficult. We consider the case when $L = (2n + 1)\Lambda$ and the above equation becomes

$$\text{sinc}\left\{\sqrt{\left[(2n+1)\,\frac{\pi}{2}\right]^2 + \left[(2n+1)\Lambda\,\frac{\Delta k_{max}}{2}\right]^2}\right\} = (-1)^n\,\frac{2q}{(2n+1)\pi} \quad . \tag{60}$$

If we define

$$\text{sinc}\left[\frac{(2n+1)}{2}\,p_n\right] = (-1)^n\,\frac{2q}{(2n+1)\pi} \quad , \tag{61}$$

then

$$\Lambda^2\,\Delta k_{max}^2 = p_n^2 \quad , \tag{62}$$

or

$$|\Delta k_{max}| = \frac{1}{\Lambda}\sqrt{p_n^2 - \pi^2} \quad . \tag{63}$$

We note that many values of p_n satisfy Eq. (61) but the value closest to and larger than π is the value applicable to the present discussion.

From Eq. (51), it is seen that θ can be maximized when $\Delta k_o = -|\Delta k_{max}|$ and

$$\theta_{max} = \sqrt{\frac{2\lambda_{ir}}{\Lambda}} \left[\left(\frac{P_n}{\pi} \right)^2 - 1 \right]^{1/4}$$

$$= \text{const.} \sqrt{\frac{N(P/A)}{|\Delta\bar{\nu}_3| \bar{\nu}_{ir}}} \quad . \tag{64}$$

By choosing $L = (2n + 1)\Lambda$ and an appropriate phase-matching angle so that $\Delta k_o = -|\Delta k_{max}|$, an upconversion efficiency better than 40% may be obtained over an acceptance angle $\alpha = 2\theta_{max}$. For the parameter values used earlier, the full acceptance angle for both cesium and sodium is about 11°, when an upconverter length equal to Λ is used. For higher values of L, the acceptance angle decreases to some extent. [A further increase in acceptance angle is possible for $n > 0$ by reducing L somewhat below $(2n + 1)\Lambda$ and allowing Δk an even larger range.]

If the parameters N, P/A and $\Delta\bar{\nu}_3$ are chosen such that $\kappa_{ir}\kappa_s \ll (\Delta k^2/2)$, then the photon conversion efficiency is given by Eq. (47) with a maximum value of $\kappa_{ir}\kappa_s L^2$. If the pump phase-matching angle is chosen such that $\Delta k_o = -\pi/L$, it will be seen that the conversion efficiency will be greater than $(4/\pi^2)\kappa_{ir}\kappa_s L^2$, over a full acceptance angle given by

$$\alpha = 2\sqrt{2\lambda_{ir}/L} \quad . \tag{65}$$

For a vapor length of 1 cm, this leads to acceptance angles of 5.1° at 10 μm (sodium) and 2.8° at 2.9 μm (cesium). These expressions for the acceptance angle, strictly speaking, are applicable only within the metal vapor. However, since the refractive index of the metal vapors at IR wavelengths is very close to unity, the same relation is valid outside the metal vapor.

We now derive a relation for the pump phase-matching angle such that Δk_o has the desired value in the above two cases. From Eq. (52), use of the small angle approximation $\cos \phi = 1 - (\phi^2/2)$ yields

$$\Delta k_o = \frac{1}{c}\left[(n_s - 1)\omega_s - (n_p - 1)2\omega_p + n_p \phi^2 \omega_p\right] \quad . \tag{66}$$

Using Eq. (53) and solving for ϕ, we obtain

$$\phi = \left[\frac{c\,\Delta k_o}{n_p \omega_p} + \frac{N}{\epsilon_o \hbar n_p}\left(\frac{\mu_{01}^2}{\Delta\omega_1} - \frac{\mu_{03}^2}{2\Delta\omega_3}\frac{\omega_s}{\omega_p}\right)\right]^{1/2} \tag{67}$$

for the required phase-matching angle. For the conditions assumed earlier, the pump phase-matching angles have values of 2.57° for sodium and 3.25° for cesium. When the pump power-density is small, so that we are in the unsaturated region, and when $N = 10^{18}$ cm^{-3}, $\Delta\nu_3 = -20$ cm^{-1}, and $L = 1$ cm the pump phase-matching angles are still 2.65° and 3.64°, respectively.

It is instructive to consider the behavior of ϕ as a function of detuning $\Delta\omega_3$ for constant L. When $\Delta\omega_3$ has a small negative value, the third term in the above equation is dominant and determines ϕ. This corresponds to the condition when the coherence length is determined by the dispersion of the upper level. When $\Delta\omega_3$ has large positive or negative values, the third term is negligible and the dispersion of the lower level determines the coherence length and ϕ. There is also a range of small positive values of $\Delta\omega_3$ for which ϕ is imaginary; in other words, pump phase-matching is not possible for these values of $\Delta\omega_3$, which correspond to detunings just below the upper level. However, it is evident that there always are IR wavelengths for which pump phase-matching can be achieved with high conversion efficiency. For active imaging, the illumination wavelength should be chosen to be such a wavelength.

The illumination wavelength or the detuning $\Delta\omega_3$ must also be chosen so that there will not be significant absorption of the sum frequency ω_s. The attenuation of the sum frequency due to absorption in a length L is described by

$$I = I_o \exp\left[- \frac{N R_o \omega_s \mu_{03}^2}{2\hbar} \frac{\Delta\omega_b L}{\Delta\omega_3^2 + \left(\frac{\Delta\omega_b}{2}\right)^2} \right] , \qquad (68)$$

where $\Delta\omega_b$ is the pressure-broadened linewidth given by*

$$\text{Cs: } 6s \rightarrow 7p \text{ (upper) } \Delta\bar{\nu}_b = 3.27 \times 10^{-20} N$$

$$\text{Na: } 3s \rightarrow 4p \text{ (total) } \Delta\bar{\nu}_b = 1.30 \times 10^{-20} N$$

At reduced pressure, the attenuations are given approximately by

$$(I/I_o)_{Na} = \exp\left[- 26.2 \times 10^{-36} \frac{N^2 L}{(\Delta\bar{\nu}_3)^2} \right] , \qquad (69)$$

and

$$(I/I_o)_{Cs} = \exp\left[- 82.8 \times 10^{-36} \frac{N^2 L}{(\Delta\bar{\nu}_3)^2} \right] . \qquad (70)$$

At $N = 10^{18}$ cm^{-3}, $\Delta\bar{\nu}_3 = -20$ cm^{-1}, L = 1 cm, $(I/I_o) = 0.94$, and $(I/I_o)_{Cs} = 0.81$. Or about 1% loss occurs at $\Delta\bar{\nu}_3 = 51$ cm^{-1} for sodium and at $\Delta\bar{\nu}_3 = 91$ cm^{-1} for cesium.

5. Acceptance Angle, IR Bandwidth, and Upconversion Efficiency for Thermal Radiation

The concepts developed above can now be applied to the more general case of the upconversion of thermal images by obtaining an expression

*R. B. Miles, "Optical Third Harmonic Generation in Metal Vapors," Internal Memorandum, Hansen Microwave Laboratory Report No. 2069, Stanford University (June 1972).

for the upconversion efficiency as a function of IR frequency, arrival angle, and pump phase-match angle.

It will be noted that the factor $K_{ir} K_s$ in Eq. (46) may be written by using Eqs. (41), (43), and (44) as

$$K_{ir} K_s = \frac{\omega_{ir} \omega_s}{(\Delta\omega_3)^2} \cdot \gamma \quad , \tag{71}$$

where

$$\gamma = \left(\frac{\pi^2 R_o^4}{h^6 c^4}\right)\left(\frac{\mu_{01}\mu_{12}\mu_{23}\mu_{03}}{\Delta\bar{\nu}_1}\right)^2 \left(\frac{N^2}{n_s n_{ir} \Delta\bar{\nu}_{atomic}}\right)\left(\frac{(P/A)^2}{\Delta\bar{\nu}_{laser}}\right) \tag{72}$$

and

$$\bar{\nu}_i = (\omega_i / 2\pi c) \quad .$$

Using Eq. (53), it can be shown that to a very good approximation n_{ir} is unity and n_s differs from unity significantly only when $\Delta\bar{\nu}_3$ is less than $\sim 1\ cm^{-1}$. Therefore γ can be considered to be independent of ω_{ir}.

Consider a particular frequency ω_{ir}^o and a pump phase-match angle ϕ^o such that the coherence length is set by the upper level at $\theta = 0$, as given by Eq. (55). Then

$$\Delta k_o^o = \frac{(n_s^o - 1)\omega_s^o}{c} = \frac{\delta}{\Delta\omega_3^o} \quad , \tag{73}$$

where

$$\delta = \frac{N\omega_s^o \mu_{03}^2}{2\epsilon_o c\hbar} \quad ; \tag{74}$$

and ω_s^o is the particular sum frequency corresponding to ω_{ir}^o.

If we define

$$\eta_{MV}^o \triangleq \frac{K_{ir}^o K_s^o}{K_{ir}^o K_s^o + \left(\frac{\Delta k_o^o}{2}\right)^2} \tag{75}$$

from Eqs. (71) through (74), it follows that

$$\gamma = \xi \left(\frac{\delta}{2}\right)^2 \frac{1}{\omega_{ir}^{o}\omega_{s}^{o}} \quad , \tag{76}$$

where

$$\xi = \eta_{MV}^{o}/(1 - \eta_{MV}^{o}) \quad . \tag{77}$$

We note that ξ and η_{MV}^{o} do not depend on N, the atomic density in the metal vapor. Using these results, Eq. (46), which is the general expression for upconversion efficiency including saturation, can be written as

$$\eta_{MV} = \frac{\xi}{\xi + \left(\frac{\Delta k \Delta\omega_3}{\delta}\right)^2 \left(\frac{\omega_{ir}^{o}\omega_{s}^{o}}{\omega_{ir}\omega_{s}}\right)} \sin^2\left[\frac{\delta L}{2\Delta\omega_3}\sqrt{\xi\,\frac{\omega_{ir}\omega_{s}}{\omega_{ir}^{o}\omega_{s}^{o}} + \left(\frac{\Delta k \Delta\omega_3}{\delta}\right)^2}\right] \tag{78a}$$

We now express Δk as a function of the general frequency ω_{ir} and incidence angle θ and a pump phase-matching angle ϕ. From Eqs. (51), (52), and (53) and approximating cos ϕ by $\left[1 - \phi^2/2\right]$, we obtain

$$\frac{\Delta k \Delta\omega_3}{\delta} \cong 1 - \left(\frac{\mu_{01}}{\mu_{03}}\right)^2 \left(\frac{2\omega_p/\omega_s}{\omega_{10} - \omega_p} + \frac{\omega_{ir}/\omega_s}{\omega_{10} - \omega_{ir}}\right)\Delta\omega_3$$

$$+ \frac{\phi^2}{2\delta}\left(\frac{2\omega_p}{c}\right)\Delta\omega_3 + \frac{\theta^2}{2\delta}\left(\frac{\omega_{ir}}{c}\right)\Delta\omega_3 \quad . \tag{78b}$$

Equation (78) expresses the upconversion efficiency as an explicit function of the variables ω_{ir}, θ, ϕ, and L. It contains , in addition to the atomic parameters and the pump frequency ω_p, the special parameters ω_{ir}, δ, and ξ (or equivalently η_{MV}^{o}). δ depends on the pressure of the metal vapor and ξ contains the dependence on the linewidth and power density of the pump. η_{MV}^{o} can be interpreted using Eqs. (46) and (75) as

the upconversion efficiency at ω_{ir}^{o} in one coherence length when the latter is determined by the upper level with the same pump and metal-vapor characteristics. The value of η_{MV}^{o} can therefore be obtained from experimental results as well as by direct calculation. It is noted that Eq. (78) is consistent in the sense that

$$\eta_{MV}^{o} = \eta_{MV} \quad (\omega = \omega_{ir}^{o},\ \theta = 0,\ \phi = \phi^{o}) \quad . \tag{79}$$

Using the atomic parameters in Table 4, it can be shown that with a laser linewidth of 0.1 cm^{-1} and at a pump power density of 1 MW cm^{-2}, η_{MV}^{o} has the values 2.97% and 17.0% for sodium and cesium, respectively. Stated differently, η_{MV}^{o} has a value of 50% for pump power densities of 5.72 MW cm^{-2} and 2.21 MW cm^{-2} for sodium and cesium, respectively. Photon conversion efficiencies of ~50% for a particular angle of incidence and IR frequency have been observed experimentally.* Therefore, $\eta_{MV}^{o} = 0.5$ or $\xi = 1$ is employed in subsequent computations (with the associated power densities).

In the upconversion of thermal images, broadband IR radiation is incident on the upconverter with a range of arrival angles. The performance of the system depends on the upconversion efficiency, which must be averaged over the IR frequencies and arrival angles and may be optimized by a proper choice of the pump phase-matching angle ϕ. The problem to be solved, therefore, is to determine the optimum combination of IR bandwidth, IR acceptance angle, and efficiency determined by a suitable choice of ϕ. This optimization problem is not amenable to an analytical solution and hence was treated numerically. The procedure is to calculate the average value of the efficiency by numerically evaluating the integral

---

*D. M. Bloom et al., "Infrared Upconversion with Resonant Two-Photon Pumped Metal Vapors," Appl. Phys. Letters, Vol. 24, No. 9, p. 427 (May 1974).

$$\eta_{av}(\theta,\phi,B) = \frac{1}{B}\int_{\omega_{ir}^{o}-B/2}^{\omega_{ir}^{o}+B/2} \eta_{MV}\,(\omega_{ir},\ \theta,\ \phi)\, d\omega_{ir} \qquad (80)$$

as a function of θ for several chosen values of the pump phase-match angle ϕ and IR bandwidth B. The optimum result is selected on the basis of the conversion efficiency and its uniformity over a large acceptance angle and IR bandwidth.

The results of some of these computations are presented in Figures 14 through 17 for several values of the pump phase-matching angle. In all cases, the values $\eta = 0.5$ (or $\xi = 1$), $L = 1$, and $B = 200\ cm^{-1}$ have been used. From these illustrations it is seen that the optimum pump phase-match angle is 2° for cesium and 1.5° for sodium. It is also seen that the photon conversion efficiency at these values is relatively uniform at 0.2 until it drops sharply at 7° for cesium and 10° for sodium. These angles are taken to be the half-acceptance angles for the upconverter. Since $n_{ir} = 1$ for metal vapors, the acceptance angles external to the upconverter are the same. The bandwidth of 200 cm^{-1} which was found to be optimum is equivalent to 0.17 μm (at 2.93 μm) for cesium and 1.67 μm (at 9.1 μm for sodium).

It was noted in the previous section that the sum frequency generated will be absorbed by the metal vapor to a degree depending on the detuning. In the foregoing, the average efficiency of upconversion over a bandwidth of 200 cm^{-1} centered at the resonant frequency was estimated. The absorption of the sum frequency generated, as given by Eqs. (69) and (70), can be estimated as

$$\eta_{abs} = \frac{1}{I_o B}\int_{\bar{\nu}_s^{o}-B/2}^{\bar{\nu}_s^{o}+B/2} I\, d\bar{\nu} \quad . \qquad (81)$$

It is found that for $L = 1$ cm and $N = 10^{18}\ cm^{-3}$, η_{abs} is 0.91 for sodium and 0.85 for cesium.

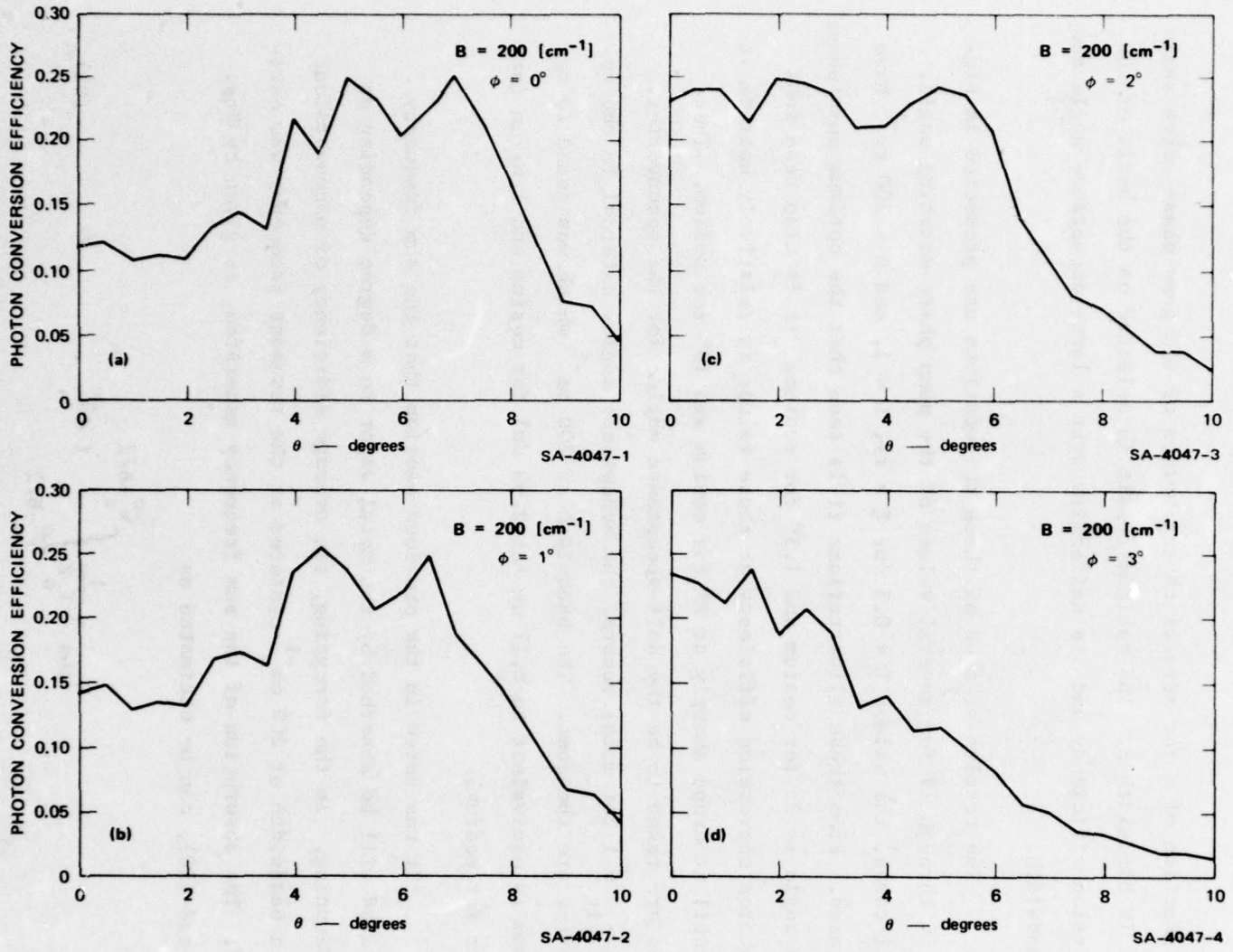

FIGURE 14 PHOTON CONVERSION EFFICIENCY OF CESIUM AS A FUNCTION OF INFRARED INCIDENCE ANGLE AND PUMP PHASE-MATCHING ANGLE

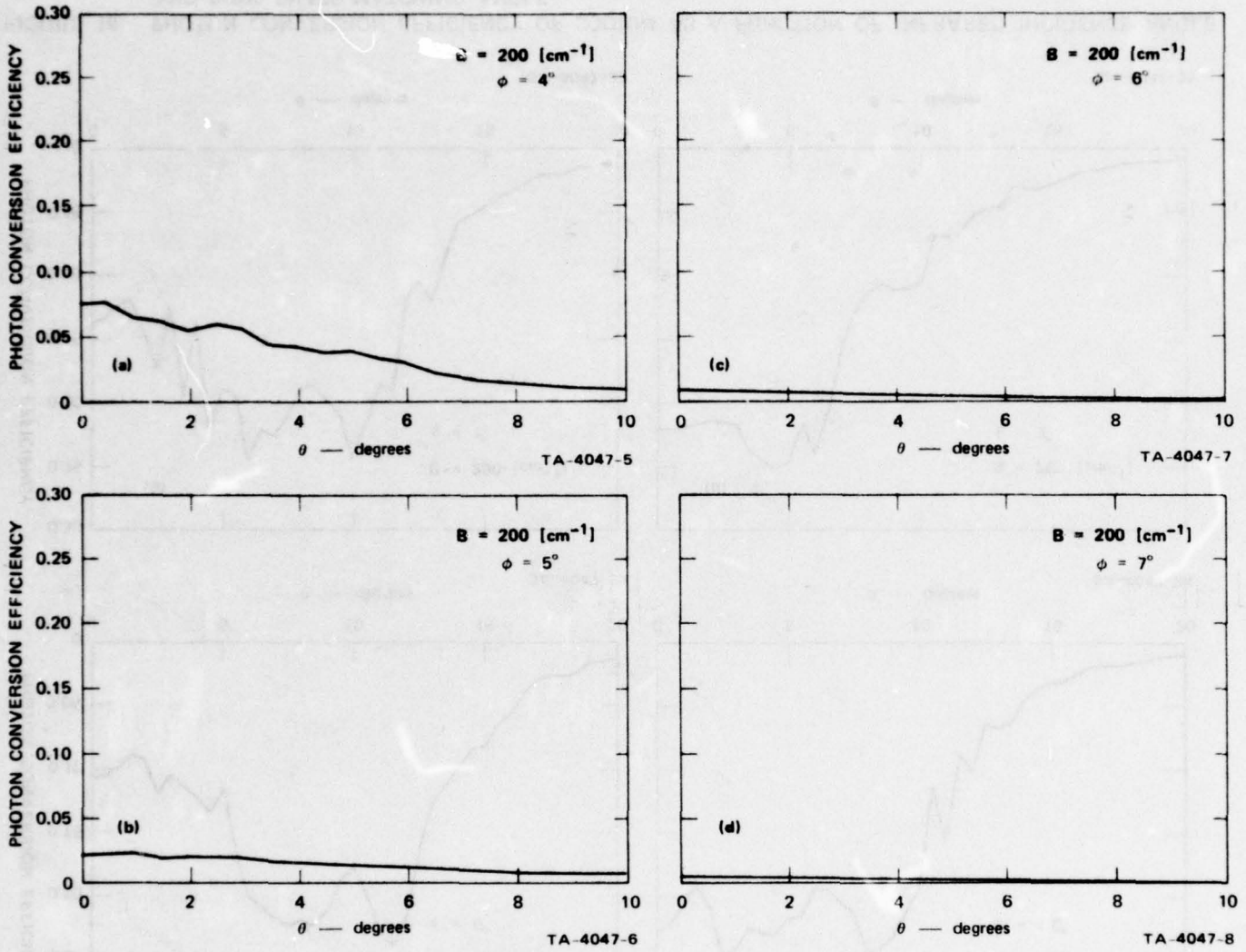

FIGURE 15 PHOTON CONVERSION EFFICIENCY OF CESIUM AS A FUNCTION OF INFRARED INCIDENCE ANGLE AND PUMP PHASE-MATCHING ANGLE

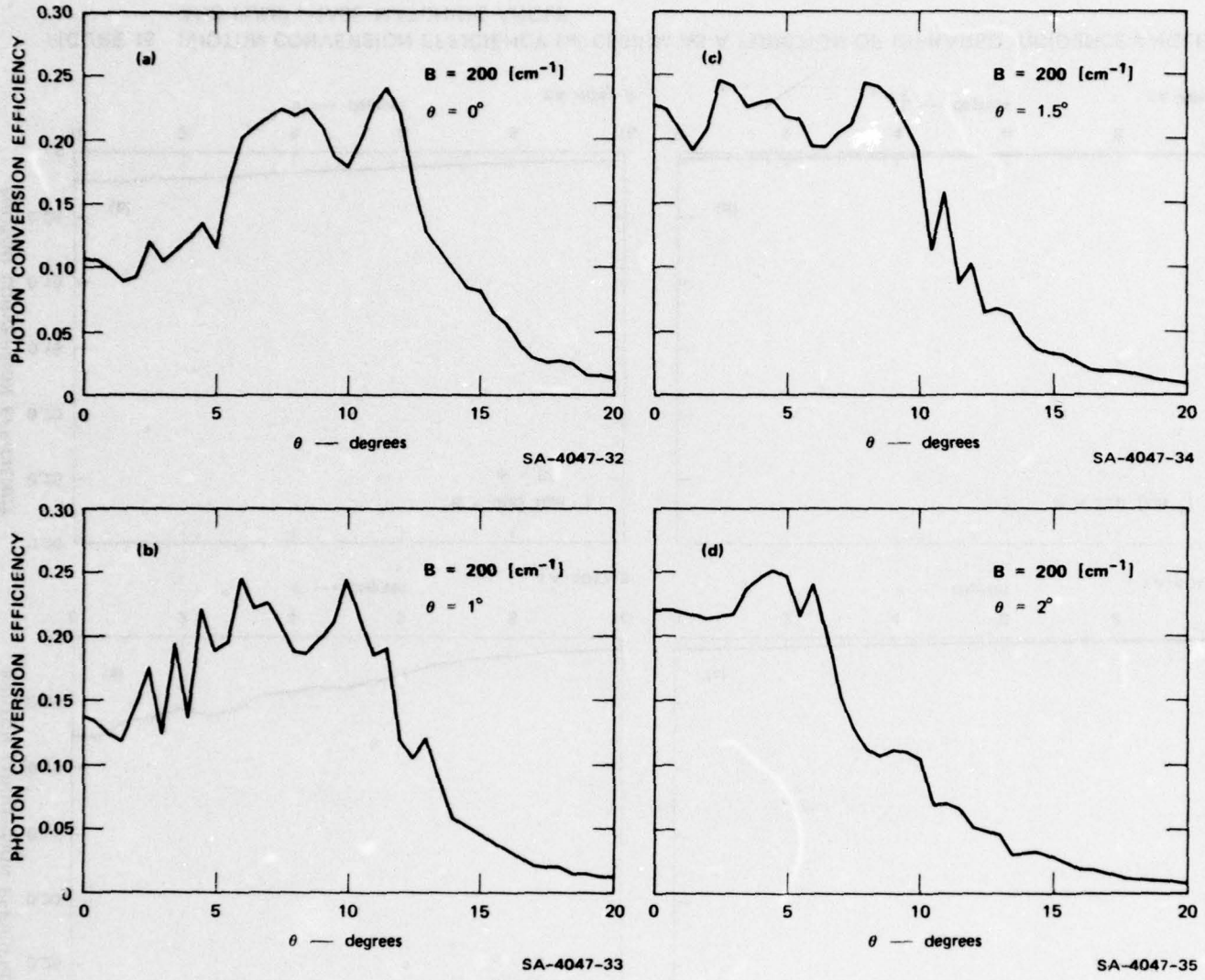

FIGURE 16 PHOTON CONVERSION EFFICIENCY OF SODIUM AS A FUNCTION OF INFRARED INCIDENCE ANGLE AND PUMP PHASE-MATCHING ANGLE

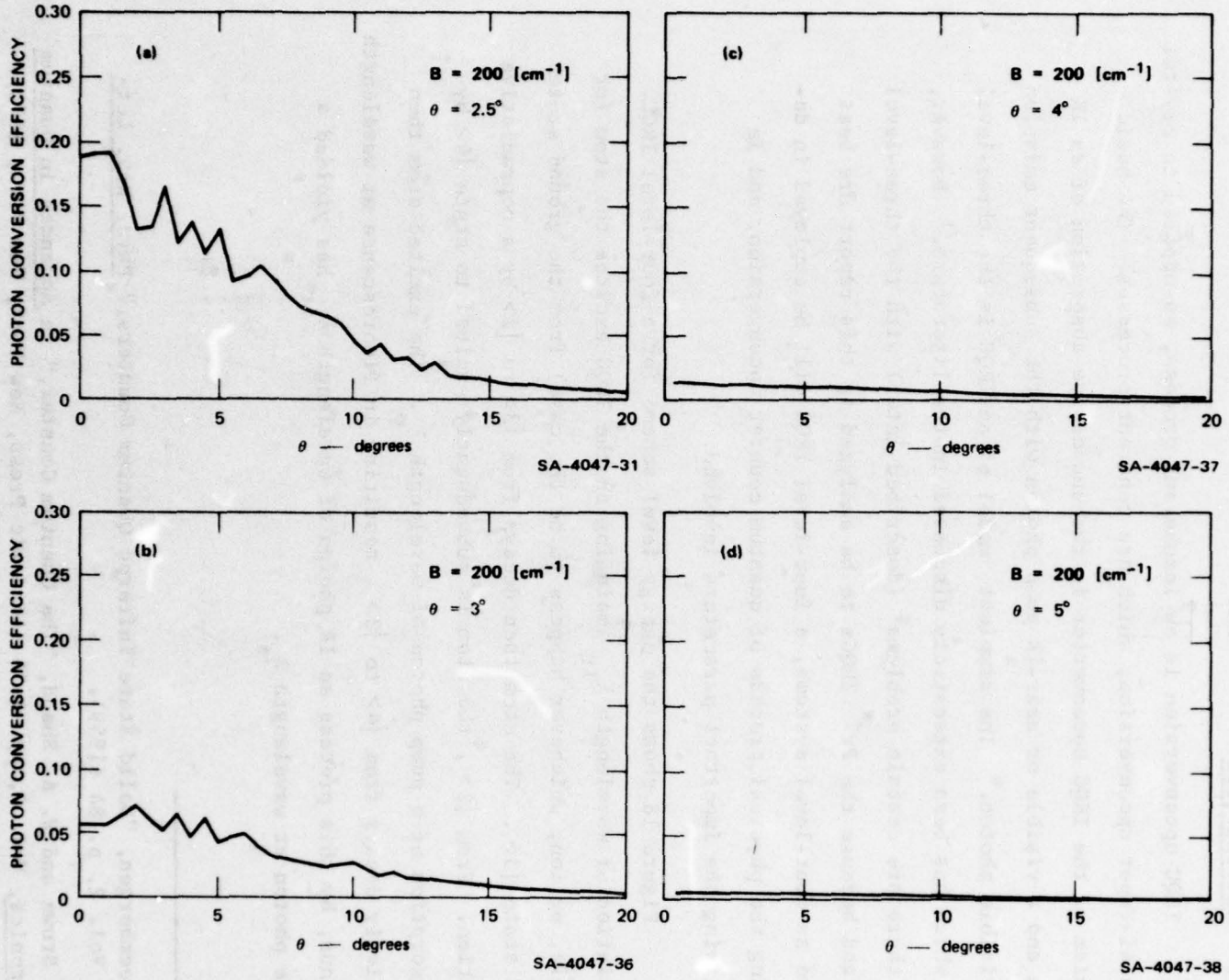

FIGURE 17 PHOTON CONVERSION EFFICIENCY OF SODIUM AS A FUNCTION OF INFRARED INCIDENCE ANGLE AND PUMP PHASE-MATCHING ANGLE

B. INFRARED QUANTUM COUNTER (IRQC)

1. Introduction

IRQC upconversion is an incoherent process, as opposed to crystal and metal-vapor upconversion, which are coherent processes. The basic mechanism of the IRQC upconverter is the successive absorption of an IR photon and a visible or near-IR pump photon with the subsequent emission of a visible photon.* The simplest model of an IRQC is the three-level IRQC, which has been extensively discussed in the literature.† However, since there are certain problems‡ (described later) with the three-level IRQC, and because the Pr^{3+} IRQCs to be analyzed in this report are best modeled as four-level systems, a four-level IRQC will be employed in describing the physical process of quantum counter upconversion, and in identifying the important parameters involved.

Figure 18 shows the energy level scheme for a four-level IRQC. IR radiation of wavelength λ_{ir} impinging on the IRQC excites the atom (or molecule, or ion, whichever happens to be the case) from the ground state $|1\rangle$ to state $|3\rangle$. The atom then decays from $|3\rangle$ to $|2\rangle$ by a nonradiative transition. From $|2\rangle$, the atom is subsequently excited to state $|4\rangle$ by the absorption of a pump photon of wavelength λ_p. The excited atom then radiatively decays from $|4\rangle$ to $|3\rangle$, resulting in fluorescence at wavelength λ_s. Thus, by this process an IR photon of wavelength λ_{ir} has yielded a visible photon at wavelength λ_s.

---

*N. Bloembergen, "Solid State Infrared Quantum Counters," Phys. Rev. Letters, Vol. 2, p. 84 (1959).

†M. R. Brown and W. A. Shand, "The Quantum Counter," in Advances in Quantum Electronics, Vol. 1, pp. 1-76 (Academic Press, New York, New York, 1970).

‡L. Esterowitz et al., "Rare Earth Infrared Quantum Counter," Appl. Optics, Vol. 7, p. 2059 (1968).

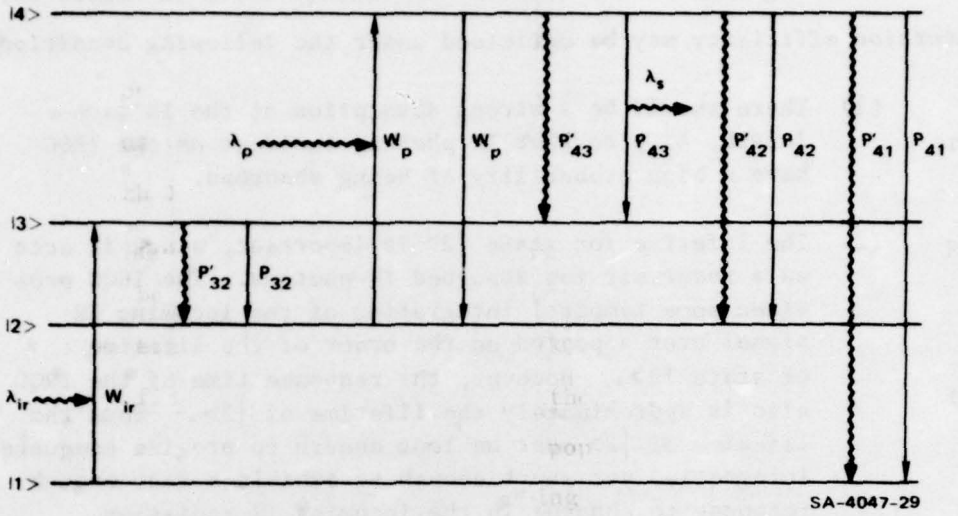

FIGURE 18 SCHEMATIC REPRESENTATION OF THE FOUR-LEVEL INFRARED QUANTUM COUNTER

If, however, no IR radiation at λ_{ir} is incident on the IRQC, state $|2\rangle$ remains unpopulated, and no output fluorescence at λ_s is observed upon pumping with λ_p, since there are no atoms in excited state $|2\rangle$ for excitation to $|4\rangle$. This means that the IRQC is transparent to the pump, since there can be no absorption at the $|2\rangle$ to $|4\rangle$ transition if $|2\rangle$ is unpopulated. Therefore, in principle, the IRQC process is "noise-free," since no output fluorescence is possible in the absence of IR photons at λ_{ir}. In practice, however, $|2\rangle$ can also be populated by thermal, Raman, and two-photon excitation processes, resulting in output fluorescence with no IR input.* Of these, the thermal excitation of $|2\rangle$ can be reduced by cooling the IRQC, and the Raman and two-photon excitations have not been significant in the Pr^{3+} IRQC upconverter.

The efficiency of IRQC upconversion depends upon the strength of the absorptions, the lifetime of state $|2\rangle$, and the radiative efficiency

---

*N. E. Byer, "Noise Considerations for Infrared Quantum Counters: the Oxygen-Fired $CdF_2:E^3$ + IRQC," J. Appl. Phys., Vol. 43, p. 3567 (1972).

of the fluorescing state. For the four-level IRQC shown in Figure 18, the upconversion efficiency may be optimized under the following conditions:

(1) There should be a strong absorption at the IR wavelength, λ_{ir}, so that IR photons incident on the IRQC have a high probability of being absorbed.

(2) The lifetime for state $|2\rangle$ is important, since it acts as a reservoir for absorbed IR photons. The IRQC provides some temporal integration of the incoming IR signal over a period on the order of the lifetime of state $|2\rangle$. However, the response time of the IRQC also is approximately the lifetime of $|2\rangle$. Thus the lifetime of $|2\rangle$ must be long enough to provide adequate integration yet short enough to exhibit a fast enough response to changes in the incoming IR radiation.

(3) The transition from state $|3\rangle$ to state $|2\rangle$ should be fast and nonradiative so that essentially all atoms excited to $|3\rangle$ end up in $|2\rangle$. This transition permits conditions (1) and (2) to be simultaneously satisfied. Notice that if $|3\rangle = |2\rangle$, a strong absorption at λ_{ir} and a long lifetime for $|2\rangle$ would be mutually incompatible. This problem is a major defect of the simpler three-level IRQC.

(4) The transition from state $|3\rangle$ to state $|4\rangle$ should be strongly allowed, since in general the stronger the pump absorption the less pump power will be needed to achieve a given quantum efficiency. For pump power below saturation levels, the photon upconversion efficiency is a linear function of the pump-absorption cross section.

(5) State $|4\rangle$ should be a strongly fluorescing state, with maximum radiative efficiency for the $|4\rangle$ to $|3\rangle$ transition.

In the four-level IRQC shown in Figure 18, after fluorescing from $|4\rangle$ to $|3\rangle$, the atom then nonradiatively decays from $|3\rangle$ to $|2\rangle$, where it is once again available for pump absorption and subsequent fluorescence. Thus, one IR photon may give rise to more than one visible photon in the output. The potential quantum efficiency is greater than unity because of this "recycling" process, depending of course upon the pump

power duration and various material parameters. For a three-level IRQC, where the fluorescence terminates at the ground state, the photon conversion efficiency is necessarily less than or equal to unity, since no recycling is possible.

The IRQC can be operated either as a CW upconverter or a pulsed upconverter, depending upon whether the pump is CW or pulsed. A recycling process, such as that described above, may not be possible for the pulsed IRQC upconverter, however, because of the pulse length being too short to allow the recycling process to occur.

Any material with a suitable set of energy levels is a potential IRQC upconverter. Table 5 summarizes the significant work done with rare-earth IRQC materials suitable for upconversion of infrared radiation with wavelengths in the 2- to 5-μm and 8- to 12-μm regions, which correspond to atmospheric transmission windows. In the rare earths, electric dipole transitions are only weakly allowed, with typical oscillator strengths of $\mathcal{F} \sim 10^{-5}$ or 10^{-6}. The significance of this is that the pump and IR transitions will be relatively weak in the rare-earth IRQC. This is not of great importance for the IR transition, since there is a large ground-state population, but it does mean that higher pump power will be required.

Later system calculations will concentrate on the Pr^{3+} $(4f^2)$ ion, since this rare-earth ion has been the most studied and has several possibilities for upconversion of wavelengths in the 2- to 5-μ region. Pr^{3+} $(4f^2)$ has been used as an IRQC material as an ion doped into a dielectric crystal* and as pure $PrCl_3$ deposited on a substrate.†,‡

---

*J. F. Porter, Jr., "Sensitivity of Pr^{3+} : $LaCl_3$ Infrared Quantum Counter," IEEE J. Quant. Electron., Vol. QE-1, p. 113 (1965).

†K. G. Sewell and W. B. Volz, "Direct Infrared Image Upconversion with a Praseodymium Chloride Quantum Counter," Appl. Phys. Letters, Vol. 23, p. 104 (1973).

‡J. R. Herrington, K. G. Sewell, and W. B. Volz, "A Thermal Imaging System Based on the $PrCl_3$ Quantum Counter," Appl. Phys. Letters, Vol. 26, p. 226 (1975).

TABLE 5

REPORTED IRQCs FOR THE 2- TO 5-μm AND 8- TO 12-μm SPECTRAL REGIONS

Material	λ_{ir} (μm)	λ_p (μm)	λ_s (μm)	Reference
$Pr^{3+}:LaCl_3$ at 300°K, 77°K, and 4.2°K	4.63 2.33 2.03 1.58 1.48	0.529 at 300°K and 77°K 0.558 at 4.2°K	0.489	(a)
15% $Pr^{3+}:LaCl_3$ at 4.2°K	2.03	0.615	0.489	(b)
2% $Tm^{3+}:LaCl_3$ at 4.2°K and 300°K	1.76	0.456	0.362	
$Sm^{3+}_x:E^{3+}_y:La_{(1-x-y)}Br_3$ proposed system	~10			(c)
15% $Pr^{3+}:LaCl_3$ at 4.2°K	2.03	0.615	0.489	(d)
Oxygen-fired $Er^{3+}:CdF_2$	1.5	0.840	0.540 0.660	(e)
$PrCl_3$ at 163°K	4.81 2.38 2.05 1.59 1.48	0.546	0.616 0.619 0.645	(f),(g)
1% $Nd^{3+}:LaCl_3$ at 200°K and 300°K	5	1.06	0.9	(h)
0.5% $Er^{3+}:BaY2F_8$	1.5	0.850	0.540	(i)

(a) J. F. Porter, Jr., "Sensitivity of $Pr^{3+}:LaCl_3$ Infrared Quantum Counter," IEEE J. Quant. Electron., Vol. QE-1, p. 113 (1965).

(b) W. B. Gandrud and H. W. Moos, "Improved Rare-Earth Trichloride Infrared Quantum Counter Sensitivity," IEEE J. Quant. Electron., Vol. QE-4, p. 249 (1968).

(c) J. C. Wright and F. K. Fong, "Multiphonon Orbit-Lattice Relaxation and Quantum Efficiency of 10-μ Infrared Quantum-Counter Upconversion in Rare-Earth-Doped Crystals," J. Appl. Phys., Vol. 42, p. 3806 (1971).

(d) J. C. Wright et al., "Laser Optical Double Resonance and Efficient Infrared Quantum Counter Upconversion in $LaCl_3:Pr^{3+}$ and $LaF_3:Pr^{3+}$," J. Appl. Phys., Vol. 44, p. 781 (1973).

(e) N. E. Byer et al., "IRQC Parameters for Er^{3+} Occupying Sites of C_2v and C_3v Symmetry in CdF_2," J. Appl. Phys., Vol. 44, p. 1733 (1973).

(f) K. G. Sewell and W. B. Volz, "Direct Infrared Image Upconversion with a Praseodymium Chloride Quantum Counter," Appl. Phys. Letters, Vol. 23, p. 104 (1973).

(g) J. R. Herrington, K. G. Sewell, and W. B. Volz, "A Thermal Imaging System Based on the $PrCl_3$ Quantum Counter," Appl. Phys. Letters, Vol. 26, p. 226 (1975).

(h) S. E. Stokowski, "Characteristics of a Nd Laser-Pumped 5-μm IRQC Detector," Paper No. 6, VIII International Quantum Electronics Conference, June 10-13, 1974.

(i) S. E. Stokowski, "Characteristics of a Laser-Pumped 1.5-μm Infrared Quantum Counter," J. Appl. Phys., Vol. 45, p. 2957 (1974).

2. Photon Conversion Efficiency of the Pr^{3+} IRQC

The IRQC photon conversion efficiency is defined as:

$$\eta_{IRQC} = \frac{\text{number of IR photons upconverted to visible photons}}{\text{number of incident IR photons}}$$

To calculate η_{IRQC}, an energy level scheme representative of the particular IRQC material to be considered is chosen and, using suitable assumptions,* the rate equations are solved.

The energy level scheme for Pr^{3+} can be represented by the four-level system shown in Figure 18. The rate equations for this four-level system are

$$\frac{dN_1}{dt} = -W_{ir}N_1 + \frac{N_2}{\tau_2} + \frac{(P'_{41} + P_{41})N_4}{\tau_4} \quad , \tag{82}$$

$$\frac{dN_2}{dt} = -\left(W_P + \frac{1}{\tau_2}\right)N_2 + \frac{(P'_{32} + P_{32})N_3}{\tau_3} + \frac{(P'_{42} + P_{42})N_4}{\tau_4} + W_P N_4 \quad , \tag{83}$$

$$\frac{dN_3}{dt} = -\frac{N_3}{\tau_3} + W_{ir}N_1 + \frac{(P'_{43} + P_{43})N_4}{\tau_4} \quad , \tag{84}$$

$$\frac{dN_4}{dt} = -\left(W_P + \frac{1}{\tau_4}\right)N_4 + W_P N_2 \quad , \tag{85}$$

where

N_i = population of state $|i\rangle$ [atoms cm^{-3}]

τ_i = lifetime of state $|i\rangle$ [sec]

P_{ij} = probability of radiative decay from $|i\rangle$ to $|j\rangle$

---

*W. F. Krupke, "Performance of Laser-Pumped Quantum Counters," IEEE J. Quant. Electron., Vol. QE-1, p. 20 (1965).

P'_{ij} = probability of nonradiative decay from $|i\rangle$ to $|j\rangle$ and radiative decay from $|i\rangle$ to $|j\rangle$ through intermediate energy levels of the IRQC that may not be pictured on its four-level representation

W_P = pump transition rate [sec^{-1}]

W_{ir} = IR transition rate [sec^{-1}]

W_{ir} and W_P may also be written as

$$W_{ir} = \sigma_{ir} J_{ir} = \sigma_{ir} I_{ir} / h\nu_{ir} \tag{86}$$

$$W_P = \sigma_P J_P = \sigma_P I_P / h\nu_P \tag{87}$$

where

σ_P = pump absorption cross section [cm^2]

σ_{ir} = infrared absorption cross section [cm^2]

J_{ir} = infrared flux [photons cm^{-2} sec^{-1}]

J_P = pump flux [photons cm^{-2} sec^{-1}]

h = Planck's constant = 6.6256×10^{-34} [J sec]

ν_{ir} and ν_P = infrared and pump frequencies [Hz]

I_{ir} and I_P = infrared and pump intensities [W cm^{-2}]

Several approximations were made to obtain Eqs. (82) through (85). Excitations due to thermal, Raman, or two-photon excitation processes were neglected. These processes have been considered separately and their effects were found to be small. It is assumed that the IRQC is cooled to reduce thermal mixing between the energy levels. The population density is assumed to be uniform over the IRQC area, and induced transitions are neglected, as are various other decay mechanisms of less importance.

Since the IRQC is an incoherent upconverter, there are no restrictions imposed by the process itself on the arrival angle of the IR radiation or the IR bandwidth that will be upconverted. The IR arrival angle is limited only by the optical system. The upconversion bandwidth is defined by the IR absorption bandwidth of the IRQC. In the case of

the two materials considered here, atmospheric attenuation reduces the useful bandwidth further.

Recently a CW Pr^{3+} (praseodymium ion) IRQC has been developed by LTV Advanced Technology Center,* and a pulsed Pr^{3+} IRQC has been developed by Varo Associates.†,‡ The LTV IRQC uses the Pr^{3+} ion doped into a dielectric crystal (the actual crystal used is proprietary information), while Varo employs $PrCl_3$ (praseodymium chloride) deposited on a substrate as the IRQC material. The IRQC parameters are given in Table 6. These parameter values were obtained through the courtesy of researchers with LTV and Varo Associates.* The basic four-level energy scheme is the same for both IRQCs although there are differences in the various parameter values.

The photon conversion efficiencies of the CW IRQC and the pulsed IRQC are developed in the following sections. For the CW IRQC the rate equations are solved under the steady-state conditions $dN_i/dt = 0$. The pulsed IRQC differs from the CW IRQC in that the pump is supplied by a pulsed rather than a CW source. Although IR radiation is continually being absorbed, no upconversion--and hence no output signal fluorescence--takes place until the IRQC is subjected to a pump pulse. For thermal or passive imaging, where the signal IR is continually incident on the IRQC, this means that a duty-cycle factor must be included that accounts for the fact that the pulsed IRQC upconverts only part of the time. An effective or time-averaged photon conversion efficiency will be derived for the pulsed IRQC.

---

*Private communication.

†K. G. Sewell and W. B. Volz, "Direct Infrared Image Upconversion with a Praseodymium Chloride Quantum Counter," Appl. Phys. Letters, Vol. 23, p. 104 (1973).

‡J. R. Herrington, K. G. Sewell, and W. B. Volz, "A Thermal Imaging System Based on the $PrCl_3$ Quantum Counter," Appl. Phys. Letters, Vol. 26, p. 226 (1975).

TABLE 6

IRQC PARAMETERS*

Parameter	LTV	Varo
λ_{ir}, μm	4.55	4.8
λ_p, μm	0.53	0.546
λ_s, μm	0.645	0.645
$\Delta\lambda_{ir}$, μm	0.6	0.5
P_{43}	0.4	0.4
τ_2, msec	50	0.7
τ_4, μsec	--	8.5
σ_p, cm^2	10^{-20}	10^{-20}
σ_{ir}, cm^2	10^{-20}	10^{-20}
n_{ir}	1.9	1.9
N_1, cm^{-3}	1.5×10^{20}	10^{22}
A, cm^2	4	4
L, μ_m	300	300
Energy per pump pulse, mJ	--	30
τ_p, nsec	--	300

* Private communication.

a. Photon Conversion Efficiency for CW IRQC

The visible fluorescence from the $|4\rangle$ to $|3\rangle$ radiative transition constitutes the upconverted signal. From the definition of η_{IRQC} and Figure 18, it follows that

$$\eta_{IRQC} = \frac{P_{43}N_4/\tau_4}{W_{ir}N_1}\left(1 - e^{-\sigma_{ir}N_1L}\right) \quad . \tag{88}$$

The factor $(1 - e^{-\sigma_{ir}N_1L})$, where N_1 is the IRQC number density and L is the length, gives the percentage of incident IR photons that are absorbed by the IRQC in a length L. Thus, to determine η_{IRQC} it is necessary to solve Eqs. (82) through (85) for N_4 in terms of N_1. Under steady-state conditions, where

$$\frac{dN_1}{dt} = \frac{dN_2}{dt} = \frac{dN_3}{dt} = \frac{dN_4}{dt} = 0 \quad ,$$

One obtains

$$N_4 = \frac{\tau_4 W_{ir} N_1}{1 + \frac{1}{W_P\tau_2} - (P'_{42} + P_{42}) - (P'_{43} + P_{43}) + \frac{\tau_4}{\tau_2}} \quad , \tag{89}$$

where it is assumed that $(P'_{32} + P_{32}) \approx 1$, or that essentially all atoms excited to $|3\rangle$ decay to $|2\rangle$. From Eq. (88)

$$\eta_{IRQC} = \frac{P_{43}(1 - e^{-\sigma_{ir}N_1L})}{1 + \frac{1}{W_P\tau_2} - (P'_{42} + P_{42}) - (P'_{43} + P_{43}) + \frac{\tau_4}{\tau_2}} \quad . \tag{90}$$

We now consider Eq. (90) in the limits of low and high pump intensities.

When the pump intensity is low such that

$$\frac{1}{W_P\tau_2} \gg \left[1 - (P'_{42} + P_{42}) - (P'_{43} + P_{43}) + \frac{\tau_4}{\tau_2}\right]$$

then

$$\eta_{IRQC} = \frac{P_{43}\tau_2\sigma_P I_P \lambda_P}{hc}\left(1 - e^{-\sigma_{ir}N_1 L}\right) \quad . \tag{91}$$

Equation (91) shows that for low pump intensities, η_{IRQC} is a linear function of the lifetime of $|2>$, the pump absorption cross section, and the pump intensity.

When the pump intensity is high such that

$$\left[1 - (P'_{42} + P_{42}) - (P'_{43} + P_{43}) + \frac{\tau_4}{\tau_2}\right] \gg \frac{1}{W_P \tau_2} \quad ,$$

then

$$\eta_{IRQC} = \frac{P_{43}\left(1 - e^{-\sigma_{ir}N_1 L}\right)}{1 - (P'_{42} + P_{42}) - (P'_{43} + P_{43}) + \frac{\tau_4}{\tau_2}} \quad . \tag{92}$$

Equation (92) gives the saturated value for η_{IRQC}; that is, the pump is strong enough so that any further increase in pump intensity will not result in more net atoms being excited from $|2>$ to $|4>$.

b. Effective Photon Conversion Efficiency for the Pulsed IRQC

For less than saturating values of pump power, and pump pulse widths less than τ_4, the photon conversion efficiency on a per-pulse basis is given by Eq. (91). To derive the effective or time-averaged photon conversion efficiency for the pulsed IRQC, we consider the following model:

It is assumed that the IRQC material is always exposed to the incoming IR radiation. In the absence of a pump pulse, state $|2>$ is populated by absorption of the incident IR radiation, and depopulated by the normal decay processes associated with its finite lifetime. The

steady-state population of $|2\rangle$ in the absence of a pump will depend only upon the lifetime of $|2\rangle$, the IR absorption cross section, the incident IR flux, and the ground-state population. The IRQC is then irradiated by a pump pulse of duration short compared to the lifetime of the state $|2\rangle$, causing atoms to be excited from $|2\rangle$ to $|4\rangle$. The atoms excited to $|4\rangle$ can then fluoresce and be detected as upconverted signal. If the time between pump pulses is greater than or equal to the lifetime of $|2\rangle$, it may be assumed that after being partially depleted by a pump pulse, $|2\rangle$ will reach its steady-state value before the next pump pulse occurs.

The effective photon conversion efficiency, η_{IRQC}^{eff}, may be obtained by considering the time-dependence of states $|2\rangle$ and $|4\rangle$. Under the assumptions that the ground-state population remains constant, a fast $|3\rangle$ to $|2\rangle$ nonradiative transition, and that thermal mixing may be neglected, in the absence of a pump the set of rate equations reduce to

$$\frac{dN_2}{dt} = -\frac{N_2}{\tau_2} + W_{ir}N_1 \quad , \tag{93}$$

with the steady-state solution

$$N_2 = \tau_2 W_{ir} N_1 \quad . \tag{94}$$

We now consider the time-dependence of $|4\rangle$ when the IRQC is subjected to a pump pulse of duration τ_P. N_4 is assumed to be unpopulated prior to the pulse, and N_2 is taken to be constant with its steady-state value, since the percentage of atoms excited to $|4\rangle$ is expected to be small. The set of rate equations reduces to

$$\frac{dN_4(t)}{dt} = -\frac{N_4(t)}{\tau_4} + W_P N_2 - W_P N_4 \quad . \tag{95}$$

If a step-function pump is turned on at $t = 0$, then the time-dependence of $|4\rangle$ is given by

$$N_4(t) = \frac{W_P\tau_4 N_2}{W_P\tau_4 + 1}\left[1 - e^{-t(W_P\tau_4+1)/\tau_4}\right] \quad . \tag{96}$$

For small x, $e^{-x} \approx 1 - x$, and thus for a pump pulse of length τ_P such that $\tau_P(W_P\tau_4 + 1) \ll \tau_4$, Eq. (96) may be approximated by

$$N_4(\tau_P) = W_P\tau_P N_2 \quad . \tag{97}$$

For the Varo IRQC (see Table 6),

$$(W_P\tau_4 + 1)\tau_P/\tau_4 \approx 0.05 \quad , \tag{98}$$

so that the preceding approximation may be considered valid. The percentage of atoms excited to $|4>$ by a single pump pulse of length τ_P is

$$\frac{N_4(\tau_P)}{N_2} \approx W_P\tau_P$$

$$= 2 \times 10^{-4} \quad , \tag{99}$$

where the fluorescent loss during the time the pulse irradiates the IRQC has been neglected, since the fluorescent lifetime is much longer than the pulse length τ_P. Thus, N_2 does remain constant to a very good approximation. For repeated pulsing, the depletion in N_2 will never be greater than the above value, provided that the pulse repetition rate is less than or equal to 1/0.7 msec, where 0.7 ms is the lifetime of $|2>$, since $|2>$ will have time to reestablish its steady-state value between pump pulses.

For the pulsed IRQC

$$\eta_{IRQC}^{eff} \triangleq \frac{\text{number of IR photons upconverted to visible photons per second}}{\text{number of IR photons incident per second}}$$

$$= \frac{(PPS)P_{43}N_4(\tau_P)}{W_{ir}N_1}\left(1 - e^{-\sigma_{ir}N_1 L}\right) \quad , \tag{100}$$

where (PPS) is the number of pump pulses per second. Employing Eqs. (87), (94), and (97), we obtain

$$\eta_{IRQC}^{eff} = \frac{P_{43}\tau_2\sigma_P I_P \lambda_P}{hc}\,\Gamma\left(1 - e^{-\sigma_{ir}N_1 L}\right) , \qquad (101)$$

with $\Gamma = (PPS)\tau_P$ the duty cycle factor, and I_P the instantaneous pump intensity. Equation (101) may be rewritten as

$$\eta_{IRQC}^{eff} = \frac{P_{43}\tau_2\sigma_P \lambda_P}{hc}\, I_P^{average}\left(1 - e^{-\sigma_{ir}N_1 L}\right) , \qquad (102)$$

where $I_P^{average} = I_P\Gamma$ is the average pump power.

In the case of the pulsed IRQC developed by Varo, an additional consideration enters into the efficiency of upconversion. Varo has observed a large, nonsignal, pump-induced fluorescence of a lifetime approximating 50 ns, which interferes with the upconverted signal to be observed. Since the pump-induced background fluorescence has a much shorter time constant than the upconverted signal fluorescence, Varo found it possible to discriminate against the pump-induced background by gating the detection system off for approximately 1.5 μs after the end of the pump pulse. The upconverted signal fluorescence is collected when the detection system is gated on from approximately 1.5 μs after the pump pulse to about 20 μs. The time discrimination collection efficiency is then defined as

$$\eta_{TD} = \frac{\text{upconverted signal fluorescence collected while detection system gated on from 1.5 μs to 20 μs}}{\text{total upconverted signal fluorescence}} .$$

Assuming, as before, a square pump pulse that turns off abruptly at τ_P, we can calculate the decay from the rate equation

$$\frac{dN_4(t)}{dt} = -\frac{N_4(t)}{\tau_4} \quad . \tag{103}$$

Taking the initial population to be $N_4(\tau_P) = W_P \tau_P N_2$, we find that

$$N_4(t) = N_4(\tau_P)\, e^{-(t-\tau_P)/\tau_4} \quad . \tag{104}$$

Therefore

$$\eta_{TD} = \exp\left[-t_{on}/\tau_4\right] - \exp\left[-t_{off}/\tau_4\right] \quad , \tag{105}$$

where t_{on} and t_{off} are the times at which the detection system is gated on and off, respectively, after the end of the pump pulse. For t_{on} = 1.5 μs, t_{off} = 20 μs, and τ_4 = 8.5 μs (Table 6), η_{TD} = 0.74.

C. NONLINEAR CRYSTALS

Nonlinear crystal upconversion has been rather thoroughly studied and reviewed.* The photon conversion efficiency in a nonlinear crystal is given by

$$\eta_{crystal} = \frac{128\pi^3 \omega_s \omega_{ir} d_{eff}^2}{10^{-7} c^3 n_s n_p n_{ir}} \left(\frac{P_p}{A}\right) L^2 \frac{\sin^2\left(\frac{1}{2}\,|\vec{\Delta k}|L\right)}{\left(\frac{1}{2}\,|\vec{\Delta k}|L\right)^2} \quad , \tag{106}$$

where d_{eff} is the effective nonlinear coefficient, P_p/A is the instantaneous pump intensity, $\vec{\Delta k} = \vec{k}_s - \vec{k}_{ir} - \vec{k}_p$ is the momentum mismatch, L is the crystal length, and n_s, n_p, n_{ir} are the indices of refraction at the sum, pump, and IR wavelengths. P_p/A has the unit watts cm^{-2}; all other units are cgs.

---

*A. Fenner Milton, "Upconversion--A Systems View," Appl. Optics, Vol. 11, p. 2311 (1972).

Equation (106) neglects saturation, which is justified for crystals at power densities of 10^6 W cm^{-2}. Equation (106) also assumes plane-wave interactions and no Poynting vector walk-off. The important parameters are the nonlinear coefficient, the pump intensity, and the active crystal length.

The acceptance angle and bandwidth of the crystal upconverter is maximized for noncritical phase-matching. Because of the birefringent effects, exact expressions for the acceptance angle and bandwidth for the thermal imaging case are difficult to obtain. However, the external acceptance angle at a single IR frequency for tangential phase-matching allowing for a phase mismatch of $|\Delta k| = (\pi/L)$ at the center of the field of view is given approximately by

$$\alpha = 2\sqrt{\frac{2n_{ir}\lambda_{ir}}{L}} \tag{107}$$

The bandwidth over which upconversion is possible depends upon the dispersion in the crystal and is usually very small except under special circumstances when for a specific pump and IR wavelengths the dispersion of the sum and IR can be matched.*

The values of the parameters for the three nonlinear crystals, $LiNbO_3$,† Ag_3AsS_3,‡,§,** and $ZnGeP_2$,†† are listed in Table 7.

---

*J. E. Midwinter, "Infrared Up Conversion in Lithium-Niobate with Large Bandwidth and Solid Acceptance Angle," Appl. Phys. Letters, Vol. 14, p. 29 (1969).

†S. E. Harris, "Tunable Optical Parametric Oscillators," Proc. IEEE, Vol. 57, p. 2096 (1969).

‡K. F. Hulme et al., "Synthetic Proustite (Ag_3AsS_3): A New Crystal for Optical Mixing," Appl. Phys. Letter, Vol. 10, p. 133 (1967).

§J. Jerphagnon and S. K. Kurtz, "Optical Nonlinear Susceptibilities: Accurate Relative Values for Quartz, Ammonium Dihydrogen Phosphate, and Potassium Dihydrogen Phosphate," Phys. Rev. B, Vol. 1, p. 1739 (1970).

**R. Byer and S. E. Harris, "Power and Bandwidth of Spontaneous Parametric Emission," Phys. Rev., Vol. 168, p. 1064 (1968).

††G. D. Boyd, E. Buehler, and F. G. Storz, "Linear and Nonlinear Optical Properties of $ZnGeP_2$ and CdSe," Appl. Phys. Letter, Vol. 18, p. 301 (1971).

TABLE 7

NONLINEAR CRYSTAL PARAMETERS

Parameter	Value		
	$LiNbO_3$*	Proustite†,‡,§	$ZnGeP_2$**
λ_{ir}, μm	2.9	10.6	10.6
λ_p, μm	1.06	1.06	1.06
λ_s, μm	0.78	0.96	0.96
$\Delta\lambda_{ir}$, μm	0.02	0.05	0.02
n_{ir}	2.1	2.68	3.07
$d^2_{eff}/n_{ir}n_p n_s$, cgs units	2.2×10^{-17}	1.6×10^{-16}	2.2×10^{-15}

*S. E. Harris, "Tunable Optical Parametric Oscillators," Proc. IEEE, Vol. 57, p. 2096 (1969).

†K. F. Hulme et al., "Synthetic Proustite (Ag_3AsS_3): A New Crystal for Optical Mixing," Appl. Phys. Letter, Vol. 10, p. 133 (1967).

‡J. Jerphagnon and S. K. Kurtz, "Optical Nonlinear Susceptibilities; Accurate Relative Values for Quartz, Ammonium, Dihydrogen Phosphate, and Potassium Dihydrogen Phosphate," Phys. Rev. B, Vol. 1, p. 1739 (1970).

§R. Byer and S. E. Harris, "Power and Bandwidth of Spontaneous Parametric Emission," Phys. Rev., Vol. 168, p. 1064 (1968).

**G. D. Boyd, E. Buehler, and F. G. Storz, "Linear and Nonlinear Optical Properties of $ZnGeP_2$ and CdSe," Appl. Phys. Letter, Vol. 18, p. 301 (1971).

To obtain an upconversion efficiency for thermal imaging, a procedure analogous to that used in the metal-vapor case should be employed to take into account the variations in Δk due to differing angles of arrival and IR wavelengths. In this report, however, it will be assumed that the crystal upconverts at its peak efficiency for $\Delta k = 0$ over the entire frequency bandwidth and angles of arrival shown in Table 7. It is realized that this is an optimistic approximation, but it will be seen that it makes little difference to the relative ranking of the various methods.

D. INFRARED PHOTODETECTORS

Direct detection of infrared radiation using cooled photovoltaic and photoconductive semiconductor detectors has been highly developed. For the purpose of comparative evaluation, the important material parameters are the quantum efficiency and the IR wavelength band over which the material has adequate sensitivity. The values of D^* shown in Table 8 for several materials were obtained from the data sheets of manufacturers. The corresponding values of quantum efficiencies are also noted. It is seen that the quantum efficiencies are in the range 0.3 to 0.7. These detectors are sensitive to radiation below their cut-off wavelength, with efficiencies of the same order. The atmospheric transmission bands usually limit their usefulness. All these detectors (except PbS) have response times less than a microsecond so that they can be used in TV-compatible FLIR systems.

TABLE 8

CHARACTERISTICS OF INFRARED DETECTORS

Material	Mode of Operation		Cut-Off Wavelength λ_2, μm	Detectivity at Cut-Off for 180° FOV, 300°K Background $D^*(\lambda_2)$, $cmHz^{1/2}W^{-1}$ Actual		Ideal[a]	Quantum Efficiency
InAs	PV	77°K	3	4×10^{11}	(b)(c)	1.3×10^{12}	0.3
PbS	PV	193°K	3	7×10^{11}	(b)(c)	9×10^{11}	0.78
InSb	PV	77°K	5	1×10^{11}	(b)(c)	1.4×10^{11}	0.71
HgCdTe	PC	77°K	12 (variable)	$1\text{-}2 \times 10^{10}$	(b)(c)	3.5×10^{10}	~0.5
	PV	77°K	12	3×10^{10}	(d)	5×10^{10}	0.6
PbSnTe	PV	77°K	12	2×10^{10}	(c)	5×10^{10}	0.4

Note: PV = photovoltaic
PC = photoconductive

(a) R. D. Hudson, Jr., Infrared System Engineering, p. 322 (John Wiley and Sons, New York, New York, 1969).

(b) Santa Barbara Research Center Data Sheet.

(c) Raytheon Data Sheet.

(d) Eltek Data Sheet.

SECTION IV

EXPECTED PERFORMANCE OF INFRARED IMAGING SYSTEMS

Drawing on the developments in the earlier sections, an evaluation is made in this section of the comparative performance of passive and active IR imaging systems based on the different approaches. The comparisons are based on practical system designs. It is assumed that a television display operating at normal frame rates will be used, so that each resolution element will be integrating for 1/30th of a second.

The various factors contributing to the efficiency of the system are discussed first. Thermal imaging system designs are then presented, accompanied by calculations of their system conversions efficiencies and noise-equivalent temperature differences. Active imaging systems using range-gated detection are then discussed. The expected signal-to-noise ratios are calculated.

Finally, other considerations in evaluating the desirability of these methods are discussed. These include the special requirements of each technique, such as pump sources and the feasibility of satisfying them, as well as estimates of the power requirements and complexity of the systems.

A. SYSTEM UPCONVERSION EFFICIENCY

The upconverter systems may be looked upon as converters of the incoming IR photons into photoelectrons from the photocathode of a low-light-level television camera. The NETD (or SNR) of these IR detection systems has been shown to depend on the IR bandwidth of the device and the quantum efficiency of the upconversion system, η, which is defined as the ratio of the number of electrons in the output of the detection

system to the number of IR photons collected from the field of view. This overall efficiency is influenced by the efficiencies of the various components in the system:

(1) Upconverter efficiency, η_{xx}: The ratio of the number of sum frequency photons produced by the upconverting medium to the number of IR photons incident on it is the efficiency of the upconverter in each case. Expressions for the upconversion efficiency of the different methods have been obtained in the previous section.

(2) Transmission efficiency, η_{opt}: The various optical components in the systems cause some loss in the IR as well as the sum frequency photons. For the purpose of this comparison, the transmittance of all optical components (except pump filters) will be taken to be unity. In the case of metal vapors, there is an additional loss of the sum frequency due to absorption by the metal vapor as discussed in Section III.

(3) Collection efficiency, η_{coll}: In the properly designed Type III coherent upconversion system, all the sum frequency radiation is collected (except for transmission losses). Thus the collection efficiency is unity for these systems. In the IRQC system, only a portion of the sum radiation emitted over 4π steradians can be collected and this loss must be taken into account. In the case of scanning FLIR systems there is a somewhat analogous loss due to scanning inefficiencies. When focal-plane arrays are used, the radiation incident on the insensitive areas separating the individual sensors in the mosaic will be lost.

(4) Duty-cycle efficiency, η_{duty}: The metal-vapor and the crystal upconverters as well as the pulsed IRQC use high peak-power pulsed lasers. Upconversion occurs only when the laser pulse is on. If P_p/A is the peak power density required to obtain the conversion efficiency, η_{xx}, and the desired average laser power is P_{av}, then it is approximately true that $\eta_{duty} = P_{av}/P_p$. In the case of the metal vapors, when pump phase-matching with two pump beams derived from the same laser, an additional factor of 0.5 must be used.

For the pulsed IRQC, using time discrimination to reduce noise, a further reduction in useful upconverted output results and is accounted for by the factor η_{TD}. It should be noted that this procedure for pulsed systems, is equivalent to increasing the electronic bandwidth of the detector.

(5) Efficiency of upconversion of different polarizations, η_{pol}: In nonlinear crystals, phase-matched upconversion is feasible only for one polarization of the incoming IR or $\eta_{pol} = 0.5$ for thermal imaging. Cesium vapor upconverts both polarizations equally well so that $\eta_{pol} = 1$, but sodium vapor upconverts the IR component parallel to the laser polarization with four times the efficiency of the orthogonal component with the result that $\eta_{pol} = 0.625$* for thermal imaging. For active imaging, $\eta_{pol} = 1$ in all cases if the backscattered radiation may be assumed to be not depolarized.

(6) Transmission of the pump filter, η_{filter}: The spectral filters used to remove the pump from the sum radiation prior to imaging also attenuate the sum radiation to a degree, depending on the narrowness of the pass band. It is believed that narrow-band-pass filters with transmissions on the order of 0.8 and with sufficient attenuation for the pump leakage can be obtained for all upconverters.

(7) Photodetector efficiency, η_{pd}: The final stage in the IR detection process is the conversion of the sum frequency photons into electrons in the visible detector. The quantum efficiencies of photodetector materials are strongly dependent on the wavelength of the radiation. The values chosen are for the best available photodetectors with low dark currents at the sum wavelength. These efficiency values may be increased considerably if image intensification can be used. The limitations of detectors for low-light-level imaging have been discussed by Milton.†

---

*E. A. Stappaerts, "Dependency of Susceptibilities on Polarization," Internal Memorandum, Hansen Microwave Laboratory, Report No. 2438, Stanford University (May 1975).

†A. Fenner Milton, "Upconversion--a Systems View," Appl. Optics, Vol. 11, p. 2311 (1972).

AD-A036 211 STANFORD RESEARCH INST MENLO PARK CALIF F/G 17/5
EVALUATION OF TECHNOLOGIES FOR INFRARED IMAGING.(U)
NOV 76 K S KRISHNAN, J S OSTREM F33615-75-C-1142
UNCLASSIFIED AFAL-TR-76-82 NL

2 OF 2
AD
A036211

END
DATE
FILMED
3-77

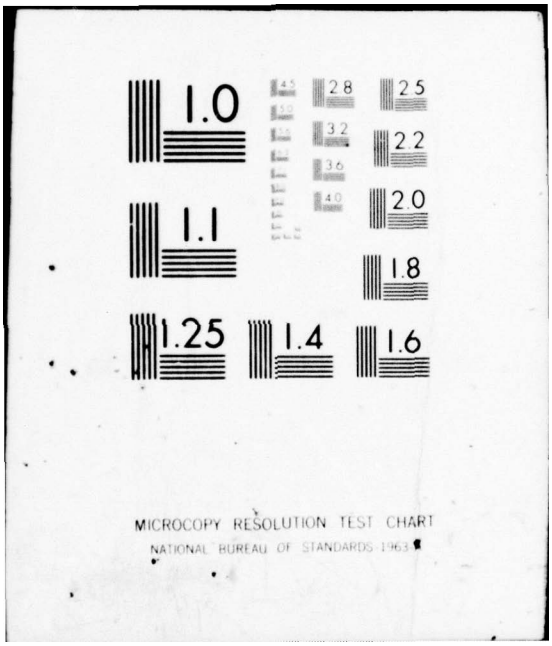
1.0
1.1
1.25
1.4
1.6
1.8
2.0
2.2
2.5
2.8
3.2
3.6
4.0
4.5
MICROCOPY RESOLUTION TEST CHART
NATIONAL BUREAU OF STANDARDS 1963-A

The overall quantum efficiency of the upconversion system is therefore given by the product of the above efficiencies

$$\eta = \eta_{xx}\,\eta_{duty}\,\eta_{TD}\,\eta_{opt}\,\eta_{coll}\,\eta_{pol}\,\eta_{filter}\,\eta_{pd} \qquad (108)$$

B. COMPARISON OF DEVICES FOR THERMAL IMAGING

In designing upconversion systems, practical considerations limit the average laser power and the upconverter diameter. It was assumed that all the upconverters will use a maximum of 20 watts of average laser power and an upconverter diameter of 2 cm. For the purposes of comparison, a 10-cm collection aperture with an f-number of two was also used to guide the design. So as to complete the design of the systems, and provide an idea of the sizes of components and overall length, it was further assumed that the visible detector can provide on the order of 300 resolution elements, each of size 20 μm, along the diameter of the visible image. This approximates the capabilities of a television camera. In the case of the upconverters, the resolution of the device was matched to that of the detector. For the direct detection system, the image diameter was defined by 300 times the resolution of the detector. The image detector is assumed to integrate for 1/30th of a second, compatible with regular TV frame rates. These design choices are summarized in Table 9.

As already seen, the coherent upconverters have a limited acceptance angle due to phase-matching requirements and the IRQC has limitations on its resolution because of the thickness of the IRQC. These characteristics, along with the other choices made above, lead to limitations on the maximum field of view for the coherent upconverters and on minimum field of view (for a given number of resolution elements) for the IRQC. So as to provide a comparison with a competing technology, passive systems based on direct detection, operating in the two atmospheric IR windows, are described.

TABLE 9

DESIGN CHOICES FOR PASSIVE INFRARED IMAGING SYSTEMS

Collection aperture	D_1	10	cm
f-number of collection aperture	$\mathcal{F}_1$	2	
Upconverter diameter	d	2	cm
Resolution of visible detector	a_d	20	μm
Number of resolution elements along image diameter	N_r	~300	
Electronic bandwidth[(a)]		30	Hz
Average power of pump laser	P_{av}	20	watts

[(a)] The detection bandwidth corresponding to the pump pulse widths is included in the duty cycle efficiency.

1. Metal-Vapor Upconverters

In Table 10, the operating characteristics of cesium and sodium metal-vapor upconverters are collected together from the developments in Section III. From these and the design principles outlined in Table 2, the system design is completed as shown in Table 10. The field of view shown is obtained from the relation

$$\alpha_{ir} = \frac{1}{2\mathcal{F}_1}\left[\sqrt{(2+\mathcal{F}_1\alpha)^2 + \frac{8\alpha\mathcal{F}_1 d}{D_1}} - (2+\mathcal{F}_1\alpha)\right] . \qquad (109)$$

The maximum number of resolution elements is obtained from Table 4. In Table 11, the upconversion system efficiency is calculated and the NETD value obtained from Eq. (17a) is presented.

TABLE 10

PASSIVE METAL-VAPOR UPCONVERTER SYSTEM DESIGN

Parameter	Cesium	Sodium
Sum wavelength, λ_s°, μm	0.4556	0.3303
IR wavelength, λ_{ir}°, μm	2.93	9.10
IR bandwidth, $\Delta\lambda_{ir}$, μm	0.17	1.66
IR acceptance angle, α, degrees	14	20
Upconversion efficiency on a pulse basis, η_{MV}	0.2	0.2
Pump power density, (P_p/A), MW cm^{-2}	2.21	5.72
Pump phase-match angle, Ø, degrees	2	1.5
Vapor length, L, cm	1	1
Vapor atomic density, N, cm^{-3}	10^{18}	10^{18}
Temperature of vapor, T, °K	782	974
Laser linewidth, $\Delta\bar{\nu}_{laser}$, cm^{-1}	0.1	0.1
Pump pulse width, τ_p, nsec	96	37
Pump pulse rate, Hz	30	30
Collection aperture, D_1, cm	10	10
Field of view, α_{ir}, degrees	2.18	2.86
Maximum number of resolution elements along diameter of field of view, N_r	754	318
D_2,[(a)] cm	2.44	2.57
f_2, cm	3.12	2.86
D_3, cm	2.44	2.57
f_3, cm	39.7	50.2

[(a)] These symbols refer to dimensions in Figure 4.

TABLE 11

PERFORMANCE OF METAL-VAPOR UPCONVERTERS

Parameter	Cesium	Sodium
η_{MV}	0.2	0.2
η_{duty}	1.44×10^{-6}	0.55×10^{-6}
η_{opt}	0.85	0.91
η_{coll}	1	1
η_{pol}	1	0.625
η_{filter}	0.8	0.8
η_{pd} (Bialkali)	0.22	0.26
System upconversion efficiency, η	4.3×10^{-8}	1.3×10^{-8}
D^{**}_{BLIP}	1.83×10^{12}	7.29×10^{10}
$\frac{\partial W}{\partial t}$	7.38×10^{-7}	5.48×10^{-5}
NETD per resolution element	456°K	9.23°K

In the design of the system, the metal vapor cell diameter forms a major constraint. From Eq. (109), it is evident there is a trade-off between the field of view, upconverter diameter, and the collection diameter (or angular resolution). It turns out that the smaller f-numbers are preferable. Increasing the angular resolution can only be done at the expense of the field of view, if the upconverter diameter is constant. Metal-vapor-cell apertures much larger than 2 cm do not seem practical, using a heat-pipe oven.

As is evident from Eq. (17b), the NETD value does not depend on the system parameters but mainly on the conversion efficiency and the IR bandwidth. Increasing the pump power or the metal-vapor pressure and/or decreasing the laser linewidth will increase the conversion efficiency. However, the value used in these calculations is already high (0.2) and therefore much improvement is unlikely. As shown in Table 11, the major inefficiency arises from the duty cycle factor, which resulted from the average power limit imposed. The quadratic dependence of efficiency on power density argues for even shorter pulses. It appears that an attractive way to significantly improve system performance will be to recirculate the pump through the upconverter. Since pump depletion is insignificant under the assumed conditions, considerable improvement in duty cycle and NETD may be achieved.

2. CW-and Pulsed-IRQC Devices

In Table 12, the characteristics of the CW- and pulsed-IRQC upconverters developed by LTV Advanced Technology Center and Varo, Inc., respectively, and discussed in Section III, are summarized. The design of the upconversion system guided by the initial choices is also presented.

Since the thickness (and diameter) of the IRQC is assumed to be the same in both the CW and pulsed versions, the design is the same for both. An f/1 system is used to collect the upconverted radiation. The angular resolution of the IRQC is poor, due to the thickness of the material and is given by the relation in Table 4. The design has to ensure that the required number of resolution elements are indeed available in the field of view.

In Table 13, the upconversion system efficiency is calculated along with NETD for the CW- and pulsed-IRQC devices. The IR bandwidth used is smaller than the respective IR absorption bandwidths because of

TABLE 12

IRQC UPCONVERTER SYSTEM DESIGN

Thickness of IRQC	L	300	μm
Diameter of IRQC	d	2	cm
Refractive index	η	1.9	
Collection aperture	D_1	10	cm
f-number of apertures	$\mathcal{F}_1$	2	
	$\mathcal{F}_2$	1	
Magnification factor	m	3.33	
Minimum angular resolution		1.65×10^{-2}	degrees
Desired number of resolution elements	N_r	300	
Field of view for 300 resolution elements		4.96	degrees
	f_1	20	cm
Choose	D_2 [(a)]	5	cm
	f_2	5	cm
	S_2	21.7	cm
	S_2'	6.5	cm

[(a)] These symbols refer to dimensions in Figure 4.

TABLE 13

PERFORMANCE OF IRQC UPCONVERTERS

Parameter	CW (LTV)	Pulsed (Varo)
Average pump laser power, P_{av}, W	20	20
Energy per pump pulse, mJ	--	33.3
Pump pulse width, τ_p, ns	CW	300
Pump pulse rate, Hz	--	600
Area to be pumped, dL, cm^2	6×10^{-2}	6×10^{-2}
Pump power density, W cm^{-2}	333	1.85×10^{6}
$\eta_{IRQC}\ \eta_{duty}$	7.8×10^{-3}	2.5×10^{-3}
η_{TD}	--	0.74
η_{opt}	1	1
$\eta_{coll} = 1/\left[4n_s\mathcal{F}_2(1 + m)\right]^2$	9.22×10^{-4}	9.22×10^{-4}
η_{pol}	1	1
η_{filter}	0.8	0.8
η_{pd} (at 0.645 μm) GaAs	0.14	0.14
System upconversion efficiency η	8.1×10^{-7}	1.86×10^{-7}
IR bandwidth, $\Delta\lambda_{ir}$, μm	0.35	0.45
D^{**}_{BLIP}	2.67×10^{11}	2.11×10^{11}
$\partial W/\partial t$	1.79×10^{-5}	2.24×10^{-5}
NETD, °K	2.53	4.14

the overlap of atmospheric absorption. In both cases, an average power of 20 watts is used for the purposes of comparison. This is somewhat higher than the approximately half-watt power levels now used by LTV and Varo. However, the power density is still in the low-intensity region, so that Eq. (91) for the efficiency is still applicable for the CW device. In the pulsed case, the interval between pump pulses at 600 Hz is still larger than τ_2 (0.7 msec) so that Eq. (102) will still describe the efficiency. This interval also provides sufficient time for the time discrimination scheme used by Varo.

Improvement in the resolution of the IRQC devices may be obtained by using larger values of $\mathcal{F}_1$, $\mathcal{F}_2$, and d, and smaller values of L. Increasing $\mathcal{F}_1$ decreases the field of view and increasing $\mathcal{F}_2$ decreases collection efficiency. Larger IRQC diameters increase the field of view and improve the resolution. The IRQC (especially the polycrystalline variety) can be fairly readily made in sizes larger than 2 cm. Furthermore, the increased area would require a smaller increase in pump power in the edge-pumping configuration. However, resolution approaching the diffraction limit without degrading other qualities, requires small thickness of the IRQC, which must still absorb most of the infrared incident on it. While the Varo device absorbs about 95% of the infrared incident on it, the LTV version absorbs only about 5%. At constant average power, the resolution of the LTV device can be improved without sacrifice in efficiency (as long as the power density is well below saturation levels). The Varo device, on the other hand, must trade off efficiency for resolution.

The conversion efficiency of the devices can be improved by operation at higher average power. The efficiency of collection of the upconverted radiation may possibly be improved by depositing on the IR side of the IRQC a film that will transmit the infrared but will reflect

the upconverted radiation. Unfortunately, this will also result in additional loss in resolution. Higher doping of the crystal will improve the performance of the CW device, if other factors remain the same.

Since absorption of the pump is negligible, if the pump photons could be utilized over and over again, say by multiple reflections, the efficiency may be improved or the average power decreased. Since the process is incoherent and angular orientation of the pump is unimportant, pump recirculation may be easier to achieve than in the case of coherent upconverters.

3. Nonlinear Crystal Upconverters

The design of the upconverter system using nonlinear crystals shown in Table 14 is exactly analogous to the metal-vapor system. Since the efficiency is linear with power density, the actual pulse length and peak power are unimportant for this comparison as long as saturation can be neglected. However, the average power of 20 watts can accommodate a power density of 1 MW cm^{-2} and a pulse length of 212 ns. This power density is well below damage thresholds in crystals.

It is seen immediately that because of the smaller acceptance angles of the crystals, the fields of view are smaller also. Consequently, even though the upconversion method is capable of better angular resolution, the number of resolution elements is smaller than for the metal vapors.

A crystal length of 1 cm was assumed and the peak efficiency was used to calculate the NETD (Table 15). It is seen that even these optimistic results are considerably poorer than the other techniques. The major reasons for this poor performance are: (1) the very narrow acceptance bandwidth of the crystals; (2) the smaller conversion efficiency of the crystals; and (3) the smaller quantum efficiency of the near infrared photodetectors. Increased IR acceptance bandwidth may be possible

TABLE 14

NONLINEAR CRYSTAL UPCONVERTER SYSTEM DESIGN

Parameter	$LiNbO_3$	Ag_3AsS_3	$ZnGeP_2$
Sum wavelength, λ_s°, μm	0.78	0.96	0.96
IR wavelength, λ_{ir}°, μm	2.93	10.6	10.6
IR bandwidth, $\Delta\lambda$, μm	0.02	0.05	0.02
Crystal diameter, d, cm	2	2	2
Crystal length, L, cm	1	1	1
f-no. of collection aperture, $\mathcal{F}_1$	2	2	2
IR acceptance angle, α, degrees	4.02	8.64	9.24
Collection aperture, D_1, cm	10	10	10
IR field of view, α_{ir}, degree	0.74	1.47	1.55
Maximum number of resolution elements along diameter, N_r	362	198	210
D_2, cm [(a)]	2.15	2.30	2.32
f_2, cm	3.68	3.40	3.37
D_3, cm	2.15	2.30	2.32
f_3, cm	38.8	29.0	28.8

(a) These symbols refer to dimensions in Figure 4.

TABLE 15

PERFORMANCE OF NONLINEAR CRYSTAL UPCONVERTERS

Parameter	L_iNbO_3	Ag_3AsS_3	$ZnGeP_2$
$\eta_{crystal}\ \eta_{duty}$	3.23×10^{-7}	5.23×10^{-7}	7.19×10^{-6}
η_{opt}	1.0	1.0	1.0
η_{coll}	1.0	1.0	1.0
η_{pol}	0.5	0.5	0.5
η_{filter}	0.8	0.8	0.8
η_{pd}	0.11 (GaAs)[a]	0.04 (In GaAsP)[a]	0.04 (In GaAsP)[a]
System upconversion efficiency, η	1.4×10^{-8}	8.4×10^{-9}	1.2×10^{-7}
D^{**}_{BLIP}	5.24×10^{12}	4.19×10^{11}	6.61×10^{11}
$\frac{\partial W}{\partial t}$	7.38×10^{-7}	4.67×10^{-5}	4.67×10^{-5}
NETD, °K	3355	94.3	39.8

[a] Varian LSE.

in special cases when tangential phase-matching is achieved, but the acceptance angle will remain small in a birefringent crystal. Reduction of the crystal length to increase acceptance angle will result in decreased efficiency of upconversion. Increases in conversion efficiency may be obtained by increasing average pump power as well as by recirculation of pump power, under the limits imposed by crystal damage the threshold of which depends both on peak power density and average power.

4. Direct-Detection Imaging Systems

So as to facilitate comparison, direct-detection systems operating in the 3-to 5-μm and 8-to 12-μm atmospheric windows are shown in Table 16. Unfortunately, all the design choices in Table 9 cannot be simultaneously satisfied with the optical resolution matching the detector resolution. Therefore, the f-numbers of the receiving optics

TABLE 16

DIRECT-DETECTION IMAGING SYSTEMS

Parameter	3- to 5-μm		8- to 12-μm
Desired number of resolution elements along image diameter, N_r		300	
Size of detector, a_d, μm		20	
Diameter of collector, D_l, cm		10	
f-number of collector, $\mathcal{F}_l$	4.1		1.6
Field of view, α_{ir}, degree	0.84		2.1
Number of resolution cells to be scanned, R		7.1×10^4	
TV frame rate, Hz		30	
Bandwidth needed, MHz		2.1	
Detector	In Sb(PV)		HgCdTe(PV)
Quantum efficiency	0.7		0.6
D^{**}_{BLIP}	1.86×10^{11}		5.39×10^{10}
$\frac{\partial W}{\partial t}$	9.08×10^{-6}		5.03×10^{-5}
$\Delta\lambda_{ir}$, μm	2		4
NETD, °K	2.1		0.28

have been chosen to match the optical resolution to the detector size of 20 μm, which represents the present capabilities in detector fabrication.

A single detector operating in the photovoltaic mode is assumed to scan the circular field of view with 300 resolution elements along the diameter. The NETD values based on these assumptions are calculated for the two atmospheric windows at 3- to 5-μm and at 8- to 12-μm, assuming that they are totally transparent in these ranges. These are optimistic assumptions but they do not significantly change the relative performance of the systems.

The performance to be expected from a focal-plane array of detectors will evidently be very much superior to the above, because of the increased integration time available.

5. System Comparisons

The data on the performance of systems based on the several techniques and materials are summarized in Table 17. The values reported assume the design choices in Table 9. At the outset it is emphasized that the concept of NETD is strictly valid only for small temperature differences, hence a direct physical meaning cannot be given to the very large NETDs shown above. However, the NETD values may still be taken as a comparative, but qualitative, measure of performance. In making comparisons, it should be recalled that all the NETD values shown are calculated at the limiting resolution of the system and that low f-number optics have been used. Furthermore, the quantum counter is resolution-limited and the coherent upconverters are limited in field of view. It is difficult to arrive at and justify a single figure of merit for all these systems with so many variable parameters.

TABLE 17

COMPARISON OF THERMAL IMAGING SYSTEMS

Technique	Material	3- to 5-μm			8- to 12-μm		
		α_{ir}, degree	N_r	NETD, °K	α_{ir}, degree	N_r	NETD, °K
Direct detection	HgCdTe (PV)				2.1	300	0.28
	In Sb (PV)	0.84	300	2.1			
Quantum counter	CW (LTV)	4.96	300	2.53			
	Pulsed (Varo)	4.96	300	4.14			
Metal vapor	Sodium				2.86	318	9.23
	Cesium	2.18	754	456			
Nonlinear crystal	$ZnGeP_2$				1.55	210	39.8
	Ag_3AsS_3				1.47	198	94.3
	$LiNbO_3$	0.74	362	3355			

α_{ir} - Planar field of view

N_r - Number of resolution elements along diameter of field of view

NETD - Noise equivalent temperature difference

On the basis of these results, thermal imaging with crystals appears hopeless unless significant improvement in material properties are achieved. Imaging with sodium vapor is considerably better than with cesium. However, for thermal imaging only the quantum counters approach the NETD performance of direct detection devices, even though one must be satisfied with poor angular resolution. The IRQC appears to be suited for applications where large area coverage is needed without scanning the focal plane. The LTV device appears superior to the Varo version.

C. COMPARISON OF DEVICES FOR ACTIVE IMAGING

The upconversion methods considered above are now evaluated for imaging with active illumination (of course, there are no lumens in the IR!), using a pulsed laser illuminator and range gating as discussed in Section II. Such an application is not possible with a detector that must scan the focal plane.

The coherent upconverters that use a pulsed pump conveniently provide range gating if the illuminating and the pump pulses are properly synchronized. Since the system is sensitive to infrared only when the pump is present, the relations developed in Section II are applicable as long as the laser return pulse is longer than the pump pulse. The IRQC on the other hand is sensitive to infrared as long as it is exposed to infrared and for times short compared to τ_2 may be considered to integrate the IR radiation in both the CW-pumped and the pulse-pumped versions considered earlier. Range gating, of course, is not possible with such a device if the lifetime τ_2 is longer than the range gate. Thermal background and backscatter of the illuminator over long paths will obscure image information even from a compact target. An external shutter will be necessary in front of the IRQC for range-gating.

We now examine several system designs for active imaging and estimate their signal-to-noise ratios. We consider systems that can operate up to ranges of 3 km with a range gate of 150 meters, or upconverter pulse lengths on the order of 1 μsec. It will be assumed that a polarized laser illuminator irradiates only the field of view of the receiver. The laser return will be considered to retain its polarization. (In the signal-shot-noise-limited mode, where most of the devices will operate, this makes little difference to the SNR.) A peak power of 10 MW and a pulse width of 10 ns will be used for all the illuminator lasers. The average power of the illuminator and the pump laser will be limited to 20 watts each. The upconverter/receiver designs will be guided by choices similar to the passive systems. These characteristics of the active systems are collected together in Table 18. The systems designs follow principles similar to the case of passive imaging except for the introduction of cooled narrow-band filters centered at the illuminator wavelength to reduce thermal background. This may not be necessary for the nonlinear crystal upconverters that already have a narrow acceptance bandwidth.

1. Metal-Vapor Upconverters

While several possibilities exist for illuminator wavelengths in the case of each of the metal vapors, the calculations will be made for the $P_2(6)$ line of the DF-laser at 3.731 μm used with cesium and the P22 line (00°1 to 02°0 band) of the CO_2 laser at 9.569 μm used with sodium. These laser lines are reasonably close to the resonance with the respective vapors without any significant absorption. In addition, the transmittance of the atmosphere for these wavelengths is excellent.

The signal-to-noise ratio of the active imaging system depends on the factor $\sqrt{\eta\tau_d}$ [Eq. (23)] and the conversion efficiency depends quadratically on the pump power density. If the average pump power is limited

TABLE 18

DESIGN CHOICES FOR ACTIVE IMAGING SYSTEMS

Illuminator	
Peak power	10 MW
Pulse length	10 ns
Average power limit (Polarized laser illuminates only field of view of receiver)	20 watt
Receiver collection aperture	10 cm
f-number of collection aperture	2
Upconverter diameter	2 cm
Resolution of visible detector	20 μm
Pump laser	
Average power	20 watt
Pulse width	1 μsec
Range gate	150 m
Range of interest	3 km
Reflectance of target	0.001

and the pulse length is defined by the range gate, then the signal-to-noise ratio may be optimized by maximizing η^q where q is the number of pulses used to obtain the image. It may be shown that the optimum condition is that [see Eq. (46)]

$$L^2 \left[\kappa_{ir} \kappa_s + \left(\frac{\Delta k}{2} \right)^2 \right] = 1.357 \quad . \tag{110}$$

When pump phase-matching is used to obtain exact phase-matching on-axis ($\theta = 0$), then the optimum upconversion efficiency is 84%. The acceptance angle may be defined by a desired minimum efficiency. From Eq. (110), it is seen that the choice of the metal-vapor length determines the trade-off between pump power and acceptance angle. A length of 1 cm is chosen

for the present comparison and the acceptance angle for a minimum of 40% of the optimized conversion efficiency is calculated. The atom density, detuning, power density, and pump phase-matching angle at which this can be achieved is listed in Table 19.

TABLE 19

ACTIVE METAL-VAPOR UPCONVERTER SYSTEM DESIGN

Parameter	Cesium	Sodium
Illuminator wavelength, λ_{ir}, μm	3.731	9.569
Sum wavelength, λ_s, μm	0.4714	0.3309
Illuminator wavenumber, $\bar{\nu}_{ir}$, cm^{-1}	2,680	1,045
$\bar{\nu}^{\circ}_{ir}$, cm^{-1}	3,411	1,098
Detuning, $\Delta\bar{\nu}_3$, cm^{-1}	-731	-53
Atom density, N, cm^{-3}	10^{18}	10^{18}
Power density, (P_p/A), W cm^{-2}	1.5×10^6	3.5×10^5
Laser linewidth, cm^{-1}	0.1	0.1
Vapor cell length, L, cm	1	1
Acceptance angle, α, degrees	2.2	3.5
Phase matching angle, Ø, degrees	2.2	2.55
Collective aperture, D_1, cm	10	10
f-number of collection aperture, $\mathcal{F}_1$	2	2
Upconverter diameter, d	2	2
Field of view, α_{ir}, degrees	0.42	0.65
Number of resolution elements along diameter, N_r	114	69
D_2, cm[(a)]	2.09	2.14
f_2, cm	3.83	3.73
D_3, cm	2.09	2.14
f_3, cm	46.9	65.3

(a) These symbols refer to dimensions in Figure 4.

For the acceptance angles shown in Table 19, the minimum conversion efficiency is 34%. No significant absorption of the sum frequencies occurs in either of the cases considered. Further, if a polarized illuminator is used, the factor η_{pol} will be unity for both cases. The system efficiency as well as the SNR per resolution element obtained from Eq. (23) is shown in Table 20.

The pump pulse rate at which the required power density may be achieved within the 20-watt average power limit is shown in Table 20 as well as the improvement in SNR obtained by averaging over a second. It is seen that the average power of the illuminator is relatively small, since only a low pump pulse repetition rate is possible.

The interrelation between various parameters, such as field of view, number of resolution elements, upconverter area, power density, vapor pressure, and so on, are similar to the case of passive imaging.

2. Shuttered, Pulsed IRQC Device

As mentioned earlier, range-gated operation with the IRQC is possible only with an external shutter. (The CW device need not be considered further since it offers no advantages.) We now examine the quantum efficiency of the pulsed IRQC, assuming that a shutter provides the range gate and the pump pulse follows shortly after the shutter closes. If the gate is open for a time (~1 μsec) short compared to the lifetime τ_2 (0.7 msec) of the IRQC, and if the time between illuminator pulses (~5 ms) is larger than τ_2, then from Eq. (93), it can be shown that the population of level two when the shutter closes, is

$$N_2(\tau_\ell) = (W_{ir} + W_\ell)N_1\tau_\ell \quad . \tag{111}$$

Here, τ_ℓ is the pulsewidth of the laser return and it is assumed that the shutter is open only during this period.

TABLE 20

METAL-VAPOR UPCONVERTER SYSTEM PERFORMANCE

Parameter	Cesium	Sodium
Peak pump power, MW	4.66	1.11
Number of pulses per second limited by pump average power of 20 watts	2.2	9.0
Average power of illuminator, W	0.22	0.9
IR filter bandwidth, μm	0.1	0.1
η_{MV} (minimum)	0.34	0.34
η_{opt} (no absorption loss)	1.0	1.0
η_{coll}	1.0	1.0
η_{pol}	1.0	1.0
η_{filter}	0.8	0.8
η_{pc}	0.20	0.26
System upconversion efficiency, η (minimum)	5.44×10^{-2}	7.07×10^{-2}
SNR (per pulse)	17	47
(per second)	25	141

If the pump pulse of duration τ_p is synchronized to appear shortly after the shutter closed, then in a manner analogous to the derivation of Eq. (100), the conversion efficiency may be shown to be

$$\eta_{IRQC}^{eff,shuttered} = \frac{\tau_\ell}{\tau_2} \eta_{IRQC}^{eff,thermal} , \qquad (112)$$

where $\eta_{IRQC}^{eff,thermal}$ is given by Eq. (100). This result simply points out the absence of long integration times in the range-gated mode of operation.

The system design for the IRQC device for active imaging does not require any changes from that for the passive case listed in Table 12 except for the addition of a polarizer, a shutter, and a cooled IR filter centered at the illuminator wavelength. The device has an absorption band at 4.8 μm of width 0.5 μm. The atmosphere has good transmittance at several wavelengths in the 4.5- to 5.0-μm range, though significant absorption occurs at others. The choice of a laser illuminator wavelength should consider these factors. A CO laser is one of the candidates for such use. An illuminator wavelength of 4.8 μm is assumed for the performance estimation.

The pump laser characteristics remain the same as those in Table 13 for the passive case, except that the pulse repetition rate is now limited by the average power of the illuminator to 200 Hz. The various efficiencies as well as the SNR for a single pulse and for an averaging period of one second are shown in Table 21.

3. Nonlinear Crystal Upconverters

In the case of nonlinear crystal upconverters, optimization of the pump power under average power limitation leads to the result that low pump powers are preferable so that the power levels should be well away from saturation. This is in contrast to the case of the metal vapors where the optimum power levels resulted in operation well into the saturation region. This difference is a consequence of the linear-power-density dependence of the upconversion efficiency of nonlinear crystals. Therefore, no modifications are necessary to the passive systems described in Table 14 for use in the active mode. The IR acceptance bandwidths of the crystals shown in this table are very narrow and will be sufficient discrimination against background.

TABLE 21

PERFORMANCE OF SHUTTERED, PULSED IRQC

Energy per pump pulse	33.3 mJ
Pump pulse width	300 ns
Number of pulses per second limited by illuminator average power of 20 watts	200 Hz
Average pump power	6.7 W
IR filter bandwidth	0.1 μm
$\eta_{IRQC}^{shuttered} = \eta_{IRQC}^{thermal} \cdot \frac{\tau_\ell}{\tau_2}$	1.94×10^{-2}
η_{TD}	0.74
η_{opt}	1
$\eta_{coll} = 1/[4n_s\mathcal{F}_2(1 + m)]^2$	9.22×10^{-4}
η_{pol}	1
η_{filter}	0.8
η_{pd} (at 0.645 μm) GaAs	0.14
System upconversion efficiency, η	1.48×10^{-6}
SNR (per pulse)	1.75×10^{-2}
(per second)	0.25

Nonlinear crystals allow considerable freedom in the choice of the illuminator and pump compared to the metal vapors and the IRQC. In the case of the latter, the properties of the medium restrict the choice to narrow ranges. The crystals evidently must be transparent at the IR, pump, and sum frequencies and angle phase-matching should be possible at

the chosen frequencies. Usually the pump is determined by the availability of a high-peak-power laser. The illuminating wavelength should not be attenuated by the atmosphere. For estimating the performance of the system, the same IR and pump wavelengths shown in Table 14 will be used.

The pump power-densities will be kept to levels such that the peak efficiency for a 1-cm crystal length will be 10% so as to stay well below saturation and optimize SNR for a given average pump power. A minimum upconversion efficiency of 4% is then assumed over the acceptance angle. Since a polarized illuminator is assumed, η_{pol} is unity. Using the intrinsic IR acceptance bandwidths of the crystals, the SNR per pulse and when averaged over one second are shown in Table 22.

4. Direct-Detection Active-Imaging Systems

In this section we calculate the SNR of an active imaging system based on direct detection using a focal plane array of IR detectors for comparison with the other methods considered above. It is noted that such arrays are not yet generally available. The system is similar to the passive imaging case described in Table 17. A collection efficiency factor of 0.5 is used to account for the radiation falling on the spaces between the detectors in the array. Using the same illumination wavelength as in the case of the metal vapors (HF and CO_2 lasers), the SNR expected on a pulsed basis or averaged over a second is calculated in Table 23. It is seen that as in the case of the IRQC, the average power of the illuminator limits the pulse repetition rate.

5. System Comparisons

The characteristics of the foregoing systems are summarized in Table 24. It should be emphasized that because of the assumption that the illuminator irradiates only the receiver field of view, comparison

TABLE 22

PERFORMANCE OF NONLINEAR CRYSTAL UPCONVERTERS

Parameter	$LiNbO_3$	Ag_3AsS_3	$ZnGeP_2$
Peak pump power, W	6.19×10^6	3.82×10^6	2.78×10^5
Number of pulses per second limited by pump average power of 20 watts	3.23	5.23	71.9
Average power of illuminator, W	0.323	0.523	7.19
IR acceptance bandwidth, μm	0.02	0.05	0.02
$\eta_{crystal}$	0.04	0.04	0.04
η_{opt}	1.0	1.0	1.0
η_{coll}	1.0	1.0	1.0
η_{pol}	1.0	1.0	1.0
η_{filter}	0.8	0.8	0.8
η_{pc}	0.11	0.04	0.04
System upconversion efficiency, η	3.52×10^{-3}	1.28×10^{-3}	1.28×10^{-3}
SNR (per pulse)	1.2	2.1	2.2
(per second)	2.1	4.9	18.4

TABLE 23

DIRECT-DETECTION ACTIVE IMAGING SYSTEMS

IR wavelength, μm	3.731	9.569
Number of resolution elements	300	300
Field of view, degrees	0.78	2
Number of pulses per second limited by average power of illuminator, Hz	200	200
IR filter bandwidth, μm	0.1	0.1
Quantum efficiency	0.7	0.6
Collection efficiency	0.5	0.5
Effective efficiency, η	0.35	0.30
SNR (per pulse)	16	15.6
(per second)	226	220

TABLE 24

COMPARISON OF ACTIVE IMAGING SYSTEMS

		3- to 5-μm			8- to 12-μm		
Technique	Material	α_{ir}, degrees	N_r	SNR/s	α_{ir}, degrees	N_r	SNR/s
Direct detection	HgCdTe (PV)				2.0	300	200
	In Sb (PV)	0.78	300	226			
Metal vapor	Sodium				0.65	69	141
	Cesium	0.42	114	25			
Nonlinear crystals	$ZnGeP_2$				1.55	210	18.4
	Ag_3AsS_3				1.47	198	4.9
	$LiNbO_3$	0.74	362	2.1			
Quantum counter	Pulsed, shuttered	4.96	300	0.25			

of the signal to noise should weigh the field of view also. (In all the cases, signal-shot-noise-limited operation is obtained.) It is seen that the IRQC has very poor characteristics and the metal vapors are superior to the crystals. Evidently, the direct-detection method based on focal-plane arrays that are being developed is superior to all other methods considered. However, the sodium metal-vapor upconverter is significantly better than any of the other upconverters and its performance is quite good in comparison to the direct-detection method. Some improvement is also possible when very small fields of view are desired.

D. GENERAL DISCUSSION OF IR UPCONVERSION FOR IMAGING

It should be emphasized that the results presented in the preceding sections are projections based on the best available information. A good deal of experimental results exist for the crystals and IRQCs. The results of this study are generally in accord with these experimental results. However, being a very new development, there is not much experimental data available on the metal vapors considered. It is nevertheless believed that the results presented are realistic.

From these results it may be concluded that the direct-detection method is superior to any of the upconverters, at their present stage of development, for passive and active imaging. For thermal imaging, the IRQC appears to have the best current performance among the upconverters because of its ability to integrate the IR, even though its resolution is poor. However, IRQCs for the more interesting 8- to 12-μm range are not well investigated. The coherent upconverters suffer because of the very short duty cycles over which they are able to upconvert. Significant improvements in their performance would result if the duty cycle could be improved.

For active imaging, where the IR acceptance bandwidth is not important, the gap between direct detection with focal-plane arrays and upconversion is very much smaller. The expectations, especially for sodium vapor, are very encouraging and can be improved considerably by developing techniques for recirculating the pump laser. Development of techniques for intracavity upconversion will reduce pump-laser-power requirements. The IRQC is not expected to be useful for active imaging. Nonlinear crystal upconverters do not appear to be competitive with metal vapors for either active or passive imaging.

The comparisons on Tables 17 and 24 are relative performance figures when the average power of the pump is limited. If ultimate performance, regardless of the pump power, is desired, the metal vapors offer the best potential among the upconversion techniques investigated. This is especially true of active imaging where performance approaching focal-plane-array detectors can be easily achieved.

Metal vapors can withstand high power densities without damage and present no particular problem in material preparation or obtaining uniformity over the field of view. Material or detector preparation plays a significant role in the other three techniques. However, both the pump and the IR wavelengths must closely match the energy level structure of the material, whereas nonlinear crystals are limited only by intrinsic absorptions. So as to take maximum advantage of the resonance denominator in metal vapors, the pump must be chosen to match the ω_{02} transition exactly. In the case of sodium, this requires a pump at 0.6856 μm and for cesium at 1.079 μm. For sodium, a parametric oscillator or a dye laser (using Cresyl violet) are possible pump sources. For cesium, experimenters at Stanford University* have been using the output from a temperature-

*E. A. Stappaerts, Stanford University, Private Communication.

tuned Nd:YAlO laser. Recently a new laser host material, lanthanum beryllate, has been announced by workers at Allied Chemical Company.* Nd-doped lanthanum beryllate has been observed to lase at 1.079 μm with nearly three times the efficiency of Nd:YAG, and appears ideally suited for use with cesium.

The efficiencies of lasers of the above type are in the neighborhood of 0.5 to 1%. Therefore, an average pump power requirement of 20 watts implies an input power of 2 to 4 KW for the pump lasers of all the upconversion systems described above. The total power requirement of the systems would not be significantly larger than this figure, since other requirements, such as the electronics or the heat-pipe oven, are small compared to the laser input power.

The system descriptions and detailed designs presented earlier give an idea of the size and complexity of the various systems. The optical systems for the upconverters are definitely more complicated than those for the direct detectors, though the absence of scanning and cooling are compensatory advantages. Even though cooling will have to be provided, the IRQC for thermal imaging appears to offer the most potential for compact design because of the end-pumping configuration. The Type III systems for the coherent upconverters will necessarily be longer than the other optical systems. All the upconverters will need in addition a low-light-level television system to detect the upconverted image. The major contributor to the size and weight of the upconverter systems will be the pump laser and power supply. An optimistic estimate for a 3-kW power supply for a pulsed laser will be on the order of 50 to 100 lb. These comments on the size, complexity, and power consumptions do not compare

---

*R. C. Morris et al., "Lanthanum Beryllate: A New Rare-Earth Ion Laser Hose," Appl. Phys. Letter, Vol. 27, p. 444 (1975).

favorably with the state-of-the-art FLIR systems, which typically weigh around 10 lb and use about 1 kW of power. However, direct-detection devices have gone through a long development and refinement procedure supported by technological advances in the related electronic device area. The upconverters have not had these advantages.

SECTION V

CONCLUSIONS AND RECOMMENDATIONS

In the earlier sections of this report, four different approaches to infrared detection and imaging have been examined. They were parametric upconversion in alkali metal vapors and nonlinear crystals, upconversion with infrared quantum counter materials, and direct detection of infrared using cooled semiconductor detectors.

Parametric upconverters have the following inherent characteristics. They require a coherent pump source and they are sensitive to the infrared only when the pump is on. Materials now available require a high power density for efficient upconversion, therefore parametric methods can upconvert only a small fraction of CW infrared radiation. (There is no mechanism for storage of the infrared photons.) The parametric process also restricts the IR bandwidth and angular acceptance of the radiation to be upconverted. The optical anisotropy of crystals further restricts these characteristics. The isotropic metal vapors are much superior to crystals in the accepted range of angles and wavelengths of the infrared radiation. A technique, called pump phase-matching, to improve the performance of metal vapors, was described earlier. The efficiency of upconversion depends on the pump power density, linearly for crystals, quadratically for metal vapors. If the average pump power is limited, this results in operation well away from saturation for crystals and in the saturation region for metal vapors. Image resolution of parametric upconverters can approach the diffraction limit with proper optical design.

The infrared quantum counter action is an incoherent process and has a significant difference in its ability to store infrared photons over a

period approximating the lifetime of the level from which the pumping takes place. The IRQC has competitive upconversion efficiency only because of this ability. The IR bandwidth of the IRQC is determined by its absorption bandwidth. There are no intrinsic limits on the angle of acceptance. The two major drawbacks of the method are its poorer resolution capability, which is related to the thickness of the crystal, and the difficulty in collecting efficiently the upconverted radiation, which is incoherently emitted in all directions.

The performances of practical systems based on these methods were compared against the state-of-the-art direct-detection devices for passive imaging. In the case of active imaging, they were compared against focal-plane array devices that are still under development. Direct detection is superior to all the upconverters considered at their present stage of development for thermal imaging. This is because of the smaller IR bandwidths of upconverters and their inability to effectively upconvert all of the incident infrared. The IRQC appears to be the best among upconverters for thermal imaging. It can be a low-cost, large field-of-view device when its low resolution is not a significant drawback. Sodium vapor appears to have the best prospects for thermal imaging among the several parametric upconverters considered. The nonlinear crystals considered are significantly poorer than the other approaches for thermal imaging.

The relative merits for active imaging present a different structure. The small IR bandwidths and duty cycles are no longer important. The performance of the sodium vapor upconverter approaches what may be achievable with direct detection using focal-plane arrays (which are not yet available). Cesium vapor and the nonlinear crystal upconverters are also better than the IRQCs, which are estimated to be so poor that they are not expected to be useful for active imaging.

Keeping in mind that the direct-detection devices have been under development for several decades assisted by progress in the energetic and motivated electronics industry, the performance of the metal vapors and quantum counters are encouraging and certainly deserve further inquiry. The concept of metal-vapor upconversion is very recent and further experimental and theoretical work is needed. Image upconversion in metal vapors has not yet been demonstrated experimentally and the promising predictions of this report for sodium need verification in the laboratory. There can be no substitute for experimentation to improve on the predicted performance as well as to realize the practical limits thereof. Furthermore, of the very many atomic and molecular systems possible, only two, sodium and cesium, have been investigated in this report. Other, possibly more efficient, systems may exist and should be discovered and examined.

In the case of IRQC, discovery and development of materials with high absorption and conversion efficiency, especially in the 8-to 12-μm region appear to be the best immediate goals. The design of practical and compact systems to improve collection efficiency is important. As is well-appreciated in the upconversion community, improvement in the performance of nonlinear crystal systems will come only with considerable improvement in materials.

Upconversion, in all cases, will benefit from the development of better photocathodes and more efficient use of the laser pump, since the latter is the major source of power consumption. In this category must be included development of efficient lasers, of intracavity techniques for upconversion, and design of pumping geometries that would allow recirculation of pump power.

REFERENCES

1. Andrews, R. A., "IR Image Parametric Up-Conversion," IEEE J. Quantum Electron., Vol. QE-6, p. 68 (1970).

2. Armstrong, J A., et al., "Interactions Between Light Waves in a Nonlinear Dielectric," Phys. Rev., Vol 127, p. 1918 (1962).

3. Bloembergen, N., "Solid State Infrared Quantum Counters," Phys. Rev. Letters, Vol. 2, p. 84 (1959).

4. Bloom, D. M., et al., "Infrared Upconversion with Resonant Two-Photon Pumped Metal Vapors," Appl. Phys. Letters, Vol. 24, No. 9, p. 427 (May 1974).

5. Boyd, G. D., E. Buehler, and F. G. Storz, "Linear and Nonlinear Optical Properties of $ZnGeP_2$ and CdSe," Appl. Phys. Letter, Vol. 18, p. 301 (1971).

6. Brown, M. R., and W. A. Shand, "The Quantum Counter," in Advances in Quantum Electronics, Vol. 1, pp. 1-76 (Academic Press, New York, New York, 1970).

7. Byer, N. E., "Noise Considerations for Infrared Quantum Counters: the Oxygen-Fired $CdF_2 : E^3$ + IRQC," J. Appl. Phys., Vol. 43, p. 3567 (1972).

8. Byer, N. E., et al., "IRQC Parameters for Er^{3+} Occupying Sites of C_2v and C_3v Symmetry in CdF_2," J. Appl. Phys., Vol. 44, p. 1733 (1973).

9. Byer, R., and S. E. Harris, "Power and Bandwidth of Spontaneous Parametric Emission," Phys. Rev., Vol. 168, p. 1064 (1968).

10. Esterowitz, L., et al., "Rare Earth Infrared Quantum Counter," Appl. Optics, Vol 7, p. 2059 (1968).

11. Falk, J., and W. B. Tiffany, "Theory of Parametric Upconversion of Thermal Images," J. Appl. Phys., Vol. 43, p. 3762 (1972).

12. Gandrud, W. B., and H. W. Moos, "Improved Rare-Earth Trichloride Infrared Quantum Counter Sensitivity," IEEE J. Quant. Electron., Vol. QE-4, p. 249 (1968).

13. Harris, S. E., "Tunable Optical Parametric Oscillators," Proc. IEEE, Vol. 57, p. 2096 (1969).

14. Harris, S. E., and D. M. Bloom, "Resonantly Two-Photon Pumped Frequency Converter," Appl. Phys. Letters, Vol. 24, p. 229 (1974).

15. Herrington, J.R., K. G. Sewell, and W. B. Volz, "A Thermal Imaging System Based on the $PrCl_3$ Quantum Counter," Appl. Phys. Letters, Vol. 26, p. 226 (1975).

16. Hudson, R. D., Jr., Infrared System Engineering, p. 322 (John Wiley and Sons, New York, New York, 1969).

17. Hulme, K. F., et al., "Synthetic Proustite (Ag_3AsS_3) : A New Crystal for Optical Mixing," Appl. Phys. Letter, Vol. 10, p. 133 (1967).

18. Jerphagnon, J., and S. K. Kurtz, "Optical Nonlinear Susceptibilities; Accurate Relative Values for Quartz, Ammonium, Dihydrogen Phosphate, and Potassium Dihydrogen Phosphate," Phys. Rev. B, Vol. 1, p. 1739 (1970).

19. Krupke, W. F., "Performance of Laser-Pumped Quantum Counters," IEEE J. Quant. Electron., Vol. QE-1, p. 20 (1965).

20. Midwinter, J. E., "Infrared Up Conversion in Lithium-Niobate with Large Bandwidth and Solid Acceptance Angle," Appl. Phys. Letters, Vol. 14, p. 29 (1969).

21. Miles, R. B., "Optical Third Harmonic Generation in Metal Vapors," Internal Memorandum, Hansen Microwave Laboratory Report No. 2069, Stanford University (June 1972).

22. Milton, A. Fenner, "Upconversion--a Systems View," Appl. Optics, Vol. 11, p. 2311 (1972).

23. Morris, R. C., et al., "Lanthanum Beryllate: A New Rare-Earth Ion Laser Host," Appl. Phys. Letter, Vol. 27, p. 444 (1975).

24. Porter, J. F., Jr., "Sensitivity of Pr^{3+} : $LaCl_3$ Infrared Quantum Counter," IEEE J. Quant. Electron., Vol. QE-1, p. 113 (1965).

25. Private Communication.

26. Sewell, K. G., and W. B. Volz, "Direct Infrared Image Upconversion with a Praseodymium Chloride Quantum Counter," Appl. Phys. Letters, Vol. 23, p. 104 (1973).

27. Stappaerts, E. A., Stanford University, Private Communication.

28. Stappaerts, E. A., "Dependency of Susceptibilities on Polarization," Internal Memorandum, Hansen Microwave Laboratory Report No. 2438, Stanford University (May 1975).

29. Stokowski, S. E., "Characteristics of a Nd Laser-Pumped 5-μm IRQC Detector," Paper No. 6, VIII International Quantum Electronics Conference June 10-13, 1974.

30. Stokowski, S. E., "Characteristics of a Laser-Pumped 1.5-μm Infrared Quantum Counter," J. Appl. Phys., Vol. 45, p. 2957 (1974).

31. Wright, J. C., and F. K. Fong, "Multiphonon Orbit-Lattice Relaxation and Quantum Efficiency of 10-μ Infrared Quantum-Counter Upconversion in Rare-Earth-Doped Crystals," J. Appl. Phys., Vol. 42, p. 3806 (1971).

32. Wright, J. C., et al., "Laser Optical Double Resonance and Efficient Infrared Quantum Counter Upconversion in $LaCl_3 : Pr^{3+}$ and $LaF_3 : Pr^{3+}$," J. Appl. Phys., Vol. 44, p. 781 (1973).

33. Zernike, F., and J. E. Midwinter, Applied Nonlinear Optics, p. 42, (John Wiley and Sons, New York, New York, 1973).

☆ U. S. GOVERNMENT PRINTING OFFICE: 1976 — 757-001/127